Journal of Systematic Palaeontology, 2022
Vol. 20, No. 1, 2093139
http://dx.doi.org/10.1080/14772019.2022.2093139

A nearly complete skeleton of a new eusphenodontian from the Upper Jurassic Morrison Formation, Wyoming, USA, provides insight into the evolution and diversity of Rhynchocephalia (Reptilia: Lepidosauria)

David G. DeMar Jr. [a]*, Marc E. H. Jones[b,c] and Matthew T. Carrano[a]

[a]*Department of Paleobiology, National Museum of Natural History, Smithsonian Institution, Washington, DC, 20560, USA;* [b]*Research Department of Cell and Developmental Biology, University College London, London, WC1E 6BT, UK;* [c]*Ecology and Evolutionary Biology, School of Biological Sciences, The University of Adelaide, North Terrace, Adelaide, South Australia 5005, Australia*

(Received 2 September 2021; accepted 18 June 2022)

We describe a new, small-bodied rhynchocephalian reptile, *Opisthiamimus gregori* gen. et sp. nov., from the Upper Jurassic Morrison Formation of Wyoming, USA. Whereas many fossil rhynchocephalians are based on isolated incomplete jaws, the holotype of *O. gregori* includes most of the skull and postcranium and therefore represents one of the most complete specimens of Rhynchocephalia known from North America. We used micro-computed tomography to examine its skeletal anatomy in detail and to develop a three-dimensional reconstruction of the skull. The skull of *O. gregori* is similar to that of several non-neosphenodontian rhynchocephalians such as *Planocephalosaurus* (e.g. large orbits) and *Clevosaurus* (e.g. parietal parasagittal crests) yet exhibits a suite of other features related to the proal shearing mechanism that becomes increasingly elaborated among more phylogenetically nested taxa such as *Sphenodon* (e.g. lateral palatine tooth row parallels maxillary tooth row along its entire length, pyramidal dentary teeth with mesial shearing crests). The postcranial skeleton of *O. gregori* exhibits characteristics typical of a terrestrial rhynchocephalian. Our phylogenetic analyses use a substantially updated data set of 118 characters and 46 taxa, and both maximum parsimony and Bayesian frameworks. Results place *O. gregori* inside Eusphenodontia but outside Neosphenodontia, and therefore in a key position for contributing to character polarity for more deeply nested clades such as Clevosauridae, Sphenodontidae and Pleurosauridae. We also erect Leptorhynchia taxon nov., composed primarily of aquatically adapted taxa (e.g. *Pleurosaurus*, *Sapheosaurus*), which is supported by both cranial and postcranial characters. Because *O. gregori* is not particularly closely related to the other named Morrison rhynchocephalians (e.g. *Opisthias rarus*), it increases both the alpha and beta taxonomic diversities within the formation. Similarly, major differences in body size and inferred diet of the Morrison taxa imply considerable concomitant palaeoecological diversity just prior to a major global decline in rhynchocephalian diversity around the close of the Jurassic.

http://zoobank.org/urn:lsid:zoobank.org:pub:888E055B-8AC1-4BD0-A37C-8CB192F79673

Keywords: Rhynchocephalia; Eusphenodontia; Late Jurassic; Morrison Formation; phylogeny; diversity

Introduction

The reptilian clade Rhynchocephalia is the sister taxon to Squamata (lizards, snakes and amphisbaenians) within Lepidosauria (Evans 1984, 2003; Gauthier *et al.* 1988; Zardoya & Meyer 1998; Evans & Jones 2010; Jones *et al.* 2013; Chambi-Trowell *et al.* 2021; see clade definitions below). Whereas Squamata is represented by more than 11,000 globally distributed species today (Uetz *et al.* 2022), Rhynchocephalia includes only a single extant species restricted to New Zealand (Hay *et al.* 2010; Cree 2014; Gemmell *et al.* 2020; Lamar *et al.* 2021). However, this pattern was strikingly different for the first 100 million years of lepidosaur evolution, after the two clades diverged sometime prior to the Middle Triassic (Jones *et al.* 2013; Simões *et al.* 2018; Burbrink *et al.* 2020). The Late Triassic and Jurassic fossil record suggests that Rhynchocephalia may have been the first to achieve a nearly global distribution and correspondingly broad ecomorphological diversity (e.g. Cocude-Michel 1963; Jones 2008; Jones *et al.* 2009b; Meloro & Jones 2012; Rauhut *et al.* 2012; Martínez *et al.* 2013; Chambi-Trowell *et al.* 2019; Kligman *et al.* 2021). Only at the close of the Jurassic did Squamata begin to overshadow Rhynchocephalia as the predominant lepidosaur clade (e.g. Evans 1995; Evans & Jones 2010; Rauhut *et al.* 2012). The fossil record of Rhynchocephalia then diminishes, first in Laurasia and

*Corresponding author. David G. DeMar, Jr Email: demard@si.edu; magnuviator@gmail.com

Published online 15 Sep 2022

later in Gondwana (Evans *et al*. 2001; Apesteguía & Novas 2003; Jones 2006b; Jones *et al*. 2009b), whereas that of squamates radically expanded (Cleary *et al*. 2018; Herrera-Flores *et al*. 2021). The pattern, pace and drivers of this Jurassic–Cretaceous transition in diversity are among the most interesting questions in lepidosaur evolution, but at present the limited fossil record makes all three aspects difficult to assess (Jones 2006b; Cleary *et al*. 2018). Indeed, the lepidosaur record is dominated by incompletely known taxa whose relationships are often poorly resolved (Evans 2003; Cleary *et al*. 2018). However, this record continues to improve, and micro-computed tomography (μCT) can enhance the discovery and communication of anatomical characters for comparative anatomy and phylogenetic analysis (e.g. Jones *et al*. 2013, 2018; K. M. Jenkins *et al*. 2017; Chambi-Trowell *et al*. 2019, 2021; Romo de Vivar *et al*. 2020; Scheyer *et al*. 2020; Simões *et al*. 2022).

North America, in particular, preserves records of rhynchocephalians spanning from the early Late Triassic (Carnian) to the late Early Cretaceous (Albian), and from East Greenland in the north to Puebla, Mexico, in the south (e.g. Throckmorton *et al.* 1981; F. A. Jenkins *et al.* 1994; Reynoso 1997, 2000; Kligman 2021). Seventeen named taxa are known, and more are likely present on the basis of poorly preserved but distinct fossils (e.g. Gilmore 1909; Simpson 1926; Rasmussen & Callison 1981; Throckmorton *et al.* 1981; Sues *et al.* 1994a, b; Reynoso 1996, 1997, 2000, 2005; Reynoso & Clark 1998; Heckert 2004; Heckert *et al.* 2008; Scheyer *et al.* 2020; Kligman *et al.* 2021; Sues & Schoch 2021; Simões *et al*. 2022). Most of these North American records are concentrated in the USA, especially the Carnian through Aptian–Albian of the Western Interior (Montana, Wyoming, Utah, Colorado, Arizona, New Mexico, Texas) and Carnian–Hettangian of the East Coast (Connecticut, Virginia, North Carolina). For a more detailed account of these records, see the Supplemental material.

The Upper Jurassic Morrison Formation of the western USA offers great potential to illuminate the evolution of Rhynchocephalia and Squamata at a time when their respective dominances were shifting. The Morrison hosted a number of palaeoenvironments where taxa from the two lepidosaur clades co-occurred (e.g. see appendices in Foster [2003] and Kirkland [2006]), including specific individual localities that indicate these groups directly cohabited certain settings. However, the Morrison lepidosaurs remain relatively poorly known, as small-bodied taxa have tended to lag behind the larger dinosaurs in their discovery and description (Carrano & Velez-Juarbe 2006). Indeed, although rhynchocephalian fossils are widespread, only three genera have been formally described: *Opisthias*, *Theretairus* and *Eilenodon* (Gilmore 1909; Simpson 1926; Rasmussen & Callison 1981), all known primarily or exclusively from jaw bones with teeth (for a more detailed account, see Supplemental material).

Consequently, the discovery of a new, small-bodied rhynchocephalian from the Upper Jurassic Morrison Formation is of special interest. In this study, we describe this new taxon in detail via direct observations and μCT scans of multiple specimens, including one of the most complete and three-dimensionally preserved rhynchocephalian skeletons from North America. As such, these specimens offer an extraordinary enhancement of our current anatomical knowledge of Jurassic Rhynchocephalia and provide a window into the evolutionary history and ecomorphological adaptations of terrestrial rhynchocephalians whose postcranial anatomy is often poorly known. Secondly, we conduct a series of phylogenetic analyses using a newly modified character/taxon dataset, which includes carefully selected outgroup and ingroup taxa and a re-evaluation of commonly used characters and character states. Results of our analysis reveal novel taxon relationships and membership within larger clades, but the overall higher-level topology remains similar to most recent studies. Lastly, we discuss aspects of the new taxon's palaeobiology (e.g. ontogeny, jaw motion) and the palaeoecological diversity of Morrison Rhynchocephalia on the basis of body size and inferred diet.

Material and methods

Institutional abbreviations

DINO, Dinosaur National Monument, Jensen, Utah, USA; **LACM**, Natural History Museum of Los Angeles County, Los Angeles, California, USA; **LDUCZ**, Grant Museum of Zoology, University College London, London, UK; **NHMUK**, Natural History Museum, London, UK; **NMNH**, National Museum of Natural History, Smithsonian Institution, Washington, DC, USA; **USNM**, National Museum of Natural History (formerly United States National Museum), Smithsonian Institution, Washington, DC, USA; **YPM**, Yale Peabody Museum of Natural History, New Haven, Connecticut, USA.

Material

The four specimens assigned to the new taxon described herein comprise a nearly complete skeleton, a partial skull with a lower jaw, an isolated partial dentary, and an atlas/axis complex (USNM PAL 722041, 720475, 720476, 720479, respectively). All specimens derive from a single locality in the Upper Jurassic Morrison Formation of northern Wyoming, USA. The holotype (USNM PAL 722041) of the new taxon is an articulated

skeleton that is nearly complete to the pelvic region. During its collection in the field, the blocky matrix encasing it split into seven or eight main pieces (and a few smaller ones), which later were reassembled in the lab into three primary blocks (P. Kroehler, pers. comm., 2022). These blocks include: (1) approximately the anterior two-thirds of the skull and lower jaws, (2) a partial right manus and carpus with the distal ends of the right radius and ulna, and (3) the posterior one-third of the skull and lower jaws and the remainder of the postcranial skeleton. Hereafter they are referred to as the 'skull,' 'hand' and 'skeletal' blocks, respectively. The skull and hand blocks were not re-attached to the skeletal block to allow for more thorough mechanical preparation and enhanced study (e.g. greater micro-CT scan resolution). The specimen is missing the tail (except for one isolated caudal), most of the pelvic girdle and hind limbs, and a small series of trunk vertebrae and associated ribs (skeletal block). Most of the missing elements are associated with broken surfaces of the blocks, and may have been present originally, although the isolated caudal suggests that some disarticulation of the tail had taken place. In all three blocks the elements (still partially embedded in matrix) are three-dimensionally preserved with some dorsoventral crushing (e.g. as seen in the skull). The anterior portion of the skull has largely been freed of matrix, exposing most of its dorsal and ventral aspects. The skeleton is exposed mostly dorsally; the hand was prepared to expose the palmar side.

For firsthand anatomical comparison and character scoring for phylogenetic analysis we also studied several USNM topotypic dentaries of *Opisthias rarus* (USNM V 2860 [holotype], 2858 ['paratype'], 6126, 6127, 6129, 6130, 6131, 6132) and *Theretairus antiquus* (USNM V 26088, USNM PAL 720482) and skeletons of *Sphenodon punctatus* (e.g. USNM 220291). High resolution digital photographs and three-dimensional (3D) volume-rendered movies of the holotype dentary of *T. antiquus* (YPM VP 013764) also were informative (provided by G. Bever).

Micro-computed tomography, three-dimensional modeling and digital imaging

To better understand the anatomy of the new fossil rhynchocephalian, we subjected most of its specimens to high resolution X-ray μCT at three institutions: Duke University, Durham, North Carolina, USA (USNM PAL 722041, holotype skull, hand and skeletal blocks); National Museum of Natural History (NMNH), Smithsonian Institution, Washington, DC, USA (USNM PAL 722041, holotype skeletal block); and the University of Hull, Hull, UK (USNM PAL 720475, referred partial skull). Several attempts were made to produce high-resolution scans of the holotype skeletal block, but its thickness prohibited acquisition of sufficiently detailed slice images of the bone (i.e. poor contrast between individual bones and between the bones and matrix). We provide the parameters of the best scan only (Supplemental material). Where interpretable, portions of the skull, lower jaws and skeleton were segmented and volumetrically rendered to show gross anatomical structures. Because little matrix surrounds the holotype skull and hand blocks, the scans of these blocks produced high-resolution images that allowed easy overall interpretation, segmentation and volumetric rendering. Mimics Research (v. 20.0) and 3D Slicer (v. 4.6.2 and 4.11.0; slicer.org) were used for segmentation and rendering. Segmentation and volumetric renderings of the referred skull were carried out in Amira 6.0; these augmented our description of the new taxon, but we include only a model of the maxilla from that specimen in the Supplemental material.

The individual volumetric renderings of the skull bones from the holotype skull block, along with several from the skeletal block (squamosal, parietal, quadrate, posterior part of mandible and posterior process of jugal, all from the right side), were exported as surface models and imported into Autodesk® Maya® 2018 Student Version for 3D reassembly and reconstruction. Because the bones of the right side of the skull were often better preserved than those on the left, we mirrored most of them to create a more symmetrical skull reconstruction. For the premaxillae and parietals, we mirrored the left and right sides and merged them together to form a more complete element. Taphonomic breakage and slight deformation of the skull bones made it difficult to fully rearticulate the skull as it was in life. As a result, some bones were slightly shifted out of natural contact when digitally reassembled (e.g. lateral process of the ectopterygoid with the maxilla and jugal).

All but one of the digital images of specimens were taken using an Olympus DSX-100 digital microscope in the Scientific Imaging Lab at the NMNH. Each of these is an extended depth of field (EDF) image, which is a combined series of multi-focused images. A Nikon D700 SLR digital camera was used to take the single image of the partial skeleton on the skeletal block (Fig. 17A; see below for block details).

Anatomical description methods, tools and terminology

Our anatomical descriptions of USNM PAL 722041 and 720475 derive from a combination of direct observations

of the fossils under stereoscopic microscopes (Zeiss Stemi SV 6 and SV 11) and via μCT scan image slices and subsequent 3D renderings and reconstructions. These primary descriptions are augmented by direct observations of the two remaining referred specimens (i.e. USNM PAL 720476, 720479).

The anatomical terminology used herein generally follows Evans (1980, 1981), Fraser (1982, 1988), Fraser & Walkden (1984), Whiteside (1986) and Apesteguía *et al.* (2012). Cranial joint terminology follows Jones *et al.* (2011), and terminology for tooth orientation follows Smith & Dodson (2003).

Phylogenetic analysis

We conducted a series of analyses to determine the phylogenetic position of the new rhynchocephalian taxon. Our data matrix, heavily modified from Hsiou *et al.* (2019; itself slightly modified from Apesteguía *et al.* 2014; see Supplemental material for details), was assembled in Mesquite v. 3.40 (build 877; Maddison & Maddison 2018). We made several additions and modifications to that dataset, some derived from other studies. Our matrix includes 46 taxa (7 outgroup, 39 ingroup) and 118 characters (95 craniodental, 23 postcranial). The late Permian-age neodiapsid reptile *Youngina capensis* Broom, 1914 was designated as the outgroup taxon. All characters were unordered and equally weighted. We ran maximum parsimony analyses using TNT v. 1.1 (Goloboff *et al.* 2008). For our first analysis, a heuristic search of 1000 replications of Wagner trees (random addition sequence) was followed by the application of the tree bisection and reconnection (TBR) branch-swapping algorithm (holding 10 trees per replicate). The most parsimonious trees (MPTs) were then exported and read in PAUP* v. 4.0a (build 169; Swofford 2003) to create consensus trees and apomorphy lists and calculate consistency and retention indices (CI and RI, respectively). Accelerated transformation (ACCTRAN) was chosen as the character state optimization criterion. Bremer (12 sub-optimal steps) and bootstrap (1000 replicates) values were calculated in TNT. Apomorphies used to diagnose taxa are based on the strict consensus, but we also provide a full list from the Adams consensus (see Supplemental material). To identify the most unstable taxa and clades among the MPTs from our parsimony analysis, we used the iterPCR (iterative positional congruence [reduced]) protocol and TNT script developed by Pol & Escapa (2009). The resultant pruned iterPCR tree reveals the multiple optimal positions of the most unstable taxa and lists the problematic characters (missing or conflicting scores) that underlie them (see Supplemental material).

We also ran a Bayesian analysis in MrBayes v. 3.2.6 x64 (Huelsenbeck & Ronquist 2001) with *Youngina capensis* again chosen as the outgroup taxon. The Bayesian analysis was run for 6,000,000 generations with a sample frequency of 1000, two runs with four chains each, and the majority rule consensus tree was calculated after a 50% burn-in. Posterior probabilities (PP) above 90% are considered strongly supported. To further test the phylogenetic affinities of the new rhynchocephalian, we added it to the 35-taxon/131-character data matrix of Simões *et al.* (2020; see Supplemental material for TNT and Nexus files) and followed the same TNT and Bayesian search criteria as above.

Clade definitions and references

We use the following clade definitions, based primarily on prior usage:

1. Lepidosauria Haeckel, 1866 *sensu* Evans 1984.
2. Rhynchocephalia Günther, 1867 represents all Lepidosauria more closely related to *Sphenodon punctatus* than to *Iguana iguana* and *Gekko gecko* (Squamata). Thus, Rhynchocephalia is the sister taxon to total-group Squamata (or Pan-Squamata). This definition is in line with both the original use (Günther 1867) and widespread current use (e.g. Jones *et al.* 2013; Cree 2014; Burbrink *et al.* 2020; de Queiroz & Gauthier 2020; Gemmell *et al.* 2020; Chambi-Trowell *et al.* 2021; Ford *et al.* 2021; Griffiths *et al.* 2021). It is operationally similar to the definition of Gauthier *et al.* (1988), Rhynchocephalia = *Gephyrosaurus* + Sphenodontida (= Sphenodontia), but more clearly accommodates the discovery of new fossil taxa (e.g. *Vellbergia*; Sobral *et al.* 2020) that potentially may be more closely related to *Sphenodon* than they are to any squamate (but not as closely related to *Sphenodon* as is *Gephyrosaurus*).
3. Sphenodontia Williston, 1925 is a less inclusive group than Rhynchocephalia, which typically is used to refer to all rhynchocephalians except *Gephyrosaurus* (e.g. Evans 2003).
4. Acrosphenodontia Chambi-Trowell, Martinelli, Whiteside, Romo de Vivar, Soares, Schultz, Gill, Benton, & Rayfield, 2021.
5. Eusphenodontia Herrera-Flores, Stubbs, Elsler & Benton, 2018.
6. Clevosauridae Bonaparte & Sues, 2006 (*sensu* Hsiou *et al.* 2015).
7. Neosphenodontia Herrera-Flores, Stubbs, Elsler & Benton, 2018.

8. Leptorhynchia taxon nov. is defined as all taxa more closely related to *Pleurosaurus goldfussi* than to *Sphenodon punctatus*. It comprises mostly aquatically adapted taxa (e.g. *P. goldfussi*) and their closest allies.
9. Pleurosauridae Lydekker, 1888 (*sensu* Simões *et al*. 2020; *non* Lydekker, 1880).
10. Saphaeosauridae Nopcsa, 1923 (*sensu* Simões *et al*. 2020; *non* Bau, 1825 *in errore* for Baur, 1895).
11. Sphenodontidae Cope, 1871 (*sensu* Simões *et al*. 2020).
12. Sphenodontinae Cope 1871 (*sensu* Simões *et al*. 2020; *non* Nopcsa, 1928).
13. Eilenodontinae Rasmussen & Callison, 1981. As likely originally intended by Rasmussen & Callison (1981), we define Eilenodontinae as all taxa more closely related to *Eilenodon robustus* and *Toxolophosaurus cloudi* than they are to *Sphenodon punctatus*. Opisthodontia Apesteguía & Novas, 2003 is "a stem-group defined as all the sphenodonts that are more closely related to *Priosphenodon* than to *Sphenodon*" (Apesteguía & Novas 2003, p. 611). Based on our phylogenetic results, Opisthodontia is redundant with Eilenodontinae. As such, and because it was erected before Opisthodontia, we prefer to use the name Eilenodontinae herein.

For a summarized listing of clade apomorphies derived from our maximum parsimony strict consensus topology, see Supplemental material.

Geological and palaeontological setting

In 1997, a new vertebrate microfossil bonebed (VMB) site was discovered in the Upper Jurassic Morrison Formation on the east side of the Bighorn Basin near Shell, Wyoming (Fig. 1) by a group of geologists led by Erik Kvale (at the time with the Indiana Geological Survey). The site occurs in a highly weathered floodplain succession of red and green mottled silty claystones near the top of a ravine. Fossils are concentrated within two distinct layers: the primary layer is dominated by dinosaur eggshell fragments and contains the majority of the vertebrate material, whereas a secondary layer with fewer fossils was deposited directly above the primary layer. Attempts to obtain a radiometric date for the site were not successful, and in addition it remains difficult to correlate the Morrison strata of the Bighorn Basin with those farther south, on the Colorado Plateau. As a result, we are not yet able to specify the stratigraphic location of these beds within the Morrison Formation, and cannot confine their age beyond the unit's broad temporal range of early Kimmeridgian–Tithonian (~156–147 mya; Foster 2007; Trujillo & Kowallis 2015; Maidment & Muxworthy 2019).

Teams from the Smithsonian Institution began working the site in 1999 and excavated a number of blocks from a 2 × 3 m quarry over several subsequent field seasons (2003, 2007, 2010, 2014). The site was named the Fox Mesa locality after a nearby landform. Work at the Fox Mesa locality has focused primarily on dense accumulations of dinosaur eggshells and associated embryonic bones (e.g. Brett-Surman *et al*. 2005; Carrano *et al*. 2013), but a rich vertebrate fauna has also been obtained. Study of this fauna is ongoing, but it includes primarily terrestrial taxa such as lepidosaurs, crocodyliforms, theropod and ornithopod dinosaurs and several groups of mammals (including triconodonts, symmetrodonts, eupantotheres and multituberculates). These remains are dominated by isolated teeth, limb shafts and vertebrae. Overall, the Fox Mesa site constitutes a rich Morrison VMB that will provide important data on taxon associations, palaeoecology and palaeoenvironment in a formation that has produced relatively few such sites compared to later (Cretaceous) strata of the Western Interior.

Relevant to this study, the layer immediately above the eggshell bed was also quarried for its fossil content. Careful examination of quarry blocks for signs of fossil content has allowed the discovery of several important associated specimens that were prepared by hand. Among these are the holotype of the new taxon described herein (found by Peter Kroehler on 10 July 2010) and the referred partial skull and isolated lower jaw (found in 2003).

Systematic palaeontology

Lepidosauria Haeckel, 1866 (*sensu* Evans 1984)
Rhynchocephalia Günther, 1867 (*sensu* Gauthier *et al*. 1988)
Sphenodontia Williston, 1925
Eusphenodontia Herrera-Flores, Stubbs, Elsler & Benton 2018
Opisthiamimus gen. nov.

Type and only species. *Opisthiamimus gregori* sp. nov.

Derivation of name. From *Opisthias* (a genus of the clade Rhynchocephalia) and the Greek 'mimos' (μῖμος, meaning mimic; latinized to mimus), referring to the morphological similarities of the dentary and dentary teeth between this taxon and *Opisthias*.

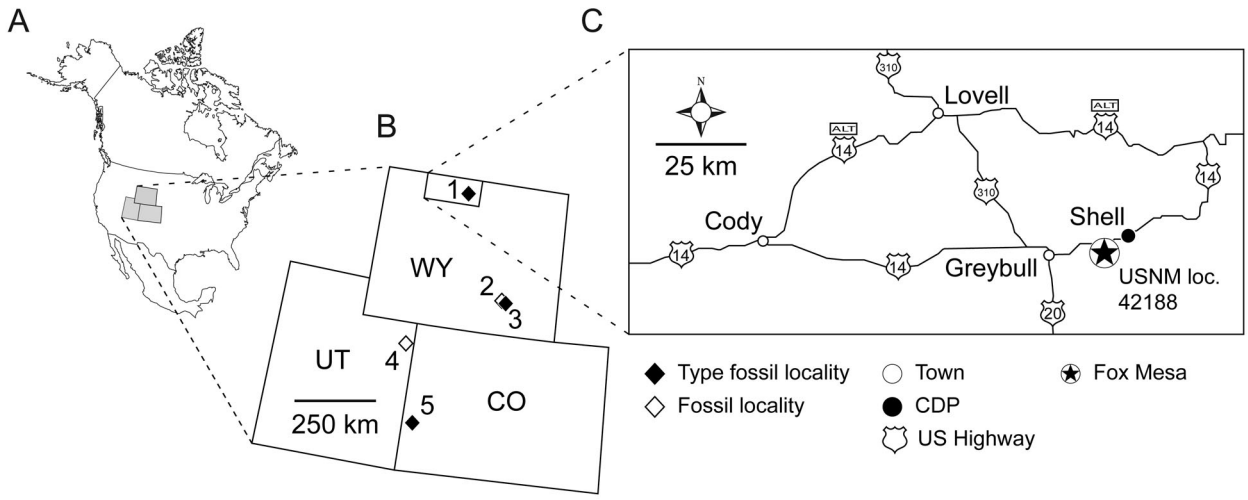

Figure 1. Geographical distributions of Rhynchocephalia of the Upper Jurassic Morrison Formation discussed within the main text and Supplemental material, including type localities of the four named taxa. **A,** map of North America with the three US states having produced Late Jurassic rhynchocephalians shaded in grey; **B,** enlargement of Wyoming, Utah and Colorado with the approximate placement of the fossil localities as numbered diamonds. Solid black diamonds designate type localities; open diamonds represent other important localities discussed in the text. Localities numbered as follows: 1, Fox Mesa, Big Horn County (type locality of *Opisthiamimus gregori* gen. et sp. nov.); 2, Ninemile Hill, Carbon County; 3, Quarry 9, Como Bluff, Albany County (type locality of *Opisthias rarus* and *Theretairus antiquus*); 4, Rainbow Park and other nearby localities, Dinosaur National Monument, Uintah County; 5, Fruita Paleontological Area, Mesa County (type locality of *Eilenodon robustus*). **C,** north-central Wyoming, enlarged from B, highlighting the type locality of *O. gregori* gen. et sp. nov. (USNM loc. 42188, Fox Mesa; encircled star). **Abbreviations: CDP**, US census-designated place; **CO**, Colorado; **loc**., locality; **USNM,** National Museum of Natural History (formerly United States National Museum), Smithsonian Institution, Washington, DC, USA; **UT**, Utah; **WY**, Wyoming.

Diagnosis. As for the type and only known species.

Opisthiamimus gregori sp. nov.
(Figs 2–14, 15A, B, M, 16–22, 23A–C, 27)

Derivation of name. The species epithet '*gregori*' recognizes Joseph Gregor, a dedicated Smithsonian volunteer who skillfully prepared the holotype and referred specimens.

Diagnosis. *Opisthiamimus gregori* gen. et sp. nov. is a small-bodied (snout-vent length ~85 mm) member of Rhynchocephalia based on the presence of four unambiguous synapomorphies: (1) jugal dorsal process extends posteriorly 33% or more of the anteroposterior length of the lower temporal fenestra; (2) lower temporal bar bowed laterally beyond the limit of the adductor chamber; (3) dentary posterior process elongate, reaching articular glenoid level; and (4) splenial absent. *Opisthiamimus gregori* is a member of Sphenodontia based on the presence of three unambiguous synapomorphies: (1) lacrimal absent; (2) distal marginal tooth attachment acrodont; and (3) weak overlap or imbrication between adjacent distal maxillary teeth. *Opisthiamimus gregori* is a member of Acrosphenodontia in possessing all 14 unambiguous character states of that major clade: (1) parietal parasagittal crest poorly developed; (2) dentary mentonian process poorly developed; (3) mandibular symphysis oval; (4) anterodorsal tip of dentary with conical, anterodorsally projected successional tooth that does not project beyond anterior margin angle of dentary; (5) mesial notch above dentary symphysis confluent with medial surface of subdental ridge/postsymphyseal lamina; (6) dentary symphysis not split by Meckelian canal; (7) precoronoid portion of dentary moderate in length and height; (8) coronoid process of dentary moderately tall; (9) mesial marginal tooth attachment acrodont; (10) distal maxillary teeth with small flanges; (11) mesiodistal length of distal dentary teeth greater than apicobasal height; (12 and 13) distal dentary teeth with a mesiolabial and mesiolingual crest; and (14) pterygoid with two tooth rows. *Opisthiamimus gregori* belongs to Eusphenodontia based on the presence of a single unambiguous synapomorphy: marginal dentition with conspicuous wear facets. *Opisthiamimus gregori* is the sister taxon to the Clevosauridae + Neosphenodontia in having a shorter fourth metacarpal relative to the third.

Opisthiamimus gregori possesses the following unique combination of unambiguous character states (autapomorphies denoted by an asterisk [*]): postfrontal lateral process bifurcated anteroposteriorly; *two

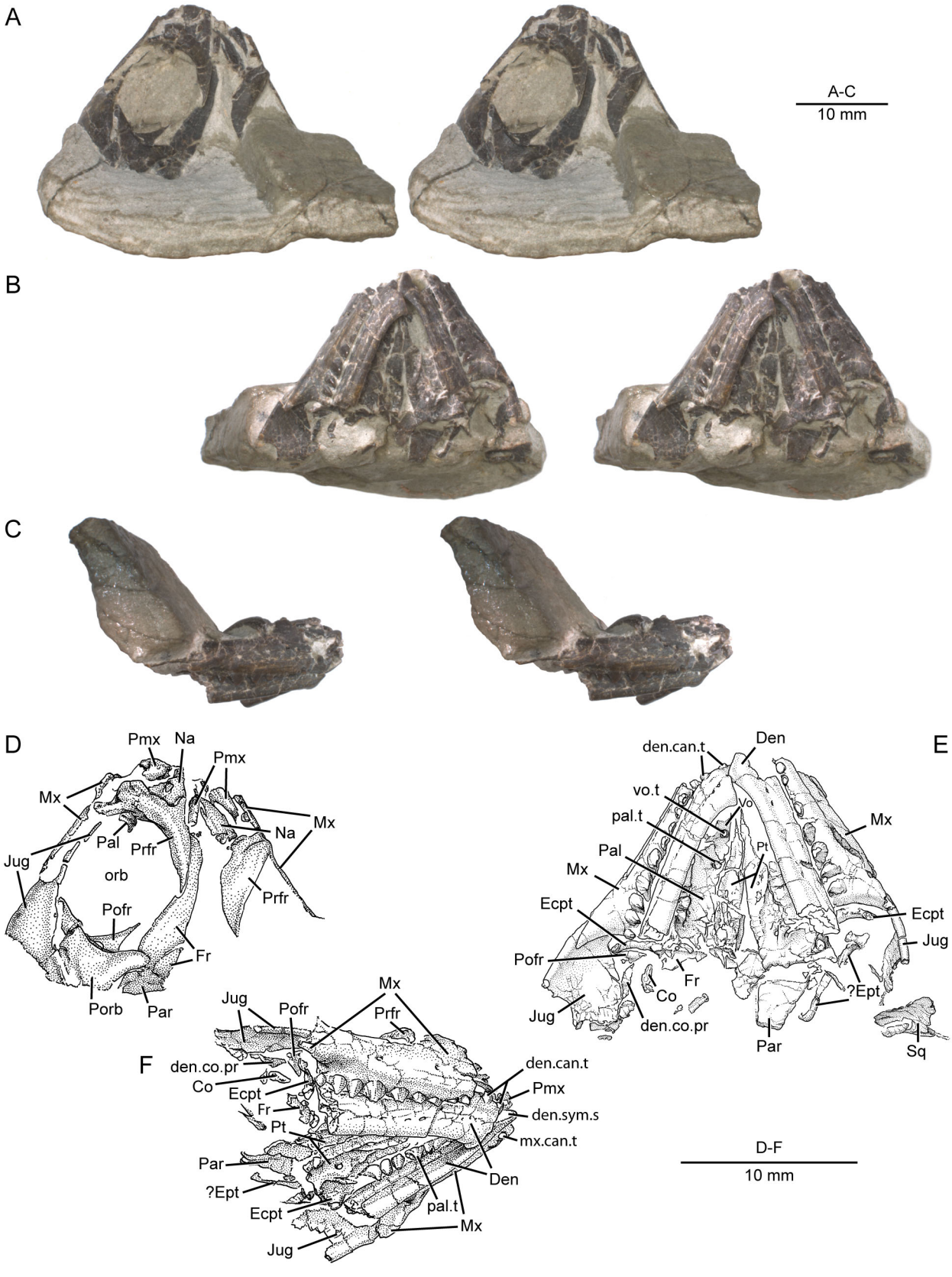
A
B
C
A-C
10 mm
D
Pmx
Na
Pmx
Mx
Mx
Na
Pal
Prfr
Jug
orb
Prfr
Pofr
Fr
Porb
Par
E
den.can.t
Den
vo.t
Vo
pal.t
Mx
Pal
Pt
Mx
Ecpt
Ecpt
Jug
Pofr
Fr
Co
?Ept
Jug
den.co.pr
Par
Sq
F
Mx
Jug
Pofr
Prfr
den.co.pr
den.can.t
Co
Ecpt
Pmx
Fr
den.sym.s
Pt
mx.can.t
Par
Den
?Ept
pal.t
Ecpt
Mx
Jug
D-F
10 mm

broadly spaced, non-hypertrophied dentary successional caniniform teeth, with the mesial caniniform positioned at the anterodorsal tip of the dentary (symphyseal); *caniniform tooth present at the mesial end of the lateral palatine tooth row, tooth similar in size (non-hypertrophied) and lingually offset to succeeding palatine teeth; palatine lateral tooth row accompanies maxillary tooth row for entire length; humerus radial condyle present and moderately expanded. *Opisthiamimus gregori* also possesses one ambiguous character state: a small posterior process on the transverse process of the second sacral vertebra.

Within Eusphenodontia, *Opisthiamimus gregori* differs unambiguously from Clevosauridae in the absence of an extensive anterolateral process of the ectopterygoid that contacts the maxillary process of the palatine. It differs unambiguously from Neosphenodontia in possessing an antorbital region of the skull between 25 and 33% the total skull length (*vs* $< 25\%$), and a maxilla excluded from the margin of the external naris by the posterodorsal process of premaxilla (*vs* entering into margin).

As compared to other named Morrison Formation rhynchocephalians, *Opisthiamimus gregori* differs from both *Opisthias rarus* and *Eilenodon robustus* in being much smaller and in possessing the following distal additional dentary teeth character states: tooth bases mesiodistally longer relative to crown height (*vs* shorter, between 50–100% of crown height); basal cross-sectional tooth shape rounded to squared (*vs* rectangular) with about equidistant mesial/distal and labial/lingual margins (*vs* labiolingually expanded); absence of tooth imbrication (*vs* weak imbrication formed by both mesial crests/flanges); and lingual and labial tooth surfaces smooth with occasional weak wrinkles (*vs* prominent ridges and grooves).

Opisthiamimus gregori differs further from *Opisthias rarus* in possessing: dentary mentonian process small (*vs* prominent); subdental ridge dorsoventrally deep at mid tooth row length relative to total height of dentary at that point ($\geq 60\%$; vs moderately deep [34–59%]); dentary symphyseal and postsymphyseal successional teeth present (*vs* only a single symphyseal successional); distal additional dentary teeth with small mesiolabial and mesiolingual crests (*vs* small flanges); and weakly overlapping distal additional maxillary teeth (*vs* moderate overlap).

Opisthiamimus gregori differs further from *Eilenodon robustus* in the following: dentary posterior process reaches the level of the articular glenoid (*vs* reaching posterior end of glenoid); articular glenoid asymmetrical mediolaterally (*vs* symmetrical); retroarticular process elongate and pronounced (*vs* small and dorsally curved); distal groove of additional dentary teeth absent (*vs* wide and poorly defined); palatine with a single lateral tooth row plus an isolated tooth (*vs* only a single lateral tooth row); and caniniform tooth present at the mesial end of the lateral palatine tooth row (*vs* absent).

Finally, *Opisthiamimus gregori* differs from *Theretairus antiquus* in possessing the following dentary and dentary teeth character states: subdental ridge dorsoventrally deep at mid tooth row length relative to total height of dentary at that point ($\geq 60\%$; *vs* moderately deep [34–59%]); occlusal wear facets well developed (*vs* poorly developed); absence of vertical striae and a mesiolingual groove on the successional teeth (*vs* present on at least one tooth); absence of non-caniniform successional teeth (*vs* present); successional caniniform teeth smaller than the largest additional teeth (*vs* distinctly larger and hypertrophied); symphyseal successional caniniform tooth present (*vs* absent); and distal dentary teeth mesiolingual crest present (*vs* absent).

Holotype. USNM PAL 722041, an articulated partial skull and skeleton.

Referred specimens. USNM PAL 720475, partial skull (left maxilla, jugal, quadrate and palatine; part of the right palatine) and lower jaw (left dentary, angular, surangular, articular and prearticular); USNM PAL 720476, partial right dentary with four teeth; USNM PAL 720479, partial atlas/axis complex.

Type locality, age and distribution. USNM locality 42188 (Fox Mesa locality), Upper Jurassic (Kimmeridgian or Tithonian), Morrison Formation, Big Horn County, north-central Wyoming, USA. Known only from the type locality, but see below for another possible Morrison Formation occurrence in the Fruita Paleontological Area, west-central Colorado, USA.

Figure 2. Anterior portion of the skull and lower jaws of the holotype specimen (USNM PAL 722041, 'skull block') of *Opisthiamimus gregori* gen. et sp. nov. **A–C,** extended depth of field stereophotopairs in **A,** dorsal, **B,** ventral and **C,** right lateral views. **D–F,** interpretive camera lucida drawings for A–C, respectively. **Abbreviations: Co**, coronoid; **Den**, dentary; **den.can.t**, dentary successional caniniform tooth; **den.co.pr**, coronoid process of the dentary; **den.sym.s**, symphyseal surface of the dentary; **Ecpt**, ectopterygoid; **?Ept**, possible epipterygoid; **Fr**, frontal; **Jug**, jugal; **Mx**, maxilla; **mx.can.t**, successional caniniform tooth of the maxilla; **Na**, nasal; **orb**, orbit; **Pal**, palatine; **pal.t**, palatine tooth; **Par**, parietal; **Pmx**, premaxilla; **Pofr**, postfrontal; **Porb**, postorbital; **Prfr**, prefrontal; **Pt**, pterygoid; **Sq**, squamosal; **Vo**, vomer; **vo.t**, vomer tooth.

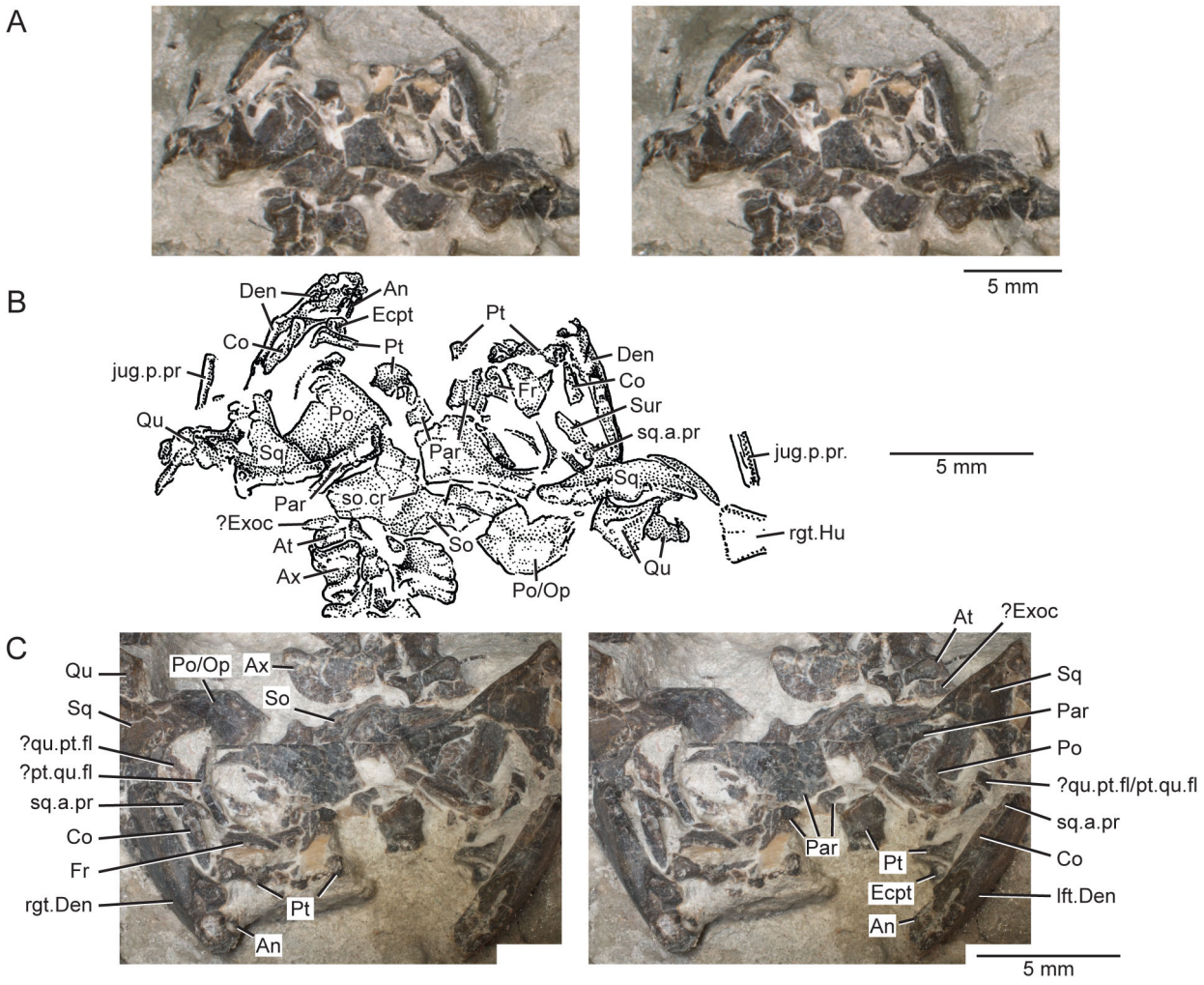

Figure 3. Posterior portion of the skull and lower jaws of the holotype specimen (USNM PAL 722041, 'skeletal block') of *Opisthiamimus gregori* gen. et sp. nov. **A,** extended depth of field (EDF) stereophotopair in dorsal view; **B,** interpretive camera lucida drawing for A; **C,** EDF stereophotopair in anterodorsal view. **Abbreviations: An**, angular; **At**, atlas or presacral vertebra no. 1; **Ax**, axis or presacral vertebra no. 2; **Co**, coronoid; **Den**, dentary; **Ecpt**, ectopterygoid; **?Exoc,** possible exoccipital; **Fr**, frontal; **jug.p.pr**, posterior process of the jugal; **lft.Den**, left dentary; **Par**, parietal; **Po**, prootic; **Po/Op**, prootic/opisthotic; **Pt**, pterygoid; **?pt.qu.fl**, possible quadrate flange of the pterygoid; **Qu**, quadrate; **?qu.pt.fl**, possible pterygoid flange of the quadrate; **rgt.Den**, right dentary; **rgt.Hu**, right humerus; **So**, supraoccipital; **so.cr**, supraoccipital crest; **Sq**, squamosal; **sq.a.pr**, anterior process of the squamosal; **Sur**, surangular.

Anatomical description

Skull and palate

Aside from being broken transversely into two parts (skull and skeletal blocks), the holotype skull (Figs 2, 3) is largely complete. The individual bones on their respective blocks are loosely articulated or in close association. However, the skull is crushed dorsoventrally, missing portions of the rostral bones, and many of the bones on the right side have been shifted slightly anteriorly relative to those on the left. Fracturing of the bones, particularly those of the palate, has complicated the identification of sutural contacts.

The skull, as digitally reassembled (Fig. 4), is triangular in dorsal view, relatively short dorsoventrally (~8.5 mm as measured between the highest and lowest points of the parietal and quadrate, respectively), and nearly as wide as it is long (~20.2 mm between the jugals *vs* ~20.5 mm between the anterior tip of the premaxilla and the back of the squamosal; Supplemental material, Table S1). Overall, the skull is moderately

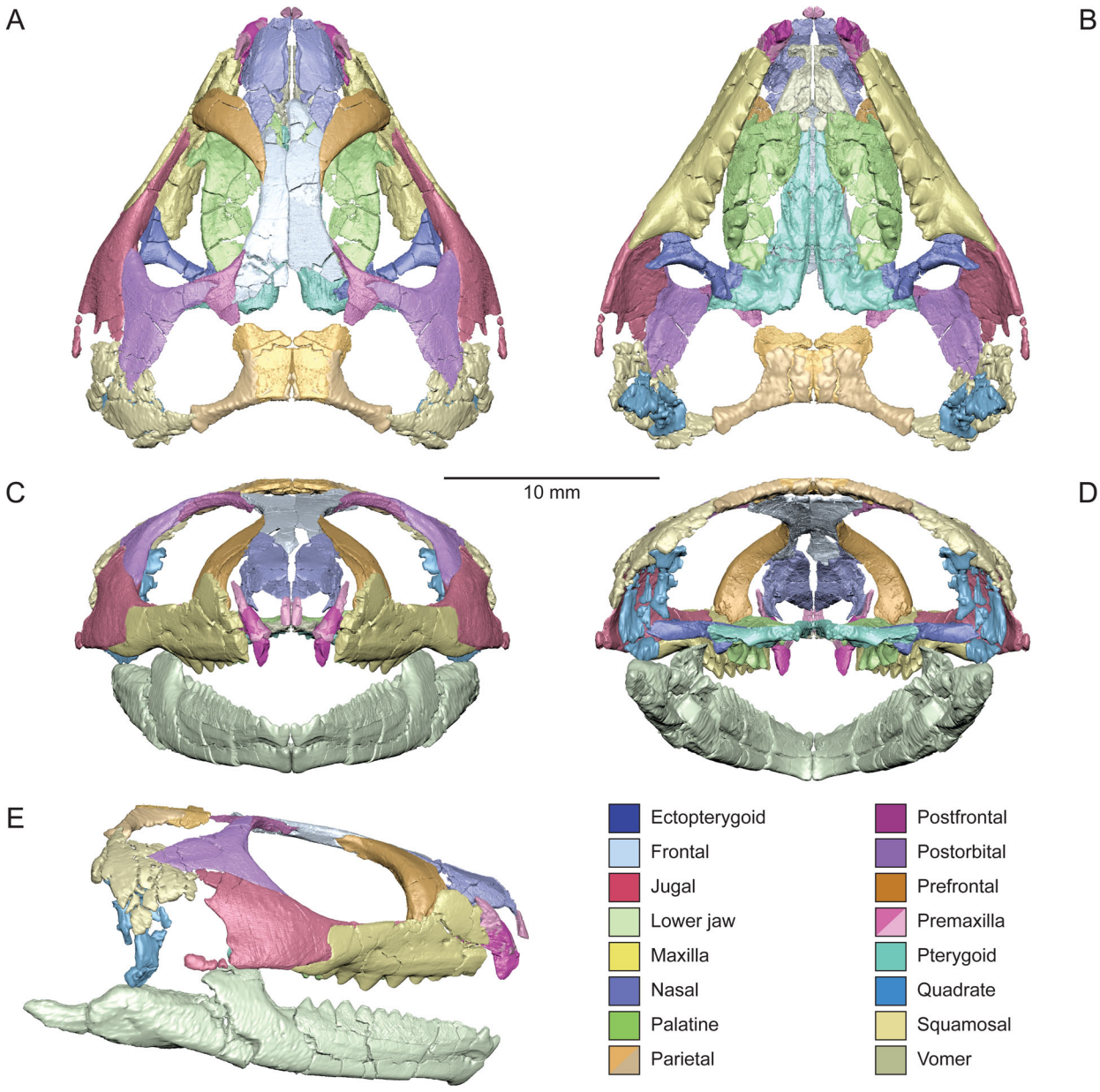

Figure 4. Virtual three-dimensional (3D) reconstruction of the skull and lower jaws of the holotype specimen (USNM PAL 722041) of *Opisthiamimus gregori* gen. et sp. nov. in **A,** dorsal, **B,** ventral, **C,** anterior, **D,** posterior and **E,** right lateral views. Colour key is at the bottom right. Solid colours indicate 3D renderings of a single bone. The mixed colours for the premaxilla and parietal indicate that for each of those bones the 3D renderings of their left and right sides were merged together to create a single, more complete version before reassembly. The left side of the skull and lower jaws is reflected from the better-preserved bones of the right side (except the vomer, pterygoid and ectopterygoid). Both left and right frontals are reassembled here.

robust with several broadly overlapping and interlocking joints that create a relatively rigid overall frame. The orbit is large and slightly more than a third of the length of the skull; it is ovoid in dorsal and lateral views and longer than it is wide or high. The upper temporal fenestra is moderate in circumference when compared to the orbit and somewhat larger than the lower temporal fenestra, which is restricted anteriorly by the broad jugal.

Note that the dentitions are described separately from the dentigerous bones themselves.

Premaxilla. The paired premaxillae (Fig. 2) are damaged; the dentigerous portion and ascending (= nasal)

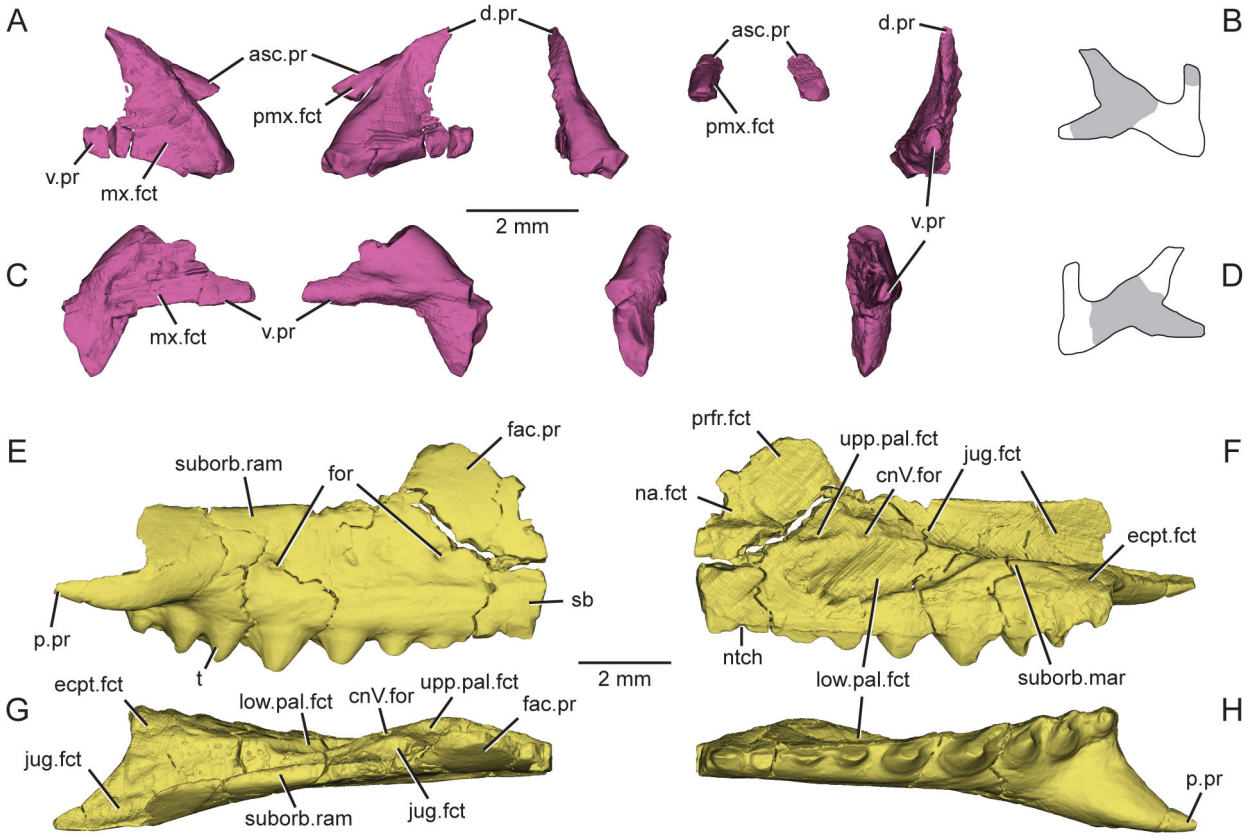

Figure 5. Virtual three-dimensional renderings of the premaxillae and maxilla of the holotype specimen (USNM PAL 722041) of *Opisthiamimus gregori* gen. et sp. nov. **A,** right premaxilla from left to right in lateral, medial, anterior and posterior views; **B,** portion of the right premaxilla (grey shade) preserved within an outline of a complete premaxilla based on *Clevosaurus hudsoni* (Fraser 1988, fig. 5); **C**, left premaxilla from left to right in lateral, medial, anterior and posterior views; **D**, portion of the left premaxilla (grey shade) as in B; **E–H,** right maxilla in **E,** right lateral, **F,** medial, **G,** dorsal and **H,** ventral views. **Abbreviations: asc.pr**, ascending process; **cnV.for**, foramen for cranial nerve five; **d.pr**, dorsal process; **ecpt.fct**, facet for the ectopterygoid; **fac.pr**, facial process; **for**, foramen; **jug.fct**, facet for the jugal; **low.pal.fct**, facet for the lower palatine process of the palatine; **mx.fct**, facet for the maxilla; **na.fct**, facet for the nasal; **ntch**, notch; **p.pr**, posterior process; **pmx.fct**, facet for the premaxilla; **prfr.fct**, facet for the prefrontal; **sb**, secondary bone; **suborb.mar**; suborbital margin; **suborb.ram**, suborbital ramus; **t**, tooth; **upp.pal.fct**, facet for the upper palatine process of the palatine; **v.pr**, ventral process.

process of each bone has largely broken away, leaving mostly the forked lateral end which includes a dorsal and ventral maxillary process (Fig. 5A–D) that is bridged by a posteriorly thinning section of bone. The complete dorsal process of the right premaxilla is exposed dorsally and wedged between the maxilla and nasal (Fig. 2A, D). In anterior view, it tapers dorsally and curves slightly dorsomedially to follow the curvature of the facial process of the maxilla. The left premaxilla is partially hidden by the left nasal, missing much of its dorsal process, and has been rotated transversely such that the medial surface of the forked lateral region faces dorsomedially. The posterior end of the ascending process of the right premaxilla is preserved, located slightly above and between the left prefrontal and right nasal. A flattened facet on its medial surface presumably articulated with the ascending process of the left premaxilla (Fig. 5A).

Maxilla. Both maxillae of the holotype (Figs 2A, C, D, F, 5E–H) are damaged, missing the premaxillary process as well as the anterior and dorsal margins of the facial process. Nevertheless, the shapes of the premaxilla and nasal indicate a relatively short, rounded snout (Fig. 4). The maxillary facial process curves weakly dorsomedially in dorsal view and has a steep posterior border. The better-preserved anterior region of the left maxilla of USNM PAL 720475 (Fig 6A, D, E) reveals a similarly steep anterior margin of the facial process and a relatively short, albeit partially incomplete, premaxillary process. The height of the maxillary facet on the right prefrontal of the holotype (see below) indicates that the

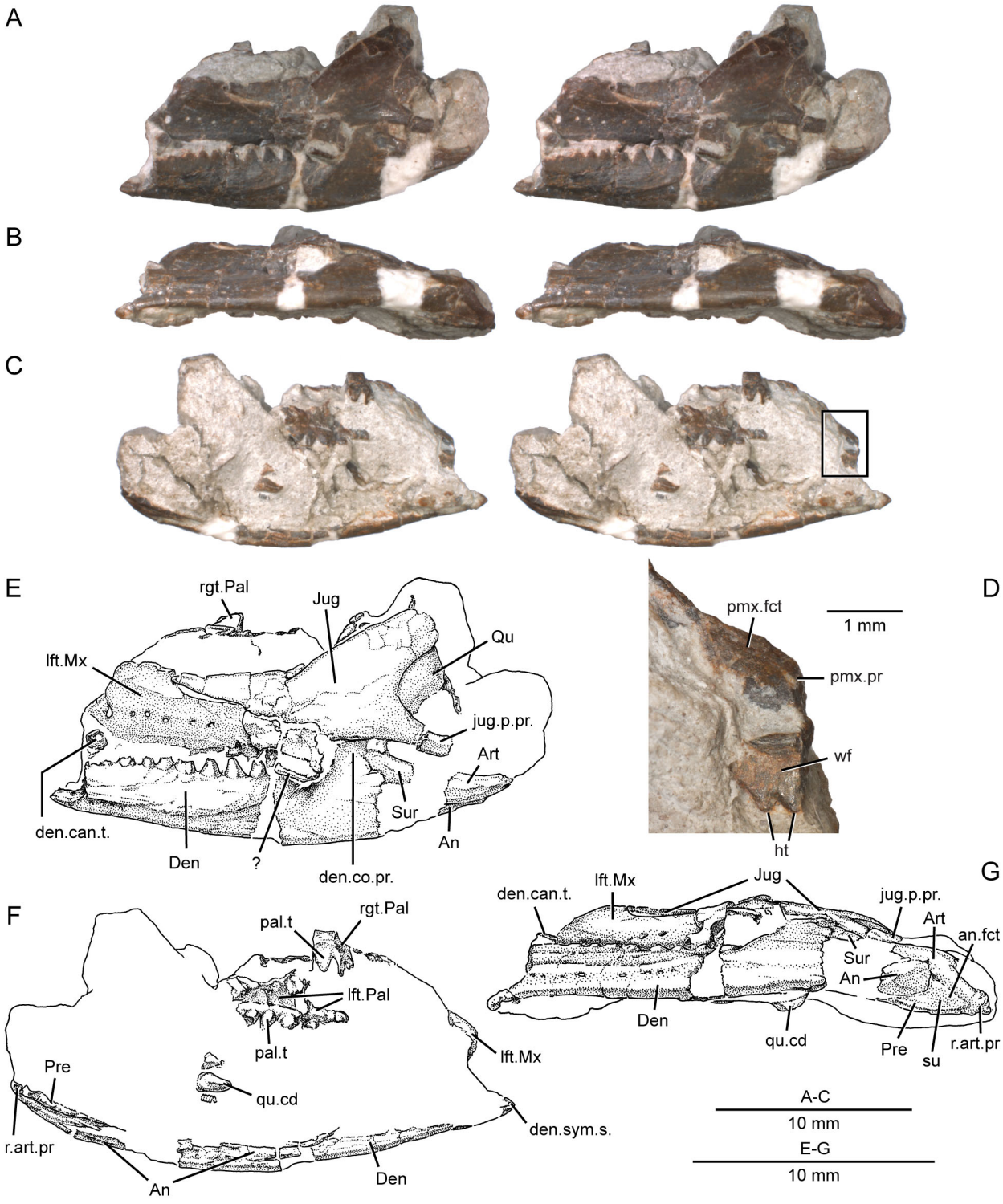

Figure 6. A referred partial skull and lower jaw (USNM PAL 720475) of *Opisthiamimus gregori* gen. et sp. nov. **A–C,** extended depth of field stereophotopairs in **A,** lateral, **B,** ventrolateral and **C,** medial views; **D,** close-up of the anterior end of the left maxilla as shown in the box in the right stereophoto in C; **E–G,** interpretive camera lucida drawings for A, C and B, respectively. **Abbreviations: An**, angular; **an.fct**, facet of the angular; **Art**, articular; **Den**, dentary; **den.can.t**, dentary successional caniniform tooth; **den.co.pr**, coronoid process of the dentary; **den.sym.s**, symphyseal surface of the dentary; **ht**, hatchling tooth; **Jug**, jugal; **jug.p.pr**, posterior process of the jugal; **left.Pal**, left palatine; **lft.Mx**, left maxilla; **pal.t**, palatine tooth; **pmx.fct**, facet for the premaxilla; **pmx.pr**, premaxillary process; **Pre**, prearticular; **Qu**, quadrate; **qu.cd**, quadrate condyle; **r.art.pr**, retroarticular process; **rgt.Pal**, right palatine; **su**, suture; **Sur**, surangular; **wf**, wear facet; **?**, unidentified bone.

facial process of the maxilla was about as tall as the suborbital ramus of the maxilla.

In lateral view, the suborbital ramus is moderately deep (Fig. 5E, F), in contrast to that of e.g. *Gephyrosaurus bridensis* (Evans 1980, fig. 31), and has a straight, horizontal dorsal margin as in *Clevosaurus hudsoni* (Fraser 1988, fig. 3b). Posteriorly, the lateral wall of the maxilla curves medially to overlap most of the lateral surface of the jugal (Fig. 5G). At the level of the last tooth position, the posterior border of the suborbital ramus is stepped downward to form a vertically oriented posterior margin. The posterior process of the maxilla tapers to a fine point but does not extend to the level of the posterior rim of the orbit (Fig. 4). In dorsal or ventral view, the posterior process is triangular and extends posterolaterally away from the tooth row, but curves slightly medially posteriorly (Fig. 5G, H). The lateral surface of the maxilla is smooth and perforated by a minimum of five or six unevenly spaced small supralabial foramina, arranged approximately parallel to the tooth row. These foramina are positioned at about mid-height of the suborbital ramus of the maxilla. The posterior-most foramen is located above the largest maxillary tooth (fourth from the rear), whereas the larger anterior-most foramen is positioned just anterior to the facial process of the maxilla, as in USNM PAL 720475 (Fig. 6A, E). Below these foramina and above the tooth row is a thickened horizontal band or lip of secondary bone.

The nasal, prefrontal, palatine, jugal and ectopterygoid facets of the maxilla are discernable in medial view (Fig. 5F). The nasal and prefrontal facets are located on the medial surface of the facial process. The lower palatine facet is an elliptical depression centred on the maxilla that would have contacted the large lower maxillary facet of the palatine. A foramen for the maxillary nerve (cranial nerve V.2: Jones *et al*. 2011; infraorbital foramen or canal of some authors: e.g. Whiteside 1986; Fraser 1988) opens posterodorsally above the palatine facet at about its mid-length. The jugal facet is an elongate dorsal groove on the medial side of the lateral wall that extends the length of the suborbital ramus. The ectopterygoid facet is triangular (akin to *Sphenodon*; Jones *et al*. 2011, fig. 30.1) and positioned on a ventromedially sloping shelf above the last two teeth at the posteromedial corner of the maxilla (Fig. 5F, G). The medial margin of the maxilla participates in bordering the suborbital fenestra for a short distance anteroposteriorly between the posterior and anterior levels of the palatine and ectopterygoid facets, respectively (Fig. 5F). We interpret the flattened, slightly grooved dorsomedial surface of the premaxillary process of the maxilla in USNM PAL 720475 as the premaxillary facet (Fig. 6D).

Nasal. Both nasals are present but damaged and separated from each other and their typical contacts (i.e. premaxilla, maxilla, frontal and prefrontal; Fig. 2A, D). As exposed, most of the left nasal is hidden below the left prefrontal laterally and partly overlies the left premaxilla anteriorly. It has been flattened along its length and lacks its anterior and posterior margins (Fig. 7A). It is also broken transversely at mid-length, with the posterior half offset sagittally relative to the anterior half. The right nasal is positioned between the ascending and dorsal processes of the right premaxilla and is overlain posteriorly by the right prefrontal. It is also tilted such that its dorsal surface slopes ventrolaterally and somewhat anteriorly; its lateral process has been bent medially with the base exposed below the right vomer in ventral view.

In dorsal view, the nasal is diamond-shaped and smooth (Fig. 7B). The left and right nasals contact each other along the midline via narrow alternating step joints; anteriorly the right overlaps the left, but posteriorly the reverse is true (Fig. 7A, B). Associated with this overlap, the dorsal external internasal suture is offset at about mid length. The posterior end of the nasal is triangular and wedged between the frontal and prefrontal (Fig. 4A); it overlaps the anterolateral surface of the frontal in a scarf joint (akin to *Sphenodon*; Jones *et al*. 2011) and forms a narrow step joint laterally with the medial edge of the prefrontal, which slightly overlaps the nasal (Fig. 7B, C). The triangular anterior process of the nasal is overlapped dorsomedially by the ascending process of the premaxilla (Fig. 4). The lateral region of the nasal, including the lateral process, is broadly triangular and slopes ventrolaterally (Fig. 7B, C). Here the nasal is partially overlapped from front to back by the premaxilla, maxilla and prefrontal. Of these contacts, only a small portion of the prefrontal facet is readily discernible, visible posterolaterally on the right nasal.

On the ventral surface, at about mid-length, a narrow ridge curves anterolaterally onto the base of the lateral process of the nasal and towards the posterodorsal margin of the external naris (Fig. 7D). This ridge separates a shallow, ovoid anteromedial depression from a similarly shaped but slightly deeper posterolateral one; a similar ridge is present in *Clevosaurus hudsoni* (Fraser 1988). In *Sphenodon punctatus*, the ventral surface of the nasal features only a single depression and lacks a ventral ridge (e.g. Jones *et al*. 2011, fig. 41). The nasal in *Gephyrosaurus bridensis* presents a more complex array of ridges that are oriented longitudinally (Evans 1980, figs 3–5). The longer sinuous ridge along the

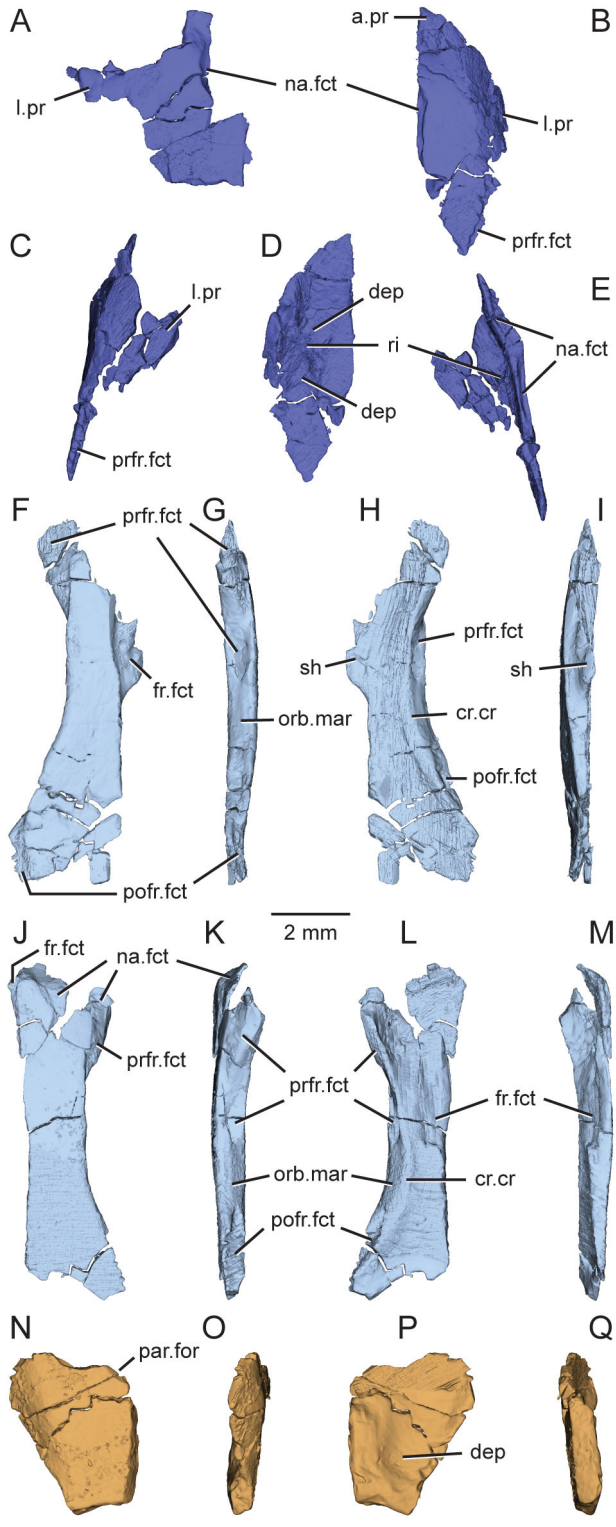

Figure 7. Virtual three-dimensional renderings of the dermal roofing bones of the skull of the holotype specimen (USNM PAL 722041) of *Opisthiamimus gregori* gen. et sp. nov. **A,** left nasal in dorsal view; **B–E,** right nasal in **B,** dorsal, **C,** right lateral, **D,** ventral and **E,** medial views; **F–I,** left frontal in **F,** dorsal, **G,** left lateral, **H,** ventral and **I,** medial views; **J–M,** right frontal in **J,** dorsal, **K,** right lateral, **L,** ventral and **M,** medial views; **N–Q,** partial left parietal in **N,** dorsal, **O,** left lateral, **P,** ventral and **Q,** medial views. Anterior is towards the top of the figure. **Abbreviations: a.pr**, anterior process; **cr.cr**, crista cranii; **dep**, depression; **fr.fct**, facet for the frontal; **l.pr**, lateral process; **na.fct**, facet for the nasal; **orb.mar**, margin of the orbit; **par.for**, parietal foramen; **pofr.fct**, facet for the postfrontal; **prfr.fct**, fact for the prefrontal; **ri**, ridge; **sh**, shelf.

midline of the nasal ('ridge 1' of Evans 1980) laterally borders a median trough that presumably housed the vestibulum anteriorly and the nasal chamber in the deeper, posterior part of the trough. A similar elongate ridge and trough are known in *Diphydontosaurus avonis* (Whiteside 1986, figs 8, 9a, b).

Prefrontal. The prefrontals are largely exposed in dorsal view but damaged anteromedially to anterolaterally (Figs 2, 8A–H). The left prefrontal is offset anteriorly relative to the right, and both have had their medial margins pushed downward.

The prefrontal is falciform in lateral view and forms the anterior and anterodorsal margins of the orbit (Figs 4, 8B, F). Medially, the prefrontal contacts the nasal anteriorly and the frontal posteriorly. The facial process of the maxilla overlaps a recessed facet on the prefrontal laterally (Fig. 8F); posterior to this overlap, the prefrontal is broadly exposed in lateral view (Fig. 4E). The ventral (= palatine) process of the prefrontal (Fig. 8A–D) extends ventrally to contact the palatine dorsally and the jugal anteromedially (see below). The ventral surface of the prefrontal is dorsally concave between the maxillary facet anteriorly and the palatine process posteriorly (Fig. 8B, C); this region likely represents the dorsal margin of the lacrimal foramen, which would have been bounded laterally by the maxilla and medially by the prefrontal. In lateral view, the gently tapering posterior (= frontal) process of the prefrontal extends posteriorly to more than one-third the length of the frontal (Fig. 4A, E). At its terminus, the dorsomedial surface of the process is narrowly faceted (Fig. 8A, E) and tapers abruptly for insertion into the recessed prefrontal facet on the lateral side of the frontal. Anterior to this contact, the concave ventromedial surface of the prefrontal cups the laterally convex anterolateral region of the frontal (Fig. 8D, H). The exposed dorsal surface of the prefrontal is smooth (akin to *Clevosaurus*; Fraser 1988) and lacks the trough that can be present in *Gephyrosaurus bridensis* (Evans 1980), *Diphydontosaurus avonis* (Whiteside 1986) and *Sphenodon punctatus* (Jones *et al*. 2011).

Lacrimal. As in all known sphenodontians, the lacrimal is absent in *Opisthiamimus gregori*.

Frontal. Both frontals exhibit moderate damage anteriorly and posteriorly (Fig. 7F–M). The left frontal is largely visible dorsally but partially covered by the left prefrontal and nasal anteriorly and by the postorbital posteriorly (Fig. 2A, D). The posterior end of the right frontal is exposed above and behind the right palatine in ventral view on the skull block (Fig. 2B, E), and as two adjacent pieces behind the right pterygoid in dorsal view on the skeletal block (Fig. 3).

The frontals (Fig. 4A, C) are narrow and elongate relative to the orbits and neighbouring elements. The dorsal surface is smooth and gently convex. In dorsal view, the anterolateral suture against the prefrontal and along the orbital margin is essentially straight; posteriorly, the frontals broaden slightly and become convex laterally between the postfrontals (Figs 4A, 7F, J). The suture between the nasals and frontals is oblique relative to the midline, and the midline junction between the paired nasals and frontals is anterior to the more lateral junction between the frontal, nasal and prefrontal (Fig. 4A). The presence of a nasofrontal fontanelle (e.g. Reynoso & Clark 1998, fig. 2) could not be determined with certainty but it likely was absent based on our reconstruction. This feature is present in immature and (variably) adult individuals of *Sphenodon punctatus* (Jones *et al*. 2011). The nasal partially overlaps the anterolateral process of the frontal (Fig. 7J, K). Posterolateral to the nasal facet, the frontal slopes ventrolaterally to underlap the prefrontal (Fig. 7J, K). Anterolaterally, the prefrontal facet of the frontal is convexly rounded laterally when viewed transversely. Posteriorly, the facet grades into a recessed groove on the side of the frontal (Fig. 7G, K), which accepts the frontal process of the prefrontal. The postfrontal clasps the laterally convex posterolateral margin of the frontal (Fig. 4A). The postfrontal facet anteriorly is recessed into the bone via a deeper horizontal groove that forms the slot portion of a horizontal slot joint with the anterior process of the postfrontal (Fig. 7G, H, K, L). Posteriorly, the facet grades into a scarf joint where the frontal partially underlaps the postfrontal (Fig. 7F, G).

The orbital margin of the frontal descends ventromedially between the pre- and postfrontals and is long relative to some rhynchocephalians such as *Sphenodon punctatus*. In dorsal view, the interfrontal suture generally follows the midline but is slightly bowed leftward anterior to mid-length (Fig. 4). For most of their length, the frontals contact each medially along a butt joint, but at about mid-length the left frontal produces a horizontal bony shelf ventrally that extends laterally beyond the sagittal plane (Fig. 7F, H, I) and onto a recessed facet of the right frontal ventromedially (Fig. 7L, M). Ventrolaterally, the crista cranii are low, blunt and broadly separated along their length (Fig. 7H, L). Anteroventrally, the frontals are dorsally concave between the prefrontal facets. The shape of the frontoparietal suture is unclear given the damage to that region; however, the frontal contacted at least the parietal medial to the postfrontal posterolaterally.

Postfrontal. Both postfrontals are partially exposed. The left postfrontal is visible anteroventral to the left postorbital in dorsal view (Fig. 2A, D), and the ventral

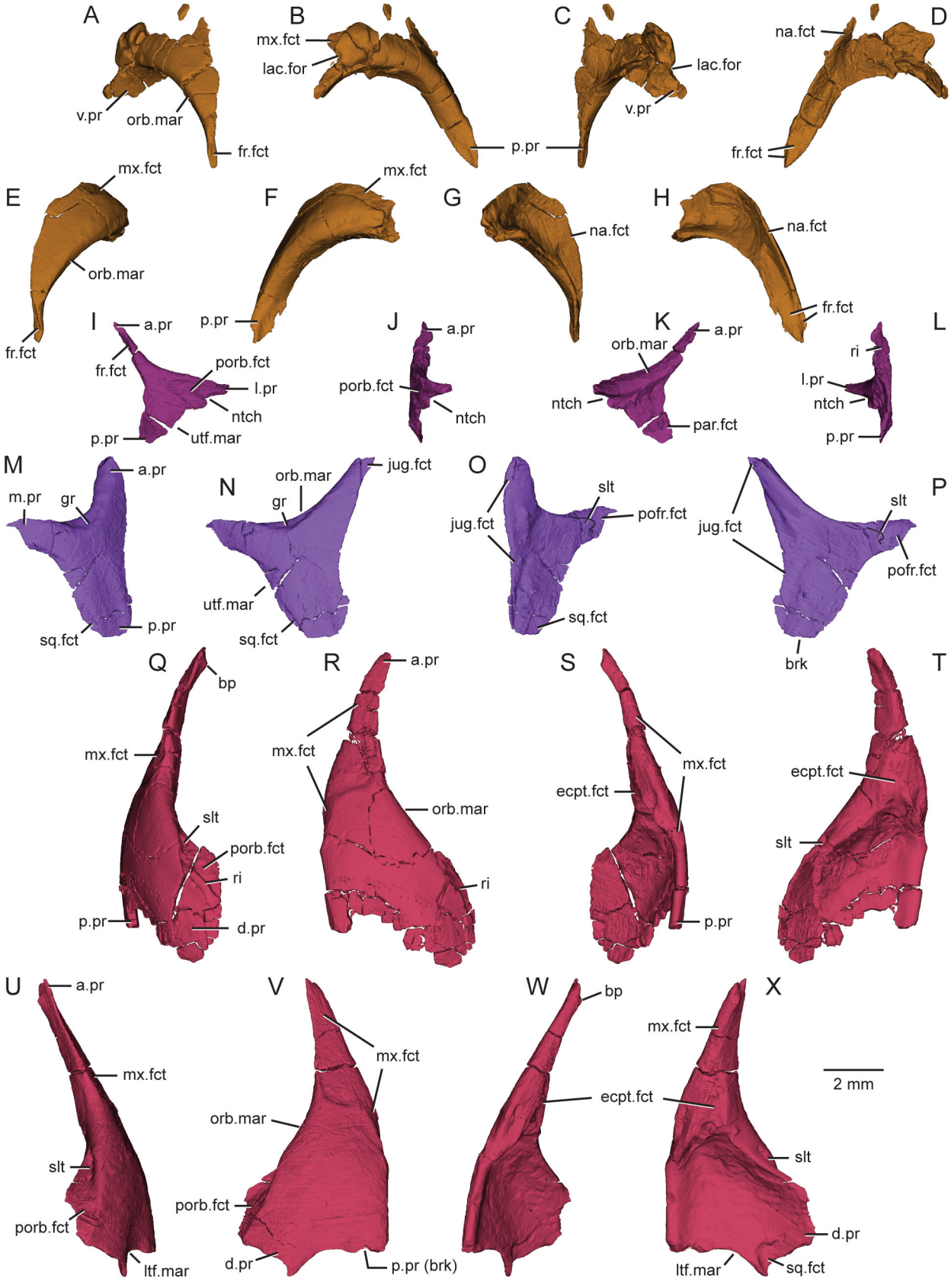
A
v.pr
orb.mar
fr.fct
B
mx.fct
lac.for
p.pr
C
lac.for
v.pr
D
na.fct
fr.fct
E
mx.fct
orb.mar
fr.fct
F
mx.fct
p.pr
G
na.fct
H
na.fct
fr.fct
I
a.pr
fr.fct
porb.fct
l.pr
ntch
p.pr
utf.mar
J
a.pr
porb.fct
ntch
K
a.pr
orb.mar
ntch
par.fct
L
ri
l.pr
ntch
p.pr
M
a.pr
m.pr
gr
sq.fct
p.pr
N
orb.mar
jug.fct
gr
utf.mar
sq.fct
O
slt
jug.fct
pofr.fct
sq.fct
P
slt
jug.fct
pofr.fct
brk
Q
bp
mx.fct
slt
porb.fct
ri
p.pr
d.pr
R
a.pr
mx.fct
orb.mar
ri
S
mx.fct
ecpt.fct
p.pr
T
ecpt.fct
slt
U
a.pr
mx.fct
slt
porb.fct
ltf.mar
V
mx.fct
orb.mar
porb.fct
d.pr
p.pr (brk)
W
bp
ecpt.fct
X
mx.fct
slt
d.pr
ltf.mar
sq.fct
2 mm

process of the right postfrontal is visible in ventral view just dorsal to the right epipterygoid (Fig. 2E).

The postfrontal (Fig. 8I–L) is a triradiate bone that clasps the frontal and parietal across the frontoparietal suture medially and is partially overlapped laterally by the postorbital (Fig. 4A). All outer margins are concave in dorsal view. The postfrontal forms the posterodorsal border of the orbit anteriorly and the anterior border of the supratemporal fenestra posteriorly. Its anterior and lateral processes, which comprise part of the orbital margin, are thick. By contrast, the posterior process, which is separated from the thickened orbital margin by a ventral ridge (Fig. 8K; akin to *Sphenodon punctatus*; Jones *et al*. 2011, fig. 53), is relatively thin. In dorsal view, the anterior process tapers to a narrow point anteriorly. The posterior process is shorter anteroposteriorly and horizontally oriented, with a broadly triangular posterior margin. The lateral process is intermediate in length and notched along its posterior border, a feature that also is present in *Clevosaurus minor* (Fraser 1988, fig. 39a). The anterior process of the postfrontal is a relatively long projection, with a medial horizontal ridge that inserts into the horizontal slot joint of the frontal (Fig. 8L). Posterior to this joint, the postfrontal overlaps the frontal posterolaterally and the parietal anterolaterally over a short distance. The postorbital facet is a triangular depression covering most of the dorsal surface of the lateral process (Fig. 8I, J). The posterior notch of the lateral process interlocked with an opposing slot on the medial end of the postorbital (Fig. 8O, P).

Postorbital. Both postorbitals are slightly fractured. The left postorbital is largely exposed in dorsal view (Fig. 2A, D); it is preserved out of articulation with and above the left postfrontal and jugal, and its ventral or jugal margin has been crumpled and bent dorsally. The posterior edge of the left postorbital is just visible to the left of the left squamosal in posterior view. Posteromedial to the jugal, the posterior edge of the process of the right postorbital is partially exposed in ventral view. Its tapering posterior end is broken transversely and bent dorsally (as revealed through 3D rendering).

The postorbital (Figs 4A, E, 8M–P) is a triradiate bone with relatively narrow anterior (= jugal) and medial (= postfrontal) processes and a wider posterior (= squamosal) process. The bone broadly enters both the posterior margin of the orbit anteriorly and the anterolateral border of the upper temporal fenestra posteromedially. It is excluded from the lower temporal fenestra by the jugal and squamosal (Fig. 4A, E), in contrast to *Sphenodon punctatus* (Jones *et al*. 2011) but similar to many other rhynchocephalians (e.g. Jones 2008, figs 3 *vs* 2, respectively). Its dorsal surface is smooth and gently convex. As with the postfrontal, the postorbital is relatively thicker anteriorly towards its orbital margin; the posterior process is thin. The orbital margin of the postfrontal is recessed and slightly grooved anterolaterally (Fig. 8M, N), presumably for attachment with the orbital fascia (Whiteside 1986). The medial margin of the postorbital gently slopes ventrally towards the upper temporal fenestra; the posterior margin of the medial process also is slightly grooved. Posteromedially, the posterior process narrowly underlaps the anterior process of the squamosal along a recessed scarf joint (Fig. 8M, N), much like in *Sphenodon* (e.g. Jones *et al*. 2011, fig. 62). The postorbital contact with the jugal is sinuous (Fig. 4A, C, E). Posteroventrally, the postorbital broadly overlaps the jugal dorsolaterally; anteroventrally, the anterior process twists slightly medially (Fig. 8P) and inserts into a 'V'-shaped slot on the dorsomedial side of the jugal (Fig. 8Q, T, U, X). The medial process features an interlocking slot and groove joint ventrally for articulation with the opposing joint of the postfrontal (Fig. 8O, P).

Jugal. The major part of each jugal is present in the skull block whereas the posterior processes are preserved in the skeletal block. In the skull block (Fig. 2), the left and right jugals are rotated somewhat medially but remain in partial contact with the maxillae laterally. Both are damaged posteriorly. The left jugal is partially exposed dorsally and ventrally; the right is mostly

Figure 8. Virtual three-dimensional renderings of the circumorbital bones of the skull of the holotype specimen (USNM PAL 722041) of *Opisthiamimus gregori* gen. et sp. nov. **A–D,** left prefrontal in **A,** dorsal, **B,** left lateral, **C,** ventral and **D,** medial views; **E–H,** right prefrontal in **E,** dorsal, **F,** right lateral, **G,** ventral and **H,** medial views; **I–L,** right postfrontal in **I,** dorsal, **J,** right lateral, **K,** ventral and **L,** medial views; **M–P,** right postorbital in **M,** dorsal, **N,** right lateral, **O,** ventral and **P,** medial views; **Q–T,** left jugal in **Q**, dorsal, **R,** left lateral, **S,** ventral and **T**, medial views; **U–X,** right jugal in **U,** dorsal, **V,** right lateral, **W,** ventral and **X,** medial views. Anterior is towards the top of the figure. **Abbreviations: a.pr**, anterior process; **bp**, bony protuberance; **brk**, break; **d.pr**, dorsal process; **ecpt.fct**, facet for the ectopterygoid; **fr.fct**, facet for the frontal; **gr**, groove; **jug.fct**, facet for the jugal; **l.pr**, lateral process; **lac.for**, lacrimal foramen; **ltf.mar**, margin of the lower temporal fenestra; **m.pr**, medial process; **mx.fct**, facet for the maxilla; **na.fct**, facet for the nasal; **ntch**, notch; **orb.mar**, margin of the orbit; **p.pr**, posterior process; **par.fct**, facet for the parietal; **pofr.fct**, facet for the postfrontal; **porb.fct**, facet for the postorbital; **ri**, ridge; **slt**, slot; **sq.fct**, facet for the squamosal; **utf.mar**, margin of the upper temporal fenestra; **v.pr**, ventral process.

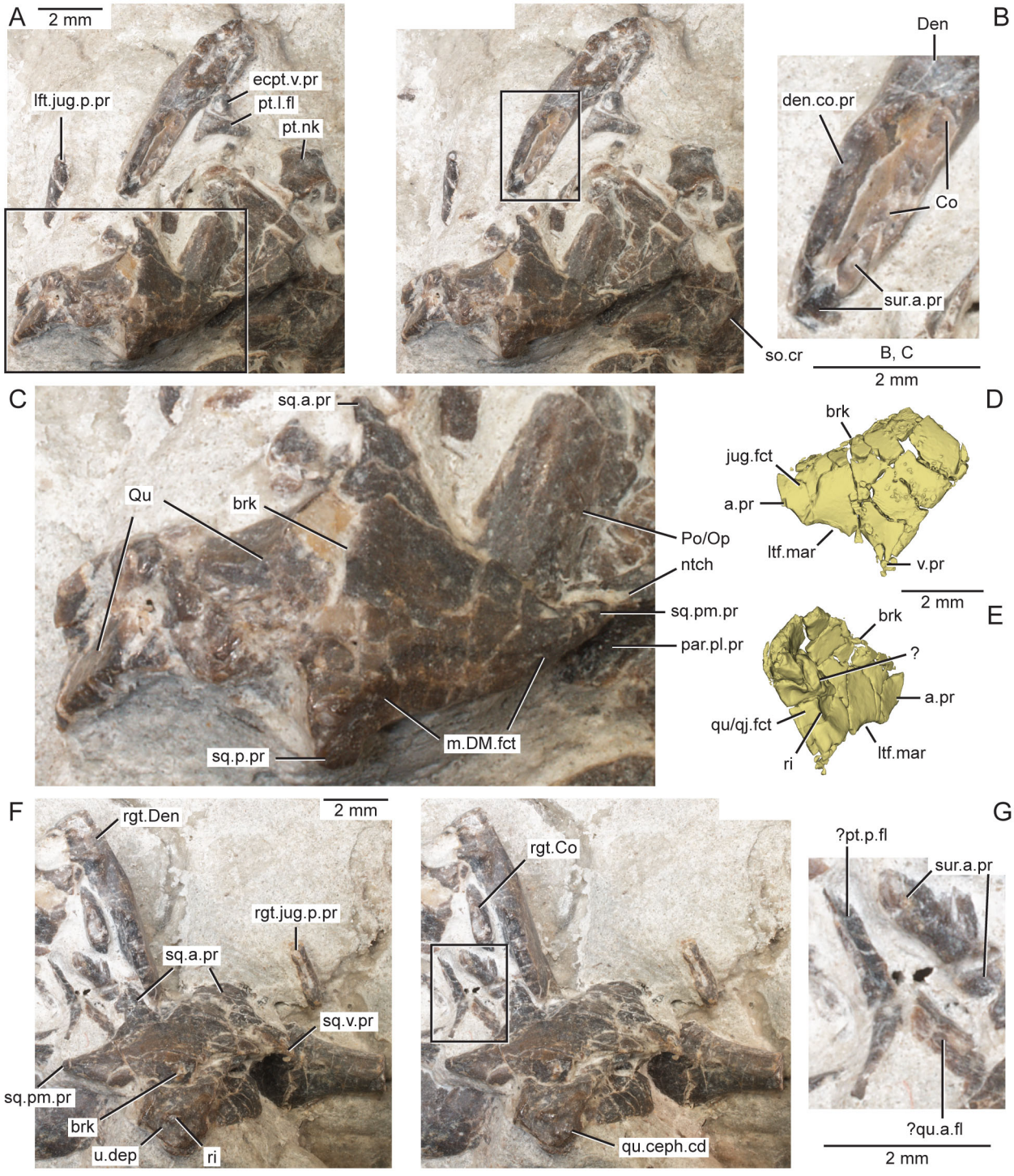
A
2 mm
lft.jug.p.pr
ecpt.v.pr
pt.l.fl
pt.nk
so.cr
B
Den
den.co.pr
Co
sur.a.pr
B, C
2 mm
C
sq.a.pr
Qu
brk
Po/Op
ntch
sq.pm.pr
par.pl.pr
m.DM.fct
sq.p.pr
D
brk
jug.fct
a.pr
ltf.mar
v.pr
2 mm
E
brk
?
a.pr
qu/qj.fct
ri
ltf.mar
F
2 mm
rgt.Den
rgt.jug.p.pr
sq.a.pr
sq.v.pr
sq.pm.pr
brk
u.dep
ri
rgt.Co
qu.ceph.cd
G
?pt.p.fl
sur.a.pr
?qu.a.fl
2 mm

exposed ventrally. In the skeletal block (Fig. 3A, B), the left posterior process is lateral to the coronoid region of the left dentary, whereas the right process is lateral to the right squamosal and its dorsal surface is broken.

The jugal is triradiate, with a long anterior (= maxillary) process, a shorter and broader dorsal (= postorbital) process, and a slender, moderately elongate posterior process (Fig. 8Q–X). Anterodorsally, the jugal forms the posteroventral margin of the orbit between the postorbital and maxilla (Fig. 4). The lower temporal fenestra is bordered anterodorsally, anteriorly and anteroventrally by the jugal. The postorbital and squamosal contact each other above the jugal and exclude it from the upper temporal fenestra. The jugal is largely hidden in lateral view by the maxilla at the level of the maxillary suborbital ramus (Fig. 4E). Behind this level of the maxilla, the lateral surface of the jugal is smooth and slightly convex, whereas the medial surface is deeply concave. Posterolaterally, its lateral surface is shallowly concave between the dorsal and posterior processes which border the lower temporal fenestra (Fig. 8U). Laterally, the anterior process of the jugal is recessed for contact with the wall of the suborbital ramus of the maxilla medially; ventromedial to the suborbital wall, the jugal slots into the grooved jugal facet atop the maxilla. At about mid-length, the jugal has a triangular facet ventromedially for contact with the ectopterygoid (akin to *Sphenodon*; Jones *et al*. 2011). The anterodorsal surface of the dorsal process of the jugal underlaps the postorbital. Here, the postorbital facet is double stepped, with the slightly grooved surface of each step separated mediolaterally by a sharp low ridge (Fig. 8Q, R). Anteroventral to this region, the jugal has a deep, 'V'-shaped slot that accepts the anterior process of the postorbital. Anteromedially and ventrally, the jugal expands slightly anteromedially to form a small bony projection (Fig. 8W). Based on our skull reconstruction, the triangular surface between this projection and the anterior edge of the jugal medially would have contacted the ventral process of the prefrontal (akin to *Clevosaurus bairdi*; Sues *et al*. 1994a, fig. 1A). The anterior end of the jugal is slightly bifurcated (akin to *Sphenodon punctatus*; Jones *et al*. 2011, fig. 31.2). In both jugals of the holotype, the posterior end of the dorsal process is broken, and therefore its posterior marginal shape and suture with the squamosal cannot be accurately determined. However, a recessed facet on the medial side of the dorsal process (Fig. 8X) indicates that the jugal at least partially overlapped the anterior process of the squamosal (above the lower temporal fenestra). In USNM PAL 720475, the left jugal preserves a nearly complete but slightly chipped dorsal process, which is broadly rounded posteriorly (Fig. 6A, E). The posterior process of the jugal is narrow mediolaterally, with subparallel dorsal and ventral margins and a broadly rounded or slightly tapered posterior margin in lateral view (Figs 3A, B, 4, 6). On the left jugal, a tiny ovoid foramen pierces the bone near the end of the posterior process laterally; this foramen could not be identified on the right due to damage, nor in USNM PAL 720475, which is missing the tip of its left jugal. On the basis of our 3D skull reconstruction (Fig. 4), the posterior process did not contact either the squamosal or quadrate/quadratojugal.

Squamosal. The left squamosal is partially preserved on two blocks: the anteroventral portion is visible in ventral view behind the left jugal on the skull block (Fig. 2B, E), and the posteromedial portion is preserved atop the left quadrate on the skeletal block (Figs 3, 9A, C). The right squamosal is preserved on the skeletal block, where it has slid forward and downward off the cephalic condyle of the right quadrate (Figs 3, 9D). Both elements are moderately fractured, with some margins missing or distorted due to crushing.

Figure 9. Details of the squamosals, articulation of the surangular and coronoid, and quadrates in the holotype specimen (USNM PAL 722041, 'skeletal block') of *Opisthiamimus gregori* gen. et sp. nov. **A,** extended depth of field (EDF) stereophotopair of the left posterolateral region of the skull in dorsal view; **B,** close-up of the surangular and coronoid bones as shown in the box in the right stereophoto in A; **C,** close-up of the medial half of the left squamosal as shown in the box in the left stereophoto in A; **D, E,** virtual three-dimensional rendering of the anteroventral portion of the left squamosal in **D,** left lateral and **E,** posteromedial views; **F,** EDF stereophotopair of the right posterolateral region of the skull in dorsal view; **G,** close-up of the possible flanges of the right quadrate and pterygoid as shown in the box in the right stereophoto in F. **Abbreviations: a.pr**, anterior process; **brk**, break; **Co**, coronoid; **den.co.pr**, coronoid process of the dentary; **ecpt.v.pr**, ventral process of the ectopterygoid; **jug.fct**, facet for the jugal; **lft.jug.p.pr**, posterior process of the left jugal; **ltf.mar**, margin of the lower temporal fenestra; **m.DM.fct**, facet for the mm. depressor mandibulae; **ntch**, notch; **par.pl.pr**, posterolateral process of the parietal; **Po/Op**, prootic/opisthotic; **pt.l.fl**, lateral flange of the pterygoid; **pt.nk**, 'neck' region of the pterygoid; **?pt.p.fl**, possible posterior or quadrate flange of the pterygoid; **Qu**, quadrate; **?qu.a.fl**, possible anterior or pterygoid flange of the quadrate; **qu.ceph.cd**, cephalic condyle of the quadrate; **qu/qj.fct**, facet for the quadrate/quadratojugal; **rgt.Co**, right coronoid; **rgt.Den**, right dentary; **rgt.jug.p.pr**, posterior process of the right jugal; **ri**, ridge; **so.cr**, supraoccipital crest; **sq.a.pr**, anterior process of the squamosal; **sq.p.pr**, posterior process of the squamosal; **sq.pm.pr**, posteromedial process of the squamosal; **sq.v.pr**, ventral process of the squamosal; **sur.a.pr**, anterior process of the surangular; **u.dep**, 'U'-shaped depression; **v.pr**, ventral process; **?**, unidentified bone fragment.

The squamosal is tetraradiate and borders the upper temporal fenestra posterolaterally and the lower temporal fenestra posterodorsally and posteriorly (Fig. 4). The surface of the bone appears smooth, with no indication of ornamentation. The anterior process is moderately broad dorsoventrally and anteriorly underlaps the posterior process of the postorbital as well as the dorsal process of the jugal. As observed on the left squamosal in the skull block (Fig. 2B, E), the jugal facet is shallowly recessed into its anterolateral surface, with a rounded posterior margin (Fig. 9D). Anterodorsally, the squamosal underlaps the ventral and posterior margins of the posterior process of the postorbital (Fig. 4). In dorsal view, the posteromedial (= parietal) process of the squamosal is triangular, curving slightly and tapering anteromedially to articulate with the posterolateral process of the parietal dorsolaterally (Figs 4, 9A, C). A short, triangular process with a bluntly rounded posterior end extends posteriorly off the posterolateral corner of the squamosal, which overlaps the cephalic condyle of the quadrate (Fig. 9C). The posterior face of the squamosal between the posterior and parietal processes slopes ventromedially away from a faint, sinuous ridge on the posterodorsal surface of the squamosal (Fig. 9C). This face is squamous and either represents an upper temporal facet or, more likely, the origin of the m. depressor mandibulae musculature as in *Sphenodon punctatus* (e.g. Jones *et al*. 2009a). Also like in *Sphenodon*, the medial side of the posterior process bears a slight indentation that presumably articulated with the paraoccipital process of the opisthotic posterolaterally (Jones *et al*. 2011). In lateral view, the triangular ventral process tapers to a narrow point ventrally, which overlaps the quadrate/quadratojugal anterolaterally (Figs 4E, 9D). The full length of the ventral process is preserved (albeit in fragments) on the left squamosal despite damage to its anterior margin. Posteromedially between the posterior and ventral processes of the squamosal, the quadrate/quadratojugal facet is represented by a shallow, dorsoventrally extended groove that is bounded anteromedially by a short parallel ridge (Fig. 9E).

Supratemporal. No supratemporal was identified and, thus, it is inferred to be absent as in most rhynchocephalians.

Parietal. Both parietals are preserved but damaged anteriorly. Except for the posterolateral process, the left parietal is largely preserved in the skull block and exposed in dorsal view behind and below the left frontal and postorbital (Fig. 2A, D); in ventral view, it is exposed above and behind the left pterygoid (Fig. 2B, E). Its posterolateral process is preserved on the skeletal block medial to the left squamosal (Figs 3, 9C). The right parietal is mostly preserved in dorsal view on the skeletal block; anteriorly, it is broken into a few pieces, with smooth impressions of some missing parts on the matrix (Fig. 3).

The paired parietals form a broad, relatively flat and unornamented parietal table (or intertemporal roof; Fig. 4). The medial half of the table is slightly lower than the lateral half. The posterolateral process of the parietal extends posterolaterally and slightly ventrally away from the parietal table. Laterally it is bifurcated, with a 'V'-shaped notch that widens laterally to accommodate the posteromedial process of the squamosal (Fig. 9C). The lateral margin of the parietal bows medially in dorsal view and slopes downward and away from a faint, 'L'-shaped parasagittal ridge that forms the dorsomedial rim of the upper temporal fenestra (Fig. 3, 4A). Anteriorly, the parietals are damaged, and therefore the shapes of the frontoparietal suture and the postfrontal facet could not be determined. Only the posterolateral margin of the parietal foramen appears to be preserved on the left parietal (Fig. 7N). Ventrally and behind the level of the presumed parietal foramen, the posteromedial and posterior margins of the parietal table are thickened, and partially border a 'U'-shaped depression on the ventral surface of the bone (Fig. 7P). The interparietal suture at this level is straight and abutting (Fig. 7Q), but it is obliterated anterior to the parietal foramen. The posterior face of the parietal, including the posterolateral process, is largely squamous and nearly vertically oriented. More laterally, the posterior surface of the posterolateral process twists such that the surface becomes increasingly posterodorsally directed (Figs 3A, 4A, 9A, C).

Quadrate and ?quadratojugal. The paired quadrates and (probably) quadratojugals are preserved on the skeletal block and adjacent to but not articulated with the squamosals (Figs 3, 9A, C, F). Based on our 3D reconstruction of the skull, the right quadrate was rotated clockwise along its dorsoventral axis, exposing part of its anterior surface in lateral view. Due to this rotation and the dorsoventral crushing and fracturing of the quadrate, we cannot be certain whether the quadratojugal is preserved (but hidden from view) and whether it was a separate bone or fused with the quadrate. These same circumstances exist with the left quadrate, which has sustained more damage. The μCT scan of the skeletal block provided little aid in identifying them due to the poor bone/bone and bone/matrix contrast. However, given that all other skull bones are accounted for in USNM PAL 722041, we hypothesize that both quadratojugals are present but currently unidentified. Much of the quadrates is hidden by matrix or other bones, and

parts of their major features were only grossly revealed through partial segmentation and 3D reconstruction (Fig. 4). The cephalic condyle of each quadrate is exposed dorsally (Fig. 9A, C, F), and the quadrates are exposed in anterolateral view down to their ventrolateral margins.

The dorsal surface of the cephalic condyle is best observed on the right quadrate, where it features a centrally placed, 'U'-shaped depression that partially encircles a low ridge for articulation with the squamosal ventrally (Fig. 9F). This depression likely is equivalent to the deep depression on the cephalic head of the quadrate as described and figured for '*Clevosaurus wangi*' by Wu (1994, fig. 3.7b; = *C. petilus* of Sues *et al*. [1994a] and *C*. sp. of Jones [2006b]). Anterolaterally, the external surfaces of the right and left quadrates have been pressed inward. Consequently, the outer wall of each lateral conch formed by the quadrate is partially caved in and distorted. We could not determine the presence of either a jugal facet or a quadratojugal foramen. A thin tympanic crest extends downward from the lateral edge of the cephalic condyle to the lateral mandibular condyle; it is laterally convex in posterior view and posteriorly concave in lateral view (Fig. 4D, E). Partial segmentation and 3D reconstruction of the right quadrate revealed a thickened vertical column or medial crest extending ventrally below the cephalic condyle (Fig. 4D). This crest borders the lateral conch medially, whereas the tympanic crest borders it laterally. Partial reconstruction of the left quadrate revealed that the lateral mandibular condyle is smaller than the medial, and that the distance between them is wider than either condyle is long anteroposteriorly. A thin sheet of bone exposed anterior to the right squamosal possibly represents the flange-like pterygoid process of the right quadrate (or perhaps the quadrate process of the right pterygoid), as commonly observed in other rhynchocephalians (Figs 3C, 9F, G). A similar piece of bone anterior to the left squamosal and prootic might also represent one of these two processes from the left side (Fig. 3C).

In USNM PAL 720475, the anterolateral surface of the left quadrate is partially exposed medial to and between the postorbital and posterior processes of the left jugal (Fig. 6A, E). Based on our 3D reconstruction, the bone has swiveled laterally relative to its dorsoventral axis (counterclockwise in dorsal view) such that its larger medial condyle is positioned anterior to its lateral condyle. The quadrate also has been tilted such that the mandibular condyles are anterior to the cephalic condyle, no longer in natural articulation with the lower jaw. Part of the medial mandibular condyle is exposed in medial view (Fig. 6C, F). The presence of a quadratojugal foramen could not be determined. However, given that no large opening was observed in the quadrate, our 3D reconstruction indicates that if the foramen is present, it likely is smaller than in *Sphenodon punctatus* (e.g. Jones *et al*. 2011, fig. 72) and perhaps closer in size to that of *Clevosaurus hudsoni* (e.g. Fraser 1988, fig. 17).

Vomer. The posterior portion of each vomer is exposed ventrally (Fig. 2B, E). The right vomer is partially hidden by matrix and the bent lateral process of the right nasal; the left is largely under matrix. The right vomer has been displaced backward to underlap the right palatine anteriorly along an artefactually long contact; a large, rounded central portion is missing. The anterior end of each bone is broken off and displaced ventrally and posteriorly.

The vomer is triangular in dorsal view, with a posteriorly concave posterolateral border that underlapped and accepted the rounded anteromedial margin of the palatine (Fig. 10A). The lateral edge of the vomer, which borders the choana medially, is curled dorsomedially (Fig. 10A) but does not form a tube as in *Gephyrosaurus bridensis* or *Diphydontosaurus avonis* (Evans 1980; Whiteside 1986). Medially, the vomers are thickened along a straight midline intervomerine joint (cf. Jones *et al*. 2011; Fig. 10D). A small worn tooth with a rounded base is visible at about mid-length anteroposteriorly on the ventromedial surface of each vomer (Figs 2E, 10C). The broken-off anterior end of each vomer (e.g. Fig. 10A–D) possibly buttressed the corresponding premaxilla posteriorly; posteromedially, the pterygoids overlapped the vomers between the palatines (Figs 4B, 10A, D). Posterodorsally, the medial surface of the vomer features a narrow, anteroposteriorly directed ridge that separates the palatine and pterygoid facets (Fig. 10A, D), much like in *Sphenodon punctatus* (e.g. Jones *et al*. 2011, fig. 25).

Palatine. Both palatines are largely exposed in ventral view (Fig. 2B, E); the prefrontal facet of the left palatine also is exposed dorsally behind the palatine process of the left prefrontal (Fig. 2A, D). The right palatine is well preserved whereas the left is damaged anteromedially. This region of the left palatine (which bears an isolated tooth) was revealed via 3D reconstruction and has been displaced anteriorly and rotated upside-down at an oblique angle to the horizontal (Fig. 10J–N). Most of the description relies on the right bone (Fig. 10O–S).

The palatine has five areas of contact, one each for the vomer anteroventrally, the prefrontal anterodorsally, the maxilla anterolaterally, the pterygoid medially and the ectopterygoid posterolaterally (Fig. 4A, B). It forms the posterior border of the choana as well as the anterior

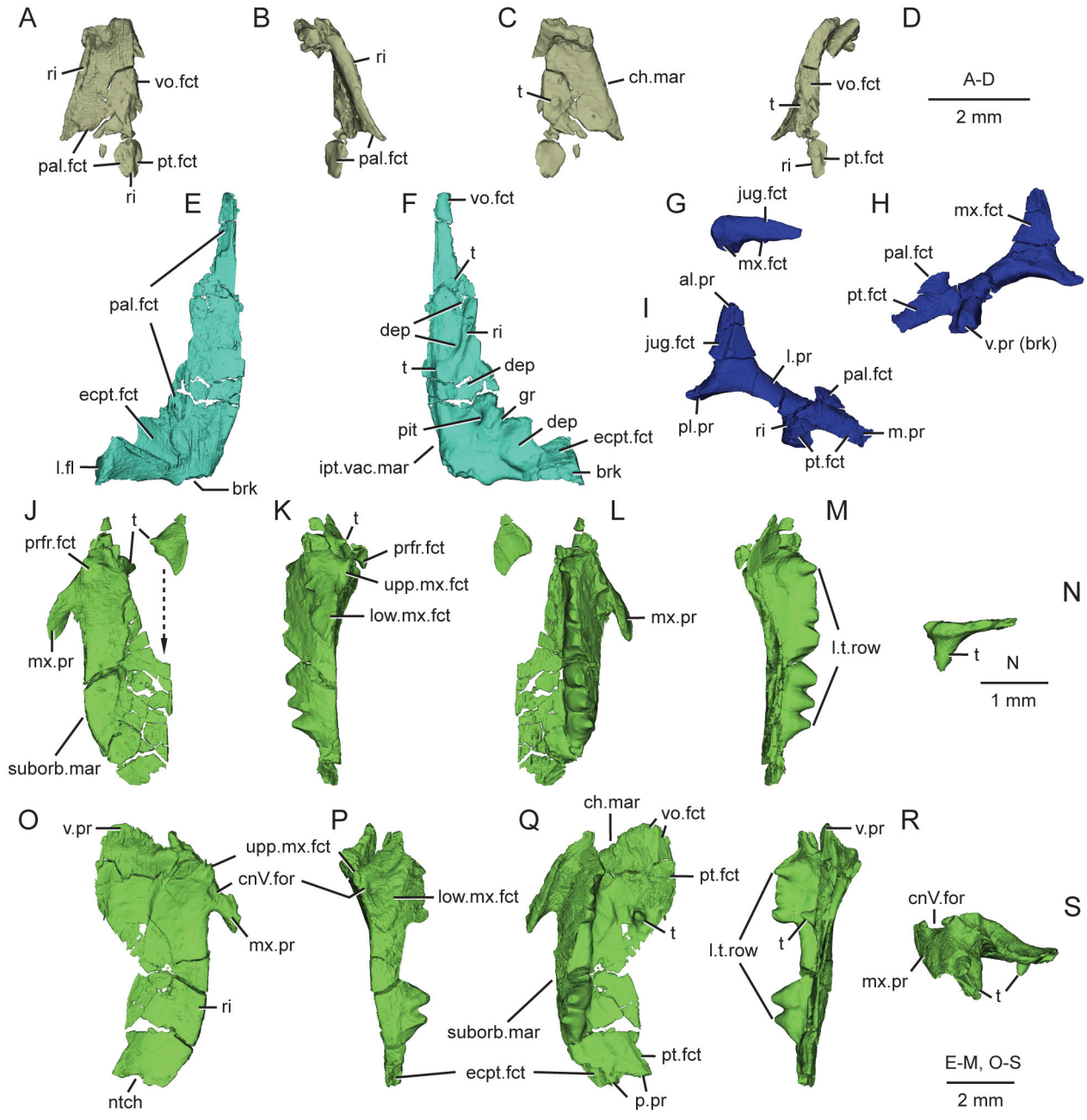

Figure 10. Virtual three-dimensional renderings of the bones of the palate of the holotype specimen (USNM PAL 722041) of *Opisthiamimus gregori* gen. et sp. nov. **A–D,** left vomer in **A,** dorsal, **B,** lateral, **C,** ventral and **D,** medial views. **E, F,** left pterygoid in **E,** dorsal and **F,** ventral views; **G,** right ectopterygoid in lateral view; **H, I,** left ectopterygoid in **H,** ventral and **I,** dorsal views; **J–M,** left palatine in **J,** dorsal, **K,** left lateral, **L,** ventral and **M,** medial views; **N,** displaced portion of the left palatine in anterior view; **O–S,** right palatine in **O,** dorsal, **P,** right lateral, **Q,** ventral, **R,** medial and **S,** anterior views. Arrow at J indicates where the displaced portion of the left palatine originated. **Abbreviations: al.pr**, anterolateral process; **brk**, break; **ch.mar**, margin of the choana; **cnV.for**, foramen for cranial nerve five; **dep**, depression; **ecpt.fct**, facet for the ectopterygoid; **gr**, groove; **ipt.vac.mar**, margin of the interpterygoid vacuity; **jug.fct**, facet for the jugal; **l.fl**, lateral flange; **l.pr**, lateral process; **l.t.row**, lateral tooth row of the palatine; **low.mx.fct**, lower maxillary facet; **m.pr**, medial process; **mx.fct**, facet for the maxilla; **mx.pr**, maxillary process; **ntch**, notch; **p.pr**, posterior process; **pal.fct**, facet for the palatine; **pit**, pit; **pl.pr**, posterolateral process; **prfr.fct**, facet for the prefrontal; **pt.fct**, facet for the pterygoid; **ri**, ridge; **suborb.mar**, margin of the suborbital fenestra; **t**, tooth; **upp.mx.fct**, upper maxillary facet; **v.pr**, ventral process; **vo.fct**, facet for the vomer.

and medial borders of the suborbital fenestra behind the maxillary process. In ventral view, the anterior half of the palatine is about twice as wide mediolaterally as the posterior half. The lateral maxillary process is divided into upper and lower facets (akin to *Sphenodon* but with a less well-developed upper facet; Jones *et al*. 2011, fig. 28). The lower facet is much larger than the upper, has an ovoid outline, and inserts into a large, recessed lower facet on the medial surface on the maxilla (Figs 5F, 10P). Between these two palatine facets is a moderate-sized foramen (Fig. 10O, P, S) for passage of the maxillary division of the trigeminal nerve (cranial nerve V.2: Jones *et al*. 2011; infraorbital foramen or canal of some authors: e.g. Whiteside 1986; Fraser 1988), which communicates with the neighbouring foramen for cranial nerve V.2 in the maxilla (see above; Fig. 5F, G). Dorsomedial to the upper maxillary facet, the dorsal surface of the palatine is indented for articulation with the palatine process of the prefrontal (Fig. 10J). From here, the dorsal surface of the palatine slopes downward posteriorly until about mid-length of the bone where it levels out and becomes shallowly concave. Medial to the prefrontal facet, the palatine steps downward (possibly due to postmortem compression) and then gently slopes ventromedially to overlap the pterygoid anterolaterally along a moderately broad and oblique scarf joint; the posterior half of the palatine-pterygoid joint presumably was much less expansive (Fig. 10Q).

The tongue-like ventral process of the palatine, which is anteromedial and ventral to the prefrontal facet, slopes anteroventrally to overlap the vomer posteriorly (Figs 4B, 10A, Q). Above the lateral tooth row, the palatine is thick dorsoventrally with a moderately broad, low dorsal ridge (Fig. 10O, P). Medial to the lateral tooth row, the bone is relatively thin (Fig. 10M, R). On the ventral surface of the broad anterior region of the palatine is a single isolated conical tooth, which occurs near the medial edge of the bone; it is located on the same coronal plane as the fourth lateral palatine tooth (counting from the anterior end; Fig. 10Q–S). The broken-off and rotated portion of the left palatine also bears an isolated tooth on its broad anterior region (Fig. 10J, N). A tooth of similar size, shape and position also is present on the left palatine of the referred specimen (USNM PAL 720475), as revealed through μCT. The better-preserved posterior end of the right palatine is notched, with two posterior processes much like in *Sphenodon punctatus* (e.g. Jones *et al*. 2011, figs 35, 37; Fig. 10O, Q); the posterior tips of these apparent processes are broken off and the notch between them may have carried nerves and blood vessels to the oral mucosa, as presumed for *S. punctatus* (Evans 2008). Each palatine bears a single row of eight lateral teeth (described below) that are nearly parallel to those in the maxilla (Figs 4B, D, 10L, Q). In dorsal or ventral view, the palatine curves posteromedially behind the tooth row to form a convex posterolateral margin, the ventrolateral face, which is indented for contact with the ectopterygoid anteromedially (Fig. 10P, Q).

Pterygoid. The anterior half or more of each pterygoid is preserved on the skull block and exposed in ventral view (Fig. 2B, E). The left pterygoid has been offset farther anteriorly relative to the right. Peripheral damage to the palatal shelf region of both pterygoids has made assessing their sutural contacts with the palatine and vomer somewhat difficult. The left pterygoid is the better preserved of the two (Fig. 10E, F) but is broken transversely just posterior to its lateral pterygoid flange (= 'transverse process' of Fraser 1988). A short, saddle-shaped tubular piece of bone is exposed dorsally on the skeletal block (Fig. 3, 9A); this element represents the 'neck' region of the left pterygoid, located between the palatal plate of the pterygoid and the quadrate flange. It terminates posteriorly at the level of its presumed contact with the basipterygoid process of the basisphenoid. The lateral end of the left pterygoid flange is broken off and preserved on the skeletal block in articulation with the ventral process of the left ectopterygoid; these bones are exposed just medial to the coronoid region of the left mandible (Figs 3, 9A). The right pterygoid is broken transversely through its pterygoid flange, and its posterior half is slightly exposed anterodorsally on the skeletal block medial to the adjoining right ectopterygoid (Fig. 3C). A thin curved bone, possibly the posterior or quadrate flange of the right pterygoid, is exposed on the skeletal block adjacent to the possible anterior or pterygoid flange of the right quadrate (Figs 3C, 9G). One of these two flanges also appears to be present on the left side, as described above for the quadrate (Fig. 3C).

The paired pterygoids taper anteriorly between the palatines and then overlap the vomers posteromedially, as noted above (Figs 4B, 10F). The pterygoids contact each other medially along most of their lengths anterior to the pterygoid flange. Behind this region, the pterygoids diverge posterolaterally to form a moderately wide and elongate interpterygoid vacuity (= pyriform recess) (Fig. 4B, 10F). The posterior half of the palatal shelf features a distinct, narrow bony ridge that extends obliquely across the ventral surface of the pterygoid (Fig. 10F). A similar but faint, edentulous, longitudinally oriented ridge is present in *Sphenodon punctatus* (e.g. Jones *et al*. 2011, figs 24, 84). Medially adjacent to this ridge are a pair of small ovoid depressions. The oblique ridge is confluent posteromedially with a low rounded ridge on the ventromedial margin of the pterygoid just anterior to the level of the interpterygoid

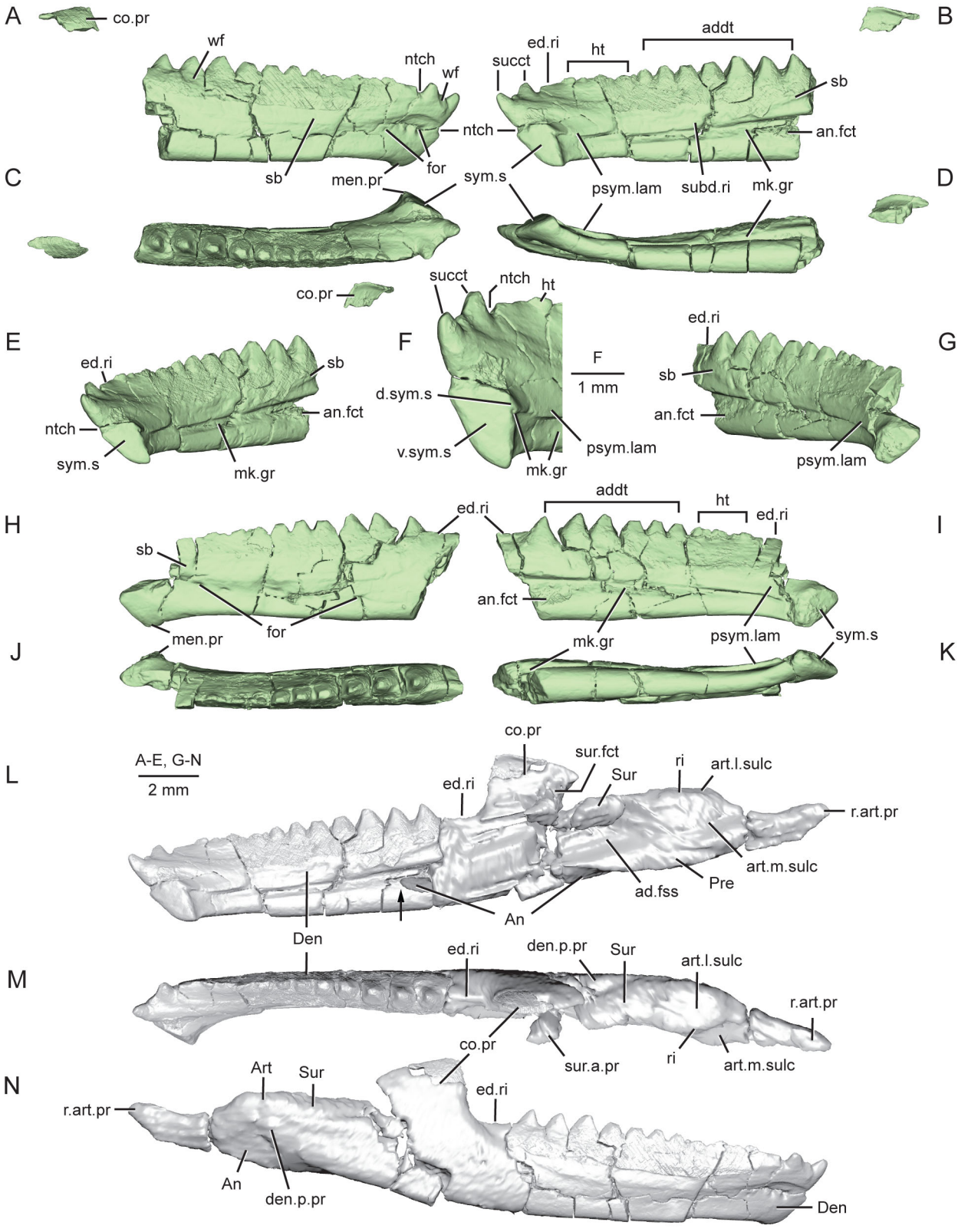
A
co.pr
wf
ntch
wf
ntch
sb
for
men.pr
B
addt
ed.ri
ht
succt
sb
an.fct
sym.s
psym.lam
subd.ri
mk.gr
C
D
co.pr
succt
ntch
ht
E
ed.ri
sb
an.fct
ntch
sym.s
mk.gr
F
d.sym.s
v.sym.s
psym.lam
mk.gr
F
1 mm
G
ed.ri
sb
an.fct
psym.lam
H
ed.ri
sb
for
men.pr
I
addt
ht
ed.ri
an.fct
mk.gr
psym.lam
sym.s
J
K
L
A-E, G-N
2 mm
co.pr
sur.fct
ri
art.l.sulc
ed.ri
Sur
r.art.pr
art.m.sulc
ad.fss
Pre
An
Den
M
ed.ri
den.p.pr
Sur
art.l.sulc
r.art.pr
co.pr
sur.a.pr
ri
art.m.sulc
N
Art
Sur
r.art.pr
ed.ri
An
den.p.pr
Den

vacuity. These merged ridges form the medial border of an oblong ventral depression anterior to the pterygoid-ectopterygoid articulation. The anteroventral face of the pterygoid flange is faceted for contact with the ventral process of the ectopterygoid (Fig. 10F), and a large, 'V'-shaped recess on the dorsal surface of the pterygoid anterior to this flange articulates with the medial process of the ectopterygoid ventrally (Fig. 10E). The pterygoid is excluded from the suborbital fenestra by the contacting ectopterygoid and palatine (Fig. 4B). Medial to the ectopterygoid articulation on the ventral surface of the pterygoid flange is a large, rounded depression with a laterally concave medial rim. Anteromedial to this depression is a short oblique groove (Fig. 10F) that appears to communicate with the posterior notch of the palatine (Figs 4B, 10O, Q). Between this groove medially and the oblong depression posterolaterally is a deep circular pit of unknown significance and function.

At about mid-length along the palatal shelf of the right pterygoid is a small, rounded mound. It bears a central excavation reminiscent of an exposed pulp cavity, and its interior (as revealed through μCT slices) is surrounded by a layer of denser tissue like that observed in the isolated palatine and vomer teeth. Furthermore, the basal diameter of the mound is comparable in size to these teeth. As such, we interpret this structure – along with a similar-looking and similarly positioned mound on the left pterygoid – to represent the bases of a pair of heavily worn pterygoid teeth (Fig. 10F). Two other pterygoid teeth also have been identified on the basis of μCT slices, positioned on the medial edge of the pterygoid near the posteromedial end of the oblique ridge (Fig. 10F). Each has an ovoid base, and the preserved crown of the left tooth is a shallow, ventromedially arcing crest, rather than conical (as in the isolated palatine teeth). We could not confidently identify any additional pterygoid teeth, but more may be present, particularly along the oblique and medial ridges described above.

Ectopterygoid. The ectopterygoids are largely complete but fractured. In ventral view, the left bone, mostly preserved on the skull block (Fig. 2B, E), is partially hidden medially by the left pterygoid and laterally by the dentary and maxilla. The end of the ventral process of the left ectopterygoid is broken off and preserved in contact with the opposing end of the pterygoid flange of the left pterygoid on the skeletal block (Figs 3, 9A). The right ectopterygoid is broken along the neck-like extension of its lateral process; the expanded lateral portion of the bone is preserved slightly disarticulated from the right maxilla and jugal in the skull block (Fig. 2B, E). The medial portion of this bone, including part of the neck and medial process of the right ectopterygoid, is partially exposed in dorsal and anterior views on the skeletal block, medial to the right dentary just behind its anterior broken surface.

The ectopterygoid articulates with the maxilla and jugal laterally and the palatine and pterygoid medially (Fig. 4A, B). In dorsal or ventral view, its expanded lateral process features a triangular anterolateral process, which is slightly more elongate and broader than the posterolateral process (Fig. 10H, I). These proportions are similar to those observed in *Sphenodon* (e.g. Jones *et al*. 2011, fig. 39) but unlike those of several species of *Clevosaurus*, in which the anterolateral process is much more elongate and contacts the posterior end of the lower maxillary process of the palatine (Fraser 1988; Jones 2006a, b). The lateral face of the ectopterygoid (Fig. 10G) contacts the jugal ventromedially; ventrally, the expanded lateral process broadly overlaps the triangular ectopterygoid facet of the maxilla posteromedially. The neck of the lateral process is rod-like; dorsoventrally, the anterior surface is anteriorly convex and the posterior surface posteriorly concave. Medially, the ectopterygoid is bifurcated into a medial and ventral process to clasp the pterygoid laterally (Figs 4A, B). Between these two processes, respectively, the posterior and dorsal surfaces of the ectopterygoid are recessed to form a 'V'-shaped pterygoid facet (Fig. 10I); a sharp ridge borders the outer perimeter of this facet. The medial process of the ectopterygoid is a straight medial extension of the lateral process and slots into a 'V'-shaped recess on the dorsal surface of the pterygoid just

Figure 11. Virtual three-dimensional renderings of the lower jaws of the holotype (USNM PAL 722041) of *Opisthiamimus gregori* gen. et sp. nov. **A–E,** part of the right dentary in **A,** right lateral, **B,** medial, **C,** dorsal, **D,** ventral and **E,** anteromedial views; **F,** close-up of the symphyseal region of the right dentary in anteromedial view; **G–K,** part of the left dentary in **G,** anteromedial, **H,** left lateral, **I,** medial, **J,** dorsal and **K,** ventral views; **L–N**, right lower jaw in **L,** medial, **M,** dorsal and **N,** right lateral views. Arrow in L indicates the anterior extent of the angular. **Abbreviations: ad.fss**, adductor fossa; **addt**, additional tooth; **An**, angular; **an.fct**, facet for the angular; **Art**, articular; **art.l.sulc**, lateral sulcus of the articular; **art.m.sulc**, medial sulcus of the articular; **co.pr**, coronoid process; **d.sym.s**, dorsal symphyseal surface; **Den**, dentary; **den.p.pr**, posterior process of the dentary; **ed.ri**, edentulous ridge; **for**, foramen; **ht**, hatchling tooth; **men.pr**, mentonian process; **mk.gr**, Meckelian groove; **ntch**, notch; **Pre**, prearticular; **psym.lam**, postsymphyseal lamina; **r.art.pr**, retroarticular process; **ri**, ridge; **sb**, secondary bone; **subd.ri**, subdental ridge; **succt**, successional tooth; **Sur**, surangular; **sur.a.pr**, anterior process of the surangular; **sur.fct**, facet for the surangular; **sym.s**, symphyseal surface; **v.sym.s**, ventral symphyseal surface; **wf**, wear facet.

anterior to its pterygoid flange (Fig. 10E). The ventral process of the ectopterygoid diverges ventromedially and somewhat posteriorly to underlap the pterygoid flange anteroventrally. A tab-like, ventrally sloping bony projection on the anteromedial surface of the ectopterygoid contacts the palatine posterolaterally, blocking the pterygoid from entering the border of the suborbital fenestra.

?Epipterygoid. An elongate strap-like bone may represent the left epipterygoid. It is exposed on the ventral surface of the skull block lateral to the left parietal and the pterygoid flange of the left pterygoid (Fig. 2B, E). This juxtaposition is close to its expected anatomical position, suggesting that the epipterygoid has rotated from a vertical orientation to a more horizontal one as a consequence of dorsoventral crushing.

It has slightly expanded ends that are twisted relative to one another. The broader end, which is preserved in an anterior position, likely represents the ventral portion of the epipterygoid and would have articulated with the dorsal surface of the pterygoid. The opposite end, which is immediately lateral to the parietal, is narrower and presumably would have approached the parietal and prootic. We could not identify the right epipterygoid.

Braincase

The braincase is somewhat crushed dorsoventrally and partially exposed dorsally on the skeletal block; it has been rotated clockwise and tilted rightward when viewed from above (Fig. 3). Portions of the supraoccipital and left prootic and opisthotic are the only easily recognizable elements of the braincase. Although these bones are fractured, no discernable sutures between them are visible, which we interpret as evidence of fusion. The dorsal rim of the foramen magnum is visible behind the midline of the supraoccipital. Neither exoccipital could be identified bordering the foramen magnum laterally; they could be missing, hidden, or fused to the opisthotic. However, a flat, thin sliver of bone lying anterior to the base of the left atlantal neural arch might be the displaced left exoccipital (Fig. 3). To the right of the supraoccipital and below the parietal process of the right squamosal is a partially exposed, dorsally convex bone with flattened surfaces that might represent a right prootic and/or opisthotic. The remainder of the braincase, including the basioccipital, basisphenoid and basipterygoid, is either hidden or unrecognizable; μCT resolution of the skeletal block was too poor to visualize these structures sufficiently for identification and description. The supraoccipital bears a low sagittal crest that is sharpest anteriorly. Posteriorly, the crest disappears where the surface of the supraoccipital swells dorsally (Figs 3, 9A). The left prootic has a prominent, thickened anterior margin.

Lower jaw

The lower jaw (Fig. 11) comprises the dentary, angular, coronoid, surangular, prearticular and articular. There is no evidence of a splenial. The coronoid process of the dentary meets the top of the tooth-bearing ramus of the dentary at about mid-length along the lower jaw (akin to *Clevosaurus hudsoni*; e.g. Reynoso 2005, fig. 3c). The two jaws meet at an unfused symphysis anteriorly.

Dentary. The dentigerous portion of each dentary is preserved on the skull block and is broken transversely behind the distal-most tooth (Fig. 2B, C, E, F). The dentaries are tightly wedged between the left and right maxillae and palatines, respectively; all but the mesial-most teeth of the right dentary are hidden between them. The dentaries are largely exposed laterally, ventrally and somewhat medially, revealing the Meckelian groove. The remainder of each dentary, including most or all the coronoid process, is preserved on the skeletal block, with mostly just the posterior process hidden from view (Fig. 3). Several major fractures extend through both dentaries. The anterior third of the right dentary is slightly offset medially along its ventral margin and a dorsal piece of its coronoid process remains on the skull block just medial to the right jugal (Fig. 2B, E). A short anterior section of the left dentary above the symphyseal notch is missing; fortunately, a smooth impression of the medial surface of this portion of the dentary, including one of the teeth, is preserved in the rock matrix (see description of teeth for details). The dentaries are not articulated at their symphysis; the left has slid slightly anteriorly and dorsally relative to the right (Fig. 2B, E).

In dorsal view, the long axis of the dentary anterior to the coronoid process is essentially straight for most of its anteroposterior length, but anteriorly it curves medially towards the symphysis (Fig. 11C, J). The tooth row generally follows this contour; however, the mesial teeth are positioned more laterally on top of the jaw than are the distal teeth. The ventral surface of the dentary ramus is broadly rounded posteriorly; anteriorly, it gently tapers mediolaterally and becomes slightly keeled behind the symphysis. Several faint longitudinal grooves extend along the ventral surface of the dentary; these grooves are fainter and less numerous relative to those observed in some specimens of *Opisthias rarus* (e.g. USNM V 2858) and other rhynchocephalians (e.g. *Eilenodon* sp.; MEHJ, pers. obs.). In mediolateral view, the ventral margin of the dentary curves downward towards the symphysis to form a small, chin-like ventral projection (= mentonian process; Fig. 11A, B, H, I). In

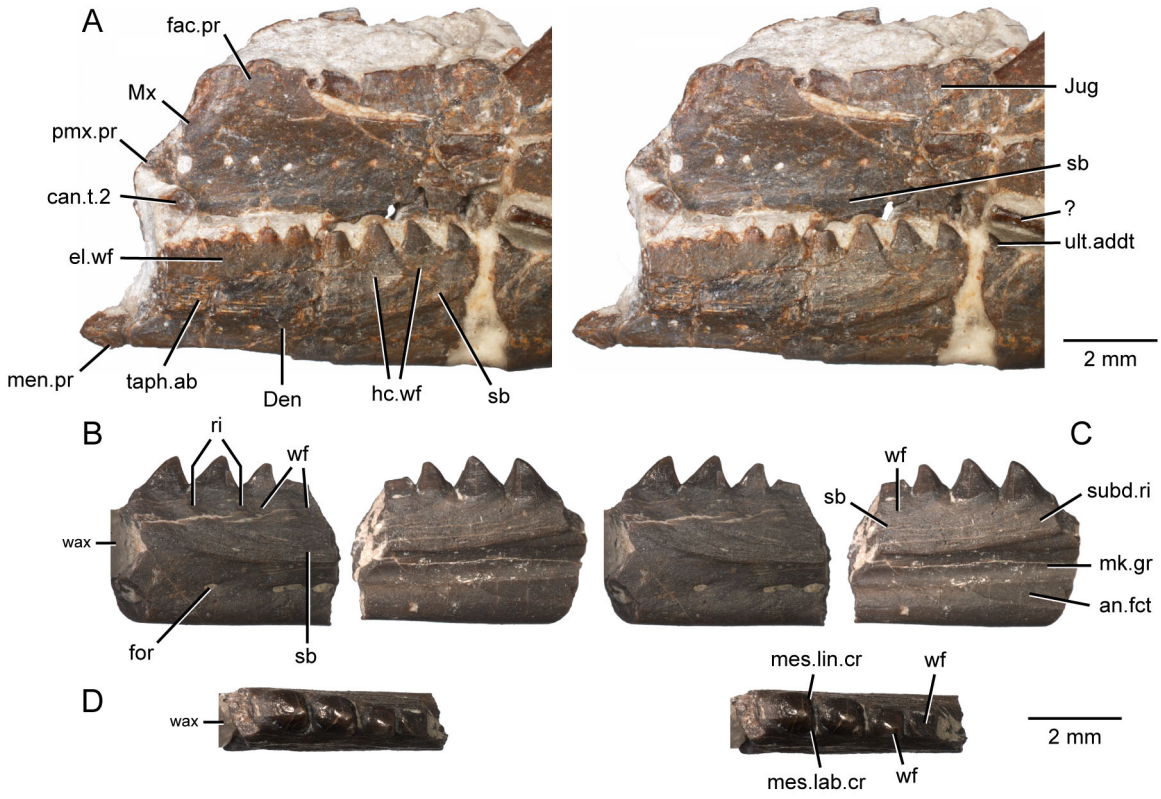

Figure 12. Extended depth of field stereophotopairs of a referred partial skull and lower jaw (USNM PAL 720475) and right dentary (USNM PAL 720476) of *Opisthiamimus gregori* gen. et sp. nov. **A,** USNM PAL 720475 in left lateral view; **B–D,** USNM PAL 720476 in **B,** lateral, **C,** medial and **D,** dorsal views. **Abbreviations: an.fct**, angular facet; **can.t.2**, second or distal successional caniniform tooth; **Den**, dentary; **el.wf**, elongate wear facet; **fac.pr**, facial process; **for**, foramen; **hc.wf**, half-circle-shaped wear facet; **Jug**, jugal; **men.pr**, mentonian process; **mes.lab.cr**, mesiolabial crest; **mes.lin.cr**, mesiolingual crest; **mk.gr**, Meckelian groove; **Mx**, maxilla; **pmx.pr**, premaxillary process; **ri**, ridge; **sb**, secondary bone; **subd.ri**, subdental ridge; **taph.ab**, taphonomic abrasion; **ult.addt**, ultimate or distal-most additional tooth; **wax**, wax; **wf**, wear facet; **?**, unidentified bone.

lateral view, the dentary surface is smooth and perforated by at least six round to ovoid small foramina; fracturing has obscured the true count. The round anteriormost foramen is the largest, positioned behind the dentary notch and below the level of the second mesial tooth (Fig. 11A). The more posterior foramina are smaller, with the last one positioned below the level of the third tooth from the rear (Fig. 11H). These foramina are positioned at about mid-height of the dentary anteriorly; more posteriorly they migrate slightly ventrally. Below the tooth row and above the lateral foramina is a thickened layer of secondary bone with a sinuous ventral outline: anteriorly the outline is convex up and posteriorly it is convex down, generally mimicking the ventral contour of the dentary (Fig. 11A). A similar layer or skirt of secondary bone occurs on the dorsomedial side of the dentary below the teeth; its ventral outline is downwardly convex and spans the tooth row (Fig. 11B, E).

Maxillary tooth wear facets just below the dentary teeth laterally have been carved into the secondary bone, which are best seen on the exposed surfaces of the referred specimens. In USNM PAL 720475, the dorsolateral surface of the dentary is polished into a single, elongate wear facet anteriorly and labial to the hatchling and first additional teeth (Fig. 12A). Posterior to this region, individual half-circle-shaped wear facets are present ventrolateral to each tooth, which abruptly decrease in size posteriorly. A prominent oblique ridge of less worn secondary bone extends posteroventrally from the distolabial margin of the fourth from last additional tooth and separates the wear facet lateral to it from the one lateral to the succeeding tooth. No wear facet is present next to the ultimate additional tooth. In USNM PAL 720476, individual lateral wear facets are separated by shallow ridges of less worn secondary bone that curve anteroventrally from about the mesiolabial edge of each tooth to about the mesiodistal

midpoint of the preceding tooth (Fig. 12B). A shallow, half-circle-shaped wear facet formed by the occluding lateral tooth row of the palatine is visible on the dorsomedial side of this dentary at the bases of the mesial two preserved additional teeth (Fig. 12C). This facet extends the mesiodistal length of the mesial-most tooth and about half the length of the succeeding one. A combination of the above listed types of wear in the dentaries of *Opisthiamimus gregori* suggest that it had primarily proal but some orthal lower jaw movements (see Discussion, below).

Medially, the Meckelian groove is within the lower half of the dentary (Fig. 11B, I). Posteriorly, it is moderately deep and narrow dorsoventrally, with distinct upper and lower borders. A tapered angular facet borders the Meckelian groove ventrally beginning at the level of the penultimate tooth (Figs 11B, I, L, 12C). Anteriorly and below the postsymphyseal lamina of the dentary (*sensu* Apesteguía *et al*. 2012, fig. 4, 'lps'), the ventral border of the groove all but disappears as it curves anteroventrally to meet the posteroventral corner of the dentary symphysis (Fig. 11F). Consequently, the Meckelian groove doubles in height as it approaches the symphysis and becomes relatively shallow mediolaterally. The ventral outline of the sharp ventral edge of the postsymphyseal lamina is slightly convex downward and does not constrict the groove dorsoventrally. Anteriorly, the postsymphyseal lamina forms the face of a small dorsal symphyseal surface at the posterodorsal edge of a prominent ventral symphysis (Fig. 11F). Here the Meckelian groove narrowly separates the dorsal and ventral facets for a short distance, which form a 'comma-shaped' symphysis much like in *Sphenodon* (Jones *et al*. 2012) and other rhynchocephalians (e.g. *Opisthias rarus*: Throckmorton *et al*. 1981, text-fig. 2A; Supplemental material, Fig. S1H, I). The face of the ventral symphysis has an ovoid outline and is nearly twice as tall as it is wide. The 'comma-shaped' symphysis is unlike that observed in *Cynosphenodon huizachalensis* (Reynoso 1996, fig. 3C), *Sphenovipera jimmysjoyi* (Reynoso 2005, fig. 2A, B), or *Opisthias* cf. *O. rarus* from Fox Mesa (based on a slender dentary, USNM PAL 720477; Supplemental material, Fig. S3), in which the ventral symphysis is larger but closer in size to the dorsal symphysis. In *Opisthiamimus gregori*, the dentary is notched (or grooved) anteriorly between the symphysis dorsally and the alveolar region of the dentary ventrally (*sensu* Evans *et al*. 2001; Jones *et al*. 2012) (Fig. 11A, B, E).

Between the ultimate tooth and the coronoid process the dentary features an edentulous ridge that slopes ventromedially onto a steep shelf (Fig. 11G, I). Although this edentulous gap could accommodate another tooth, there is no evidence of one, nor is there a pit for a developing tooth like in some of the largest dentaries of *Opisthias rarus* (USNM V 6130) including the holotype (USNM V 2860; Fig. 15I, K; Supplemental material, Fig. S1A, C). Furthermore, these dentaries, and other similar-sized topotypic specimens referred to *O. rarus* (e.g. USNM V 6126, 6129, 6132) as well as the 'paratype' (USNM V 2858; Fig. 15H, J, L; Supplemental material, Fig. S1D, F), all possess a tooth row that leaves little to no room anterior to the coronoid process; this anatomical trait is also present in *Theretairus antiquus* (Simpson 1926, fig. 1). The presence and length of the tooth gap in USNM PAL 722041 (and apparently in USNM PAL 720475; Fig. 12A) is similar to that observed in small to large specimens of *Clevosaurus hudsoni* (e.g. Fraser 1988, figs 19, 20, 23).

In lateral view, the coronoid process is rectangular, with its maximum width exceeding its maximum height (Fig. 11L, N). The long axis of the process forms an angle of 116° from a horizontal line drawn anteriorly through the tooth bases. The margin of the coronoid process is slightly convex dorsally but concavo-convex anteriorly and concave posteriorly. The process is moderately tall and extends well above the tooth crowns. Its posteromedial surface features a moderately deep, rounded facet for the anterior process of the surangular (Fig. 11L). This facet is vacant and exposed on the right dentary, but on the left, it is in its natural articulation with the anterior process (Fig. 9A, B). Based on a complete 3D reconstruction of the left lower jaw (not shown), the mandibular foramen is positioned where the posterior base of the coronoid process meets the anterodorsal part of the posterior process. The moderately elongate posterior process tapers posteriorly and terminates at about the midlength of the articular cotyle or glenoid (Fig. 11N).

Coronoid. The left coronoid is visible in dorsal view on the skeletal block and is tightly sutured to the left dentary (Fig. 9A, B). The bone is thin mediolaterally and its dorsal margin is broken off, revealing its squamous lateral contact with the coronoid process of the dentary medially. Posteriorly, it is bifurcated to form the slot portion of a slot joint with the anterior process of the surangular. The remainder of the left coronoid is hidden by matrix and bone. The ovoid bone immediately anterior to the anterior process of the right surangular on the skeletal block is the right coronoid (Figs 3, 9F). The dorsal tip of this bone is found medial to the broken-off top of the coronoid process of the right dentary in the skull block (Fig. 2B, E).

Angular. The tapering anterior end of each angular is preserved in articulation with its respective dentary on

the skull block. Here, the angular is found on the medial side of the dentary bordering the Meckelian canal ventrally. On the skeletal block, a short exposure of the left angular is visible in dorsal and medial views, whereas only a transverse section of the right element is visible in anterior view (Fig. 3).

The angular is an elongate twisting bone with tapering anterior and posterior ends. The angular extends anteriorly to a level below the penultimate dentary tooth and less than one-quarter of the length of the dentary ramus anterior to the coronoid process (Fig. 11L). From here, the bone extends posteriorly along the ventromedial surface of the dentary. As it approaches the prearticular, it begins to twist onto the ventral surface of the dentary where it is hidden in medial view by the prearticular posteroventrally (see below). Behind this point in lateral view, the face of the angular is oriented ventrolaterally and exposed below the articular (Fig. 11N). In USNM PAL 720475, the posterior-most end of the angular is relatively broad but missing its tip (Fig. 6B, G). It is displaced laterally to expose part of the posteriorly tapering angular facet on the ventral and ventrolateral surfaces of the prearticular and surangular, respectively (Fig. 6B, G).

Articular complex (surangular, prearticular, articular). Of the three bones of the articular complex, only the anterior ends of the surangulars are exposed on the skeletal block; consequently, the degree of fusion between these bones is uncertain. The 3D reconstructions of the left and right articular complexes allow for a general description of this compound element as a unit. USNM PAL 720475 provides additional details not observable in the holotype, although it is also missing portions of these bones.

The exposed left surangular is articulated with its corresponding dentary and coronoid. The broken anterodorsal end of the element is teardrop-shaped in horizontal cross section, with the tapered anterior margin slotting into the back of the coronoid (Fig. 9A, B). Laterally and slightly more posteriorly, the surangular fits into a depression (the surangular facet) on the medial side of the coronoid process of the dentary (see above). The anterior end of the right surangular is exposed below and anterior to the right squamosal and medial to the right dentary (Fig. 3). Crushing of the skull has bent this portion of the bone ventromedially away from the dentary (Fig. 9F, G).

The surangular overlaps the posterior process of the dentary dorsolaterally to enclose the mandibular foramen dorsally and form the dorsal border of the adductor fossa medially. In dorsal view, the articular surface for contact with the quadrate is ovoid in marginal outline and oriented at an oblique angle anterolaterally/posteromedially (Fig. 11M). A low ridge extending parallel to the long axis of the mandibular ramus divides the articular surface into medial and lateral sulci; the lateral sulcus is narrower, shallower and set higher on the articular relative to the medial one. A straight, tight suture between the surangular and prearticular is visible in ventral view on USNM PAL 720475, extending anteroposteriorly along the exposed angular facet and onto the base of the retroarticular process (Fig. 6B, G). This suture does not extend entirely through the retroarticular process, indicating partial fusion between the surangular and prearticular.

The prearticular has a sharply rounded ventromedial edge that extends anteriorly from the retroarticular process past the posterior border of the dentary coronoid process (Fig. 11L); poor μCT scan resolution inhibits defining its anterior-most portion. Lateral to this ridge, the prearticular contacts the angular along its length, mostly hiding it from medial view. The upper margin of the prearticular anteriorly borders the adductor fossa ventrally. The posterior retroarticular process is elongate. In dorsal or ventral view, it extends to a sharply rounded point posteriorly; in medial or lateral view, the process gently curves posterodorsally (Fig. 11L, M). The elongate, tapering shape of the retroarticular process is similar to that observed, for example, in *Clevosaurus hudsoni* (Fraser 1988, fig. 19) but unlike the short, posteriorly blunt process of *Sphenodon* (e.g. Jones *et al*. 2009a, figs 6, 36). The tip of the retroarticular process in USNM PAL 720475 is broken off (Fig. 6).

Dentition

The marginal dentition is acrodont (i.e. attached to the crest of the jawbone with no indication of roots). Ankylosis is complete, with a layer of secondary bone that obscures the tooth bases of more mature (i.e. non-hatchling) teeth.

Premaxillary teeth. No premaxillary teeth are preserved.

Maxillary teeth. Between the holotype and referred specimens, we have identified the hatchling, successional caniniform and additional teeth. Both maxillae of the holotype (USNM PAL 722041) preserve or have spaces for at least nine teeth (Figs 5E, F, H, 13). The mesial-most teeth are not preserved in the holotype, but two more mesial teeth are preserved in USNM PAL 720475, for a total of at least 11 (Fig. 6C, D; Supplemental material, Fig. S4). Based on our 3D skull reconstruction (Fig. 4), we estimate that only one or two more mesial teeth occurred in the maxilla, for a maximum of 12 or 13 teeth. The lingual faces of the two mesial teeth in USNM PAL 720475 are slightly polished

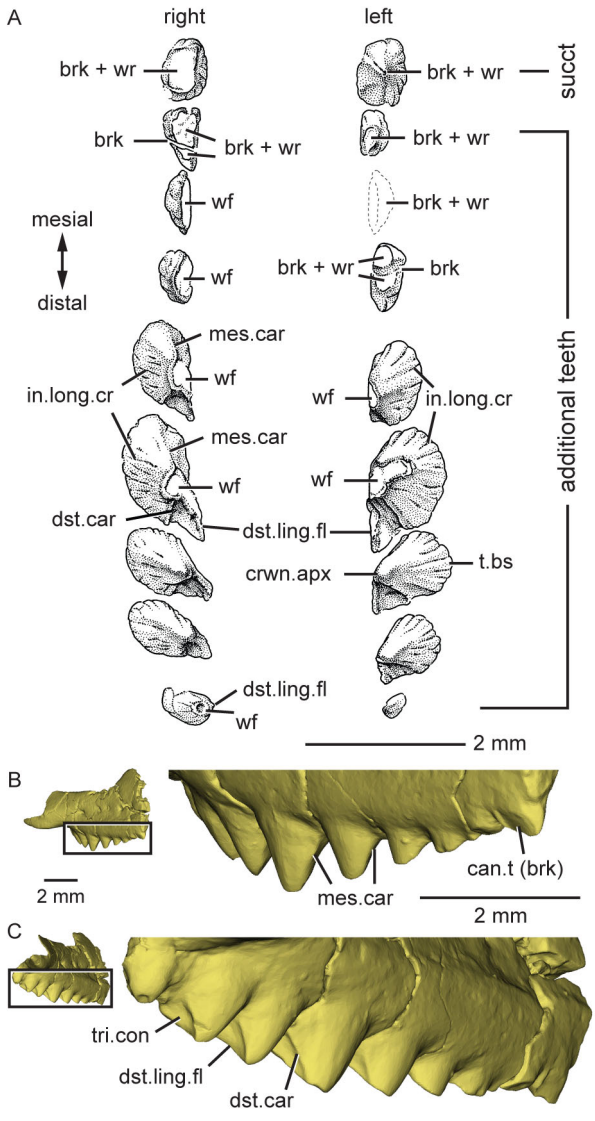

Figure 13. The maxillary teeth of *Opisthiamimus gregori* gen. et sp. nov. **A,** interpretative camera lucida drawing of the teeth of the holotype specimen (USNM PAL 722041) in occlusal view; **B, C,** virtual three-dimensional renderings of the right maxilla with close-ups of its teeth in the holotype specimen in **B,** anterolateral/mesiolabial and **C,** posterolateral/distolabial views. The boxes in B and C indicate the respective magnified regions to the right. **Abbreviations: brk**, break; **can.t**, successional caniniform tooth; **crwn.apx**, tooth crown apex; **dst.car**, distal carina; **dst.ling.fl**, distolingual flange; **in.long.cr**, internal longitudinal cracks of the tooth enamel; **mes.car**, mesial carina; **succt**, successional tooth; **t.bs**, tooth base; **tri.con**, triangular concavity; **wf**, wear facet; **wr**, non-occlusal wear.

but not extensively worn, and there are no apparent ridges or grooves adorning them (Fig. 6D). The mesial-most tooth is triangular in lingual view and slightly larger than the succeeding tooth, which is bluntly rounded across its apex. Because of the size disparity in these two teeth we interpret them as representing part of the hatchling dentition (Supplemental material, Fig. S4).

The preserved mesial four teeth of the holotype are moderately to heavily worn, whereas the five distal-most teeth have moderate to no apparent wear (Fig. 13A). Excluding the mesial-most preserved tooth, the teeth increase in size distally to the fourth from the rear before decreasing to the ultimate tooth (Figs 5E, F, H, 13A). In occlusal view, the six mesial teeth are approximately in line with each other mesiodistally, whereas the last three teeth become increasingly lingually positioned. The base of the mesial-most preserved tooth is ovoid in outline and labiolingually compressed. In labial view, this tooth is separated from its immediate successor by a notch and is more deeply implanted into the maxilla (Figs 5F, 13B). This tooth on the right maxilla preserves part of the crown, revealing it likely was subconical; it is triangular in lingual and labial views. The labial and lingual surfaces of this crown are moderately worn, thus exposing its internal dentine to form a sharp, mesiodistally oriented apical crest. Taken together, these features support identifying this tooth as a successional caniniform, as in *Sphenodon punctatus*. Three-dimensional rendering of USNM PAL 720475 revealed a nearly complete, labiolingually compressed conical tooth at the same position and behind the two hatchling teeth (Fig. 6D; Supplemental material, Fig. S4), which we similarly identify as a caniniform.

The next three teeth in the holotype (as observed on the right maxilla) probably do not represent hatchling teeth. Such teeth in rhynchocephalians typically alternate in size (Robinson 1976), and there is no evidence of smaller hatchling teeth in this specimen or in USNM PAL 720475. Thus, we interpret these three teeth as the mesial additional series distal to the successional caniniform (Fig. 13A). In occlusal view, they are hemispherical in outline, with a rounded labial margin and a lingual side that is flattened due to occlusal wear.

The five distal-most teeth represent the mature additional teeth; these are basically conical aside from the distolingual flange (see below). The two largest additional teeth are more labiolingually compressed, with a mesiodistally longer base and a subtle mesial carina (Fig. 13B). On the distal margin of these five teeth, a sharp ridge or carina extends along a slight mesially convex arc from the apex towards the tooth base; it is subtle on the small ultimate tooth (Fig. 13A, C). A well-developed flange on the lingual side of the largest four additional teeth extends distolingually towards the tooth base from the apex. This flange is sharp in the unworn crowns (e.g. penultimate and third from last right additional teeth). In the largest additional teeth, the

lingual surface is worn across the apex to the base of the distolingual flange, which forms a moderately wide, elongate wear facet. On the largest additional tooth of the left maxilla, this facet extends across the apex and onto the labial side of the tooth, where it is grooved and extends basally to about half the height of the crown (Fig. 13A). In labial view, the distolingual flanges of the third, fourth and fifth additional teeth from the rear are partially hidden from view because each flange extends distally past the mesial margin of the successive tooth. The labial surface of the tooth between this flange and the distal carina is gently concave and triangular in outline when viewed distolabially and occlusally (Fig. 13C). In labial view, the mesial four mature additional teeth appear slightly recurved (Fig. 5E). The ultimate additional tooth is much smaller compared to the others; on the right maxilla, it has a rounded, concave wear facet on the labial side of the apex, and its mesial carina and distolingual flange are subtle and more ridge-like (Fig. 13A). Externally, the enamel is mostly smooth with faint longitudinal wrinkles; its translucent nature reveals internal longitudinal cracks, preservational in nature, in most teeth (Fig. 13A).

Dentary teeth. Hatchling, successional (including caniniform) and additional teeth are all present in the dentary of *Opisthiamimus gregori*. In the holotype, only the mesial two teeth of the right dentary are exposed (Figs 2C, F, 14A, B); the remaining dentary teeth were 3D reconstructed to reveal the hatchling and additional series (Fig. 11). The right dentary preserves the entire tooth row; the left is missing the mesial-most teeth. A total of 13 or 14 teeth are inferred for both jaws (the uncertainty lies with the unexposed and worn hatchling teeth).

The exposed mesial two teeth of the right dentary represent post-hatchling successional caniniform teeth (Fig. 14A–C). The mesial-most tooth in USNM PAL 722041 is situated at the extreme anterodorsal end of the dentary above the symphyseal notch and here is referred to as a symphyseal successional caniniform tooth. It is conical and slightly procumbent, and its lingual and labial sides are separated by a blunt, lingually offset longitudinal carina on both the mesial and distal margins (Fig. 14C). The apex and distolabial surfaces are slightly worn. This tooth occurs at a similar position as the probable symphyseal caniniform observed in the holotype dentary of *Opisthias rarus* (Gilmore 1909; Fig. 15G, I, K; Supplemental material, Fig. S1G, H). The next prominent tooth represents a second successional caniniform tooth. The presence of a non-symphyseal caniniform sets *Opisthiamimus gregori* apart from *O. rarus*, which has either only one possible symphyseal caniniform (holotype) or none (‘paratype’; e.g. Evans & Fraser 1992; Fig. 15H, J, L; Supplemental material, Fig. S1G–I). The second caniniform is similar in size and shape to the symphyseal caniniform but is more upright and bears slightly more occlusal wear, which extends onto and across its entire mesiolabial surface (Fig. 14A, B). Between the caniniform teeth on the dorsolateral surface of the dentary is a shallow ‘V’-shaped wear facet that is continuous with the distolabial and mesiolabial wear facets of those teeth. Both caniniforms are set deeper into the jaw than are the succeeding hatchling teeth and the possible remnant of a hatchling tooth positioned between the caniniforms (Fig. 14C). As in the holotype of *O. rarus* (Supplemental material, Fig. S1H), a small notch in the occlusal surface of the dentary occurs just distal to the symphyseal successional tooth. A similar but slightly larger and deeper notch also occurs behind the distal caniniform, much like the one observed behind the caniniform in a specimen of *Sphenodon punctatus* (Jones 2006a, fig. 2.22; Fig. 11A, F). In the left dentary, this notch is inferred on the basis of a wedge-shaped piece of matrix immediately distal to the caniniform impression and mesial to the dentary impression; Fig. 14D). The presence of two caniniform teeth in *O. gregori* is similar to the condition in *Theretairus antiquus* (Simpson 1926; Supplemental material, Fig. S2A–E), but the paired caniniforms in *T. antiquus* are hypertrophied and positioned behind the anterior end of the dentary (i.e. non symphyseal).

The caniniform teeth on the left dentary are missing along with a short anterior section of the bone. However, a smooth triangular impression – presumably of the lingual side of a second caniniform – is preserved in the rock; it is consistent in size, shape and placement with its right counterpart (Fig. 14D). In USNM PAL 720475, a broken, dorsally worn, diamond-shaped structure lateral to the premaxillary process of the left maxilla and above the hatchling dentition of the left dentary probably represents the second caniniform; it is attached atop part of the missing anterodorsal region of that dentary (Figs 6A, E, 12A).

A short section of the right dentary is exposed immediately behind the notch of the second caniniform tooth and is edentulous along its dorsal summit (Figs 11B, E, 14A, B); μCT slices revealed no evidence of any worn hatchling teeth in this region. A similar edentulous region also appears to be present on the left dentary, based on the 3D rendering and the smooth, straight dorsal margin of its impression in the matrix (Figs 11I, 14D). Behind the edentulous portion of both dentaries, the hatchling dentition is represented by several small, bluntly triangular teeth that alternate in size (Fig. 11B, I). The smaller hatchling teeth are about half the size of the larger ones. There are five or six hatchling teeth on each dentary, which are set much more shallowly on the

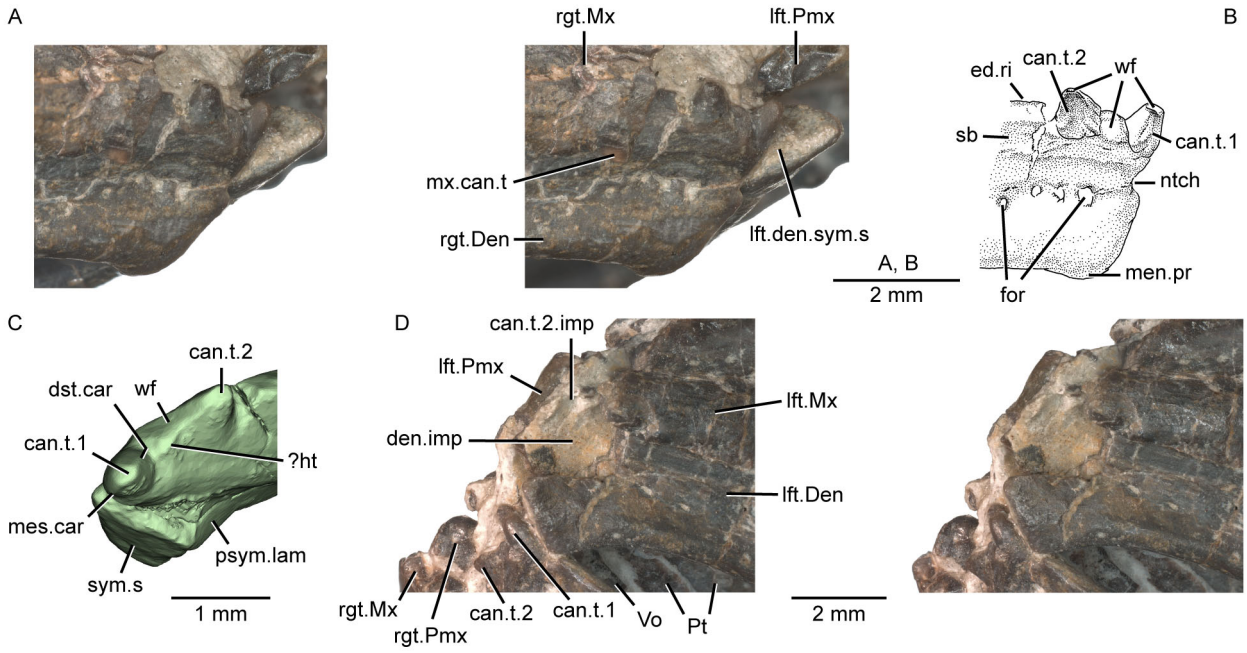

Figure 14. Dentary successional caniniform teeth of the holotype (USNM PAL 722041, 'skull block') of *Opisthiamimus gregori* gen. et sp. nov. **A,** extended depth of field (EDF) stereophotopair of the anterior end of the upper and lower jaws in right lateral view; **B,** interpretive camera lucida drawing of the anterior end of the right dentary in right lateral view; **C,** virtual three-dimensional rendering of the anterior end of the right dentary in anterodorsal and slightly medial views; **D,** EDF stereophotopair of the anterior end of the upper and lower jaws in left lateral and ventral views. **Abbreviations: can.t.1**, first or symphyseal successional caniniform tooth; **can.t.2**, second or distal successional caniniform tooth; **can.t.2.imp**, impression of the second or distal successional caniniform tooth; **den.imp**, dentary impression; **dst.car**, distal carina; **ed.ri**, edentulous ridge; **for**, foramen; **?ht**, possible remnant of a hatchling tooth; **lft.Den**, left dentary; **lft.den.sym.s**, symphyseal surface of the left dentary; **lft.Max**, left maxilla; **lft.Pmx**, left premaxilla; **men.pr**, mentonian process; **mes.car**, mesial carina; **mx.can.t**, successional caniniform tooth of the maxilla; **ntch**, notch; **psym.lam**, postsymphyseal lamina; **Pt**, pterygoid; **rgt.Den**, right dentary; **rgt.Max**, right maxilla; **rgt.Pmx**, right premaxilla; **sb**, secondary bone; **sym.s**, symphyseal surface; **Vo**, vomer; **wf**, wear facet.

jaw summit relative to the caniniforms and subsequent additional teeth (see below). Three-dimensional reconstructions show that both hatchling tooth series appear to have apical and labial wear; they are bluntly rounded or flattened apically, with flattened labial sides.

The larger teeth behind the hatchling dentition represent the additional tooth series (Fig. 11B, I). In USNM PAL 722041, there are seven right and six or seven left additional dentary teeth. They are conical or pyramidal overall with a slightly concave mesial face, a convex distal face and a mesially inclined apex. These teeth increase in size distally until the third or second from the last tooth in the right and left dentaries, respectively, decreasing slightly thereafter. The apically unworn teeth are lower-crowned and blunter relative to those at a similar position in the dentary of *Opisthias rarus* (Fig. 15A *vs* Fig. 15C, E, respectively). When measured in lingual aspect, the unworn additional teeth are nearly equal to or slightly longer mesiodistally than they are tall apicobasally. In occlusal view, they are about equal or, more often, longer mesiodistally than they are wide labiolingually (i.e. length/width $>$ 1). The mesial-most additional tooth is asymmetrical in occlusal view with a flattened labial face and broadly rounded lingual surface. This tooth bears weak mesiolabial and distolabial crests. More distally along the tooth row, the labial and lingual halves of the additional teeth become more symmetrical, and the entire tooth more pyramidal. The lingual or labial profile of the distal-most four or five teeth is concavo-convex, with the apex offset mesial to the transverse midline (e.g. Fig. 12). The lingual surface of the second additional tooth in the holotype is slightly flattened, thus creating weak mesiolingual and distolingual longitudinal crests. The mesiolingual crest becomes slightly better developed in the larger, more distal teeth as the lingual surface becomes flatter and the mesial face slightly concave. The distolingual crest also becomes slightly more prevalent as the distal face of the teeth becomes flatter. In some rhynchocephalians these crests are typically referred to as flanges, but they are weakly developed in *Opisthiamimus gregori* and better described as crests (= 'small flanges' *sensu* Evans *et al.* 2001; Säilä 2005). In the last two teeth the distal surface

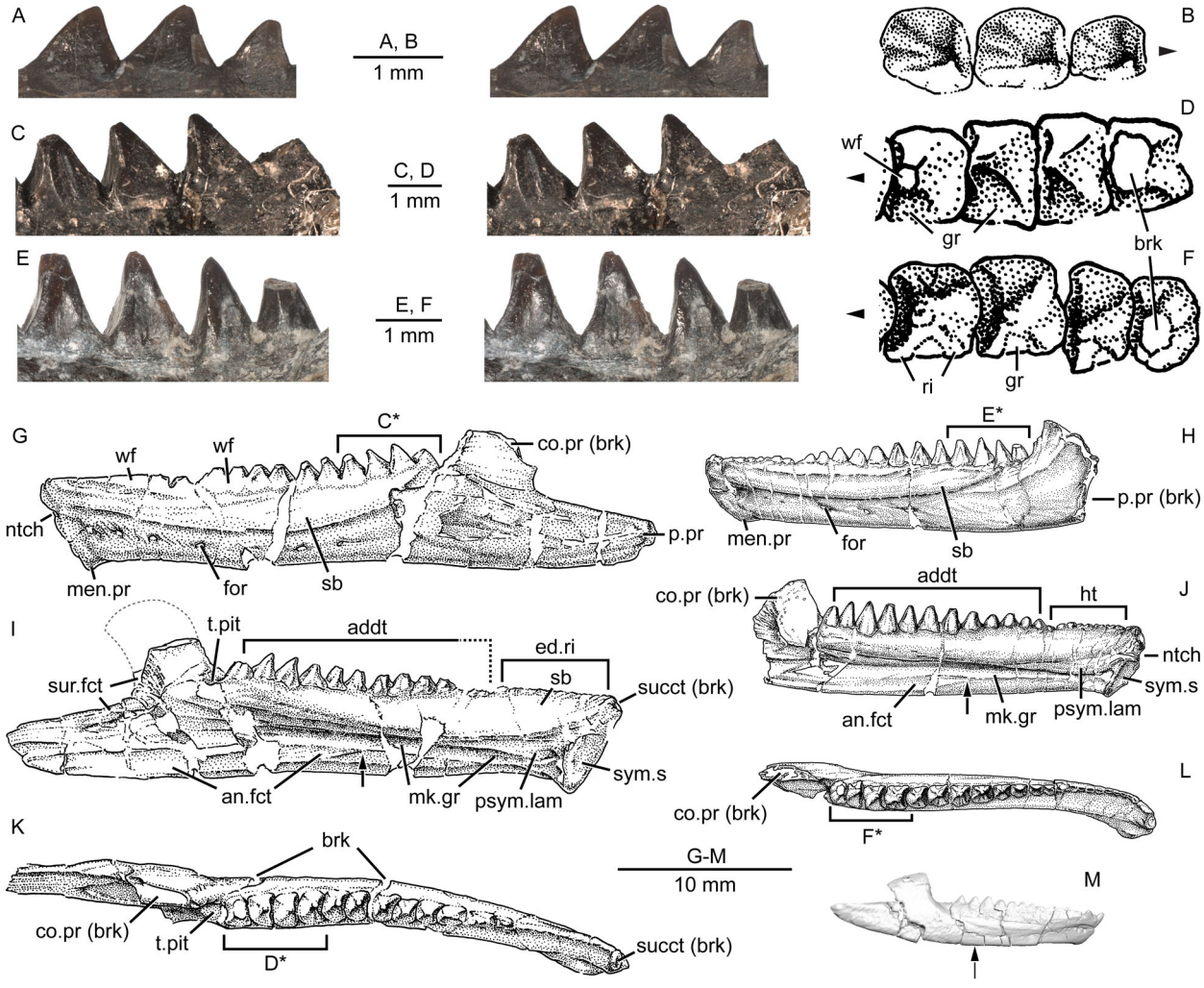

Figure 15. Dentary additional teeth of *Opisthiamimus gregori* gen. et sp. nov. and *Opisthias rarus*. **A,** extended depth of field (EDF) stereophotopair of the distal-most additional teeth of a referred dentary (USNM PAL 720476) of *O. gregori* in labial view; **B,** interpretive camera lucida drawing of the distal-most additional teeth of USNM PAL 720476 in occlusal view; **C,** EDF stereophotopair of the distal-most additional teeth of the holotype dentary (USNM V 2860) of *O. rarus* in labial view; **D,** interpretive camera lucida drawing of the distal-most additional teeth of USNM V 2860 in occlusal view; **E,** EDF stereophotopair of the distal-most additional teeth of the 'paratype' dentary (USNM V 2858) of *O. rarus* in labial view; **F,** interpretive camera lucida drawing of the distal-most additional teeth of USNM V 2858 in occlusal view; **G–L,** interpretive camera lucida drawings of the holotype and 'paratype' specimens of *O. rarus*, respectively, in **G** and **H,** lateral, **I** and **J,** medial, and **K** and **L,** dorsal views; **M,** virtual three-dimensional rendering of the holotype right dentary of *O. gregori* in right lateral view. C*, D*, E* and F*, regions of the tooth row shown in C, D, E and F, respectively. Arrows in B, D and F point mesially. Arrows in I, J and M indicate the anterior extent of the angular. Dashed line in I outlines the coronoid process of the dentary as illustrated in Gilmore (1909, fig. 1). **Abbreviations: addt**, additional tooth; **an.fct**, facet for the angular; **brk**, break; **co.pr**, coronoid process; **ed.ri**, edentulous ridge; **for**, foramen; **gr**, groove or escape structure; **ht**, hatchling tooth; **men.pr**, mentonian process; **mk.gr**, Meckelian groove; **ntch**, notch; **p.pr**, posterior process; **psym.lam**, postsymphyseal lamina; **ri**, ridge; **sb**, secondary bone; **succt**, successional tooth; **sur.fct**, facet for the surangular; **sym.s**, symphyseal surface; **t.pit**, empty tooth pit; **wf**, wear facet.

of the crown is convexly rounded, and the distolabial and distolingual crests are faint or absent. Unlike the distal-most six or seven teeth in the holotype and 'paratype' of *O. rarus* (Fig.15G–L; Supplemental material, Fig. S1), the lingual and, more so, labial sides of the distal-most additional teeth in USNM PAL 722041, 720475 and 720476 all lack prominent triangular depressions and/or longitudinal ridges between the mesial and distal crests (e.g. Fig. 15A, B *vs* Fig. 15C–F; see also Throckmorton *et al*. 1981, text-fig. 5). Conversely, they are mostly smooth, with some teeth possessing only faint vertical enamel wrinkles.

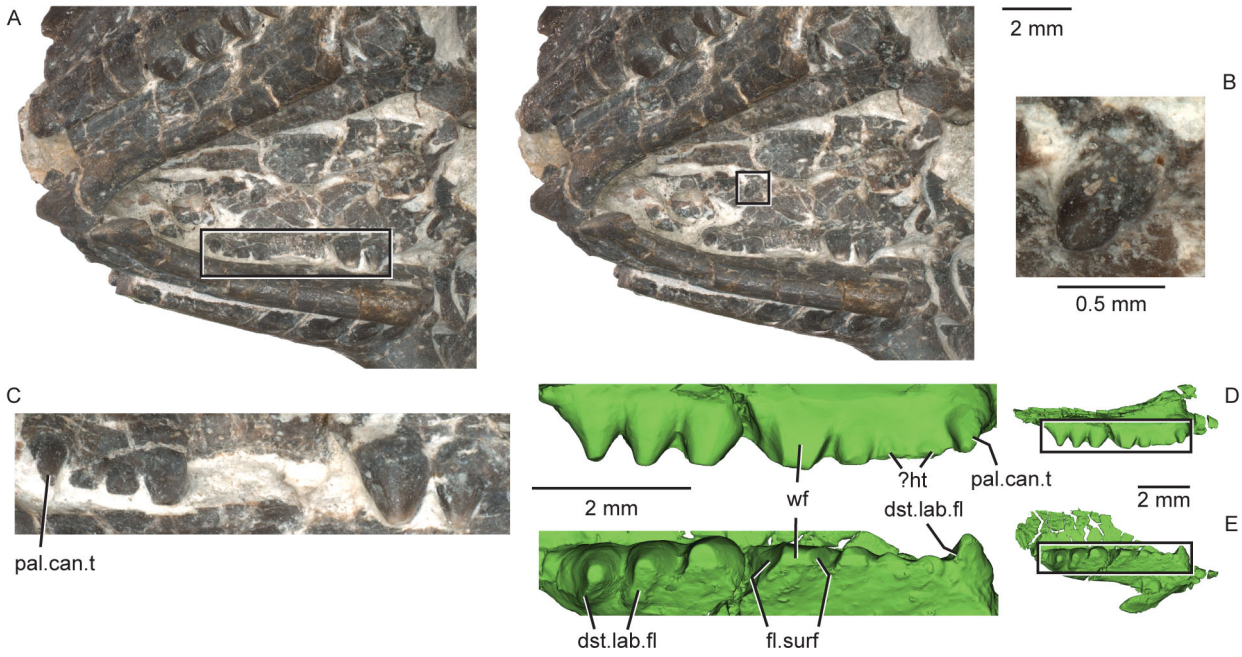

Figure 16. The palatine teeth of the holotype specimen (USNM PAL 722041, 'skull block') of *Opisthiamimus gregori* gen. et sp. nov. **A,** extended depth of field stereophotopair of the palatal region of the skull in left ventrolateral view; **B,** close-up of the isolated palatine tooth of the right palatine in occlusomedial view as shown in the box in the right stereophoto in A; **C,** close-up of the lateral tooth row of the right palatine in occlusolingual view as shown in the box in the left stereophoto in A; **D, E,** virtual three-dimensional renderings of the left palatine lateral tooth row in **D,** lingual, and **E,** occlusal views. Boxes at D and E indicate the regions of the left palatine enlarged and labeled to their left. **Abbreviations: dst.lab.fl**, distolabial flange; **fl.surf**, flattened surface; **?ht**, hatchling teeth or shallowly set mature teeth; **pal.can.t**, caniniform tooth of the palatine; **wf**, wear facet.

The description above is based on the 3D reconstructed holotype dentition, but the fully exposed additional teeth of the isolated partial right dentary (USNM PAL 720476) better show many of these features. The enamelled surfaces of these teeth are smooth, and the mesial and distal crests are weakly defined both labially and lingually relative to, for example, the small flanges in *O. rarus* (Fig. 15C, E; Supplemental material, Fig. S1) and the large flanges in *Clevosaurus hudsoni* (Fraser 1988, fig. 19) and *Priosphenodon avelasi* (Apesteguía & Novas 2003, fig. 1f; LeBlanc *et al*. 2020, fig. 1E, F). The labial and lingual surfaces appear subtly polished but not extensively worn (Fig. 12B–D). Similarly, the exposed labial surfaces of the dentary teeth in USNM PAL 720475 are slightly more polished (Fig. 12A). No obvious enamel-dentine junction is evident. Very little to no mesiodistal overlap or imbrication is apparent between the additional dentary teeth in *Opisthiamimus gregori*.

Palatine teeth. The palatine bears a single isolated conical tooth near the medial edge of the bone and a lateral row of enlarged teeth that is sub-parallel to the maxillary dentition (Fig. 16). A total of eight lateral teeth are preserved on the left palatine (Figs 10K–M, 16D, E), whereas six are evident on the right plus spaces for two others (the fifth and sixth teeth are missing; Figs 10P–R, 16C). All palatine teeth exhibit some occlusal wear. The mesial-most tooth is moderate in size, conical with a weak and narrow distolabial flange, and lingually offset relative to the successive teeth (Figs 10L, Q, 16E). This tooth represents a palatine caniniform, which is like that observed in *Sphenodon punctatus*. However, in *S. punctatus* the caniniform is considerably larger (hypertrophied) and in line with the successive palatine teeth (e.g. Jones *et al*. 2011, figs 28, 29, 35). The tip of each caniniform is worn flat. The successive palatine teeth increase in size until the ultimate (on the right) or penultimate (on the left) tooth; the last tooth on the left is slightly smaller than the penultimate one. The second and third teeth are the smallest and set shallowly on the bone; they are perhaps hatchling teeth, worn nearly flat apically and labially (Fig. 16D). The fourth tooth is similar in shape but slightly larger and more robust than the caniniform and more greatly worn apically.

The fifth tooth of the left palatine exhibits such extensive wear that the dentine is exposed across the entire apical and lingual surfaces of the tooth. Its mesial and

distal faces are flattened relative to the rounded contours of the other palatine teeth (Figs 10L, 16D, E); a tooth at a similar position in the left palatine of USNM PAL 720475) also has the flattened mesial and distal surfaces. The last two and three teeth of the right and left palatines, respectively, are shaped like inflated cones, with faint wrinkled enamel, weak vertical ridges and a distolabial flange. Near their base, these teeth bulge lingually beyond their attachment with the palatine. The crown tip and distolabial flange of all of these teeth exhibit wear, which becomes weaker more distally along this portion of the tooth row. In USNM PAL 720475, the larger and more distal tooth on the poorly preserved right palatine exhibits extensive labial wear (Fig. 6C, F). The isolated single tooth set near the medial edge of the palatine is conical and about equal in size to the palatine caniniform and exhibits some occlusal wear (Figs 10Q–S, 16A, B).

Postcranial axial skeleton

A total of 24 partial to complete vertebrae are preserved in USNM PAL 722041, 22 presacral and two sacral vertebrae (Fig. 17). A short section of the presacral column is missing between presacrals 15 and the seventh from the last presacral. Given the size of the vertebrae surrounding the gap *vs* its length, we estimate that only two or three additional vertebrae were present, for a total of 24 or 25 presacral vertebrae. This value is consistent with that observed or estimated in other Jurassic rhynchocephalians (Hoffstetter & Gasc 1969; Müller *et al*. 2010), and most rhynchocephalians have fewer than 25 presacrals, whereas *Sphenodon punctatus* has 25 (Günther 1867; Hoffstetter & Gasc 1969). The number of cervical vertebrae is either seven or eight, depending on whether the well-developed rib of the eighth vertebra contacted the sternum distally (Hoffstetter & Gasc 1969).

The vertebrae are mostly articulated and arranged in a slight 'S'-shaped configuration (Fig. 17). The anterior cervical vertebrae including the atlas and axis are rotated rightward, exposing their left sides. More posterior vertebrae are positioned increasingly upright in the matrix, exposing more of their dorsal surfaces. Minor damage occurs in all vertebrae, and most neural spines are either abraded dorsally or broken off near their bases. Nevertheless, given how short the dorsally abraded (*vs* broken) neural spines are (e.g. in presacrals 14 and 15) and how narrow the bases of the broken spines are in most other non-cervical presacrals, we predict that the spines likely were not tall as in *Sphenodon punctatus* (e.g. Hoffstetter & Gasc 1969, figs 27–30) but more similar to those of *Clevosaurus hudsoni* (e.g. Fraser 1988, fig. 25). The axis and third cervical vertebra have the best-preserved neural spines (Fig. 18A, B). A horizontal fracture occurs through the left neural arch of the first four cervical vertebrae including the atlas and axis; although this fracture occurs at the contact between the base of the neural arch and the top of the centrum (here, the neurocentral junction) in these vertebrae, it does not indicate unfused neurocentral sutures (*contra* our earlier interpretation; DeMar *et al*. 2018). The centra are deeply amphicoelous and notochordal as evidenced through our μCT scan. A thickened rim of bony tissue surrounds the perimeter of the anterior and posterior cotyles. Evidence of free intercentra is lacking.

Atlas and axis. A proatlas was not observed. Only the left neural arch of the atlas is exposed; the atlantal centrum (odontoid process) and right neural arch are presumably hidden by matrix and bone (Fig. 18A, B). The left neural arch is broken horizontally at about mid-height to reveal an elliptical cross-section. In lateral view (above the fracture), the dorsal surface of the atlantal neural arch is concave and arches upward posterodorsally. The anterior margin of the short anterior process is anteriorly convex. The posterior margin of the posterior process is beveled dorsally. Below the fracture, the lower half of the neural arch (= 'foot' of Evans 1981) is inflated and more bulbous, exhibiting a broadly rounded ventral margin. In *Sphenodon punctatus* and other rhynchocephalians such as *Clevosaurus hudsoni*, the first or atlantal intercentrum articulates with the ventromedial side of the atlantal neural arch foot (Jones *et al*. 2009a; O'Brien *et al*. 2018). This element does not appear to be preserved in USNM PAL 722041 (at least not on the left side). The flat, thin sliver of bone lying anterior to the base of the left atlantal neural arch is not the first intercentrum but might be a displaced left exoccipital (see above).

The axis features a dorsoventrally tall neural arch and spine (Fig. 18A, B). The spine is moderately elongated anteroposteriorly, but its length is far less than its combined height with the neural arch. In lateral view, the dorsal margin of the neural spine is flat and gently sloped anteroventrally. More anteriorly, the neural spine steeply descends along a broadly rounded arc. At the base of the arc, the anterior edge of the neural arch is inset posteriorly and then descends nearly vertically to the top of the centrum. A little less than halfway up this margin is a small but distinct, triangular prezygapophysis; its articular surface faces slightly dorsolaterally. The outline of the neural spine is posteriorly concave, and its posterior face bears a concave vertical furrow bounded by lateral ridges that connect ventrally with the postzygapophyses. Within the furrow, a small bony spur or accessory process is centrally placed at the base of

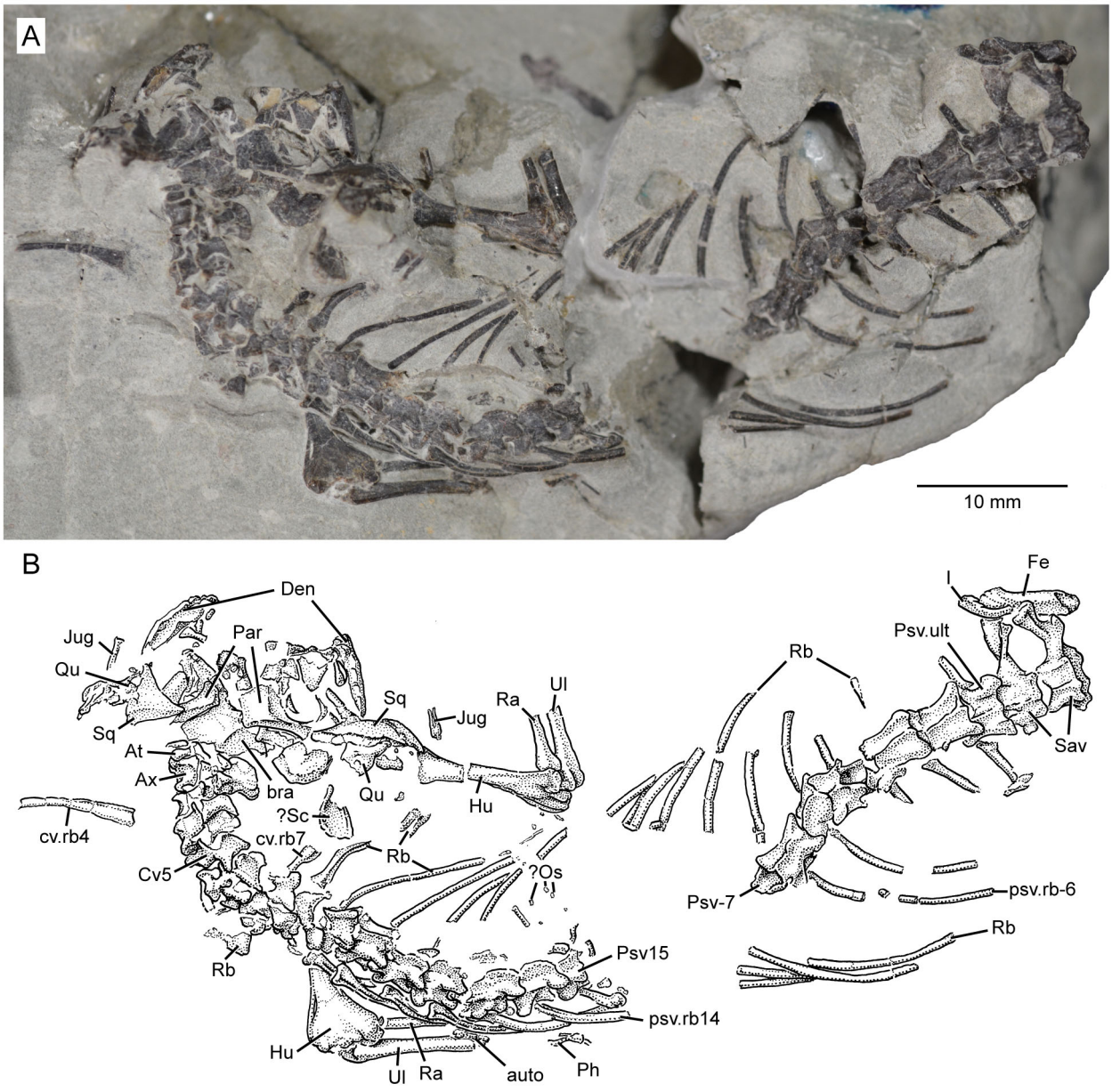

Figure 17. Partial skeleton of the holotype specimen (USNM PAL 722041, 'skeletal block') of *Opisthiamimus gregori* gen. et sp. nov. **A,** digital photograph in dorsal view; **B,** interpretive camera lucida drawing for A. **Abbreviations: At**, atlas or presacral vertebra no. 1; **auto**, autopodium; **Ax**, axis or presacral vertebra no. 2; **bra**, braincase; **Cv5**, cervical or presacral vertebra no. 5; **cv.rb4**, cervical rib no. 4; **cv.rb7**, cervical rib no. 7; **Den**, dentary; **Fe**, femur; **Hu**, humerus; **I**, ilium; **Jug**, jugal; **?Os**, possible osteoderm; **Par**, parietal; **Ph**, phalanx; **Psv15**, presacral vertebra no. 15; **Psv-7**, seventh from last presacral vertebra; **psv.rb14**, presacral rib no. 14; **psv.rb-6**, sixth from last presacral rib; **Psv.ult**, ultimate or last presacral vertebra; **Qu**, quadrate; **Ra**, radius; **Rb**, rib; **Sav**, sacral vertebra; **?Sc**, possible scapula; **Sq**, squamosal; **Ul**, ulna.

the neural spine (*sensu* Fraser 1988). The postzygapophysis is prominent, and its ovate articular surface faces gently ventrolaterally. In cross-section, the lateral face of the neural arch and spine is steep. The neural arch below the zygapophyses is anteroposteriorly short relative to the condition in subsequent presacral vertebrae.

The axis centrum is similarly short and ventrally concave in lateral view. The partially exposed ventral surface exhibits an hourglass shape, due to the concave lateral centrum surfaces. Anteroventrally, the centrum is flattened, slightly wider mediolaterally, and anteriorly convex along its anterior margin. This portion of the

centrum represents the axial (second) intercentrum, which is fused to the axial centrum without evident sutures. In *Sphenodon punctatus*, this fusion occurs in adults (Hoffstetter & Gasc 1969; Jones *et al*. 2009a), but at least in one presumed adult specimen of *Clevosaurus hudsoni* (NHMUK PV R36832), the axis intercentrum is fused not with its centrum but instead with the atlantal centrum (odontoid process; see O'Brien *et al*. 2018, fig. 14d–h). The atlantal centrum is fused to the axial centrum in *Gephyrosaurus bridensis*, as demarcated by a ridge along its dorsal boundary (Evans 1981, fig. 3D). Neither the axial centrum nor the intercentrum bears a transverse process; in *Sphenodon* there are small protuberances that do not support a rib (Hoffstetter & Gasc 1969; Jones *et al*. 2009a).

An isolated, partial and slightly deformed atlas-axis complex (USNM PAL 720479) recovered from screen-washed sediment of the Fox Mesa locality is referred to *Opisthiamimus gregori* on the basis of its similar size and morphology (Fig. 18C–L). This specimen reveals additional features not visible on the type specimen of *O. gregori*. Here, the atlas-axis complex is formed by fusion of the atlantal centrum (odontoid process) with the axial centrum, which in turn (as in the holotype, USNM PAL 722041) is fused with the axial intercentrum anteroventrally. The neural arch and spine of the axis are missing; the arch is broken horizontally at about the level where it contacted the centrum dorsolaterally. Portions of the lateral and ventrolateral surfaces of this element are broken where the atlas and axis centra and axis intercentrum are fused. A short, shallow transverse groove demarcates the dorsal boundary between the atlas and axis centra (Fig. 18C, H); this feature is similar to the dorsal ridge in *Gephyrosaurus bridensis* (Evans 1981, fig. 3D). In dorsal view, the atlas centrum is somewhat arrowhead-shaped, with a broad posterior end that tapers anteriorly to form a bluntly rounded anterior margin. The dorsal surface of the atlas centrum has a bilateral pair of ovoid depressions (Fig. 18C, H); ventrally, it is transversely and longitudinally convex and roughened for articulation with the atlantal intercentrum (Fig. 18D–F, I–K). The posterior cotyle of the axial centrum is slightly deformed by plastic deformation; it is ovoid and deeply amphicoelous (Fig. 18G, L).

Postaxial cervical vertebrae. The neural spines of the five (possibly six) postaxial cervical vertebrae are shorter in dorsoventral height and anteroposterior length than that of the axis (Figs 17, 18A, B). The prezygapophyses are well developed, and a horizontal interzygapophyseal ridge spans the length of the neural arch between the pre- and postzygapophyses. This ridge separates the lateral wall of the neural arch from its more gently sloping roof (Fig. 18A, B).

The centrum of the fourth cervical vertebra (c4) bears a small bony projection on its anterolateral surface, just below the centrum/neural arch boundary (= neurocentral junction), which likely represents a non-rib-bearing diapophysis (Fig. 18A, B); no rib-bearing feature is present in the third cervical vertebra (c3). The fifth cervical vertebra (c5) features the first prominent transverse process; here, the diapophysis is connected to the parapophysis by a narrow ridge of bone, thus forming an anteroposteriorly flattened, lemniscate (∞) synapophysis. The diapophyseal portion spans the neurocentral junction and is situated about midway along the neural arch anteroposteriorly. The parapophyseal portion is set on the lateral side of the centrum just behind the anterior cotyle. In lateral view, the synapophysis is oriented anteroventrally-to-posterodorsally; in dorsal view, it extends a short distance laterally. In the following two (likely three) cervical vertebrae (c6–?c8), the synapophyses become slightly more robust, with a broader bony ridge connecting the diapophysis and parapophysis. In these three vertebrae, the diapophysis is slightly larger than the parapophysis; in c5, they are more equal in size. The synapophyses in c6–?c8 also are more laterally elongate and sequentially begin to migrate slightly higher up onto the lateral side of the neural arch and centrum. Where exposed (c4, c6, ?c8), the accessory process at the posterior base of the neural spine is present but smaller relative to that of the axis. The cervical centra are shorter than those of the dorsal series (e.g. the third and fourth cervical centra are ~1.6 mm and 1.7 mm, respectively, *vs* ~3 mm in the fourth dorsal [12th presacral]). The zygosphene-zygantrum joint is obscured by matrix, tight articulation, or damage along most of the cervical series; however, the left zygantrum of c4 is visible in posterior view and shows a dorsomedially inclined articular surface.

Post-cervical presacral (dorsal) vertebrae. Because of the uncertainty regarding the position of the cervicodorsal junction (i.e. after presacral eight or nine) and in the total number of presacrals (at least two are missing), we count individual vertebrae based on their relative positions anterior or posterior to the missing section of presacral vertebrae (Figs 17, 19). Those anterior to the missing section are counted relative to the atlas (i.e. presacrals 8–15); the seven presacrals posterior to the missing section are counted relative to the last (ultimate) presacral (e.g. sixth from last presacral or Psv-6 in Fig. 19B).

In general, the post-cervical presacral vertebrae differ from the postaxial cervicals in being more elongate anteroposteriorly, having weaker and laterally shorter

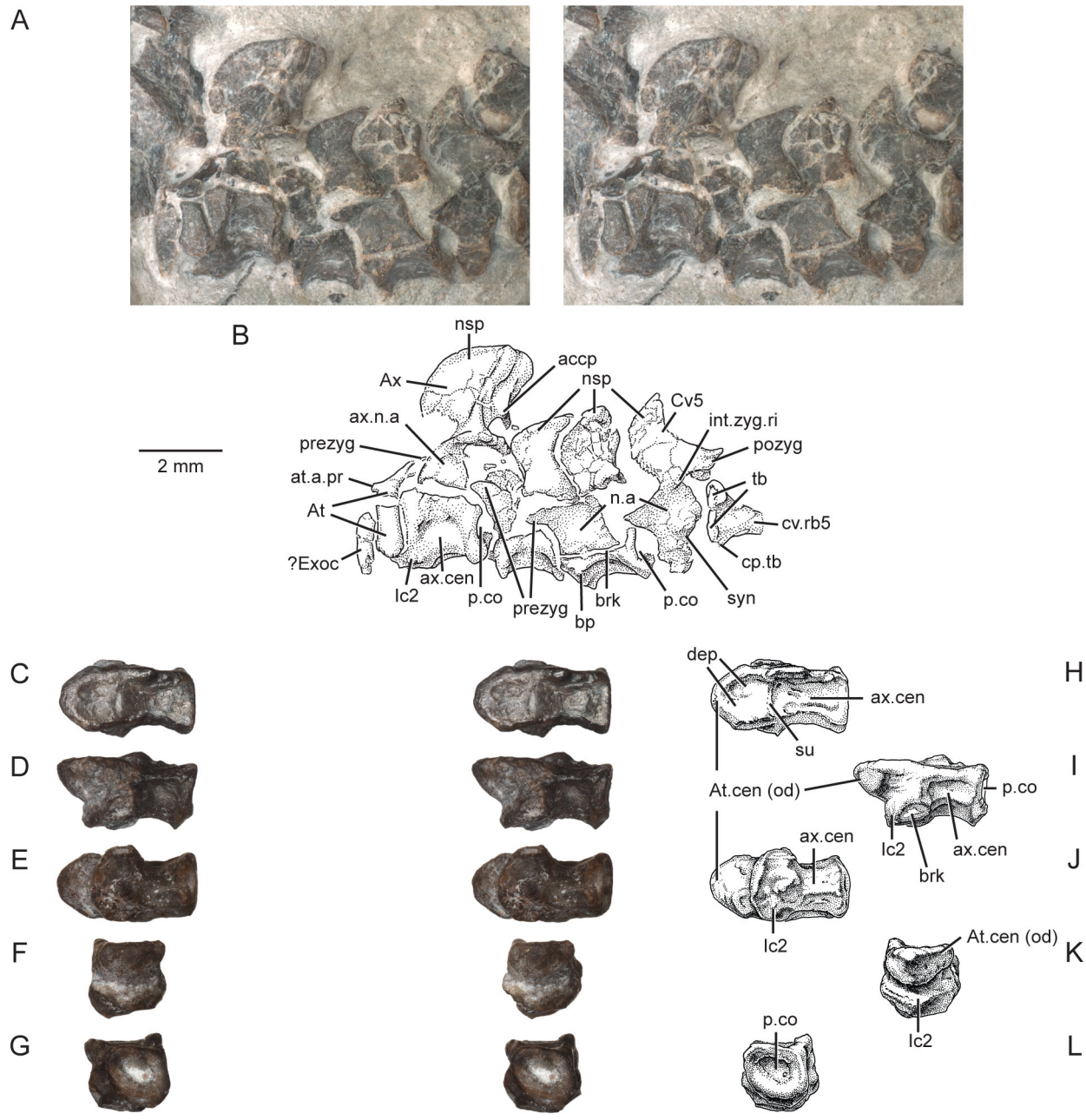

Figure 18. Anterior cervical vertebrae of *Opisthiamimus gregori* gen. et sp. nov. **A,** extended depth of field (EDF) stereophotopair of the anterior cervical series in left lateral view of the holotype specimen (USNM PAL 722041, 'skeletal block'); **B,** interpretive camera lucida drawing for A; **C–G,** EDF stereophotopairs of a referred partial atlas/axis complex (USNM PAL 720479) in **C,** dorsal, **D,** left lateral, **E,** ventral, **F,** anterior and **G,** posterior views; **H–L,** interpretive camera lucida drawings for C–G, respectively. **Abbreviations: accp**, accessory process; **At**, atlas vertebra; **at.a.pr**, anterior process of the atlas; **At.cen (od)**, atlas centrum or odontoid process; **Ax**, axis vertebra; **ax.cen**, centrum of the axis vertebra; **ax.n.a**, neural arch of the axis vertebra; **bp**, bony protuberance; **brk**, break; **cp.tb**, capitular protuberance of the tuberculum; **Cv5**, fifth cervical vertebra; **cv.rb5**, cervical rib no. 5; **dep**, depression; **?Exoc**, possible exoccipital; **Ic2**, second intercentrum; **int.zyg.ri**, interzygapophyseal ridge; **n.a.**, neural arch; **nsp**, neural spine; **p.co**, posterior cotyle; **pozyg**, postzygapophysis; **prezyg**, prezygapophysis; **su**, suture; **syn**, synapophysis; **tb**, tuberculum.

synapophyses, and bearing lower neural arch roofs. Following the trend observed in the cervical vertebrae, the synapophysis continues to migrate up the lateral wall until it is completely placed on the side of the neural arch; this transition occurs around presacral 14 (Fig. 19A). At this point in the dorsal series, the

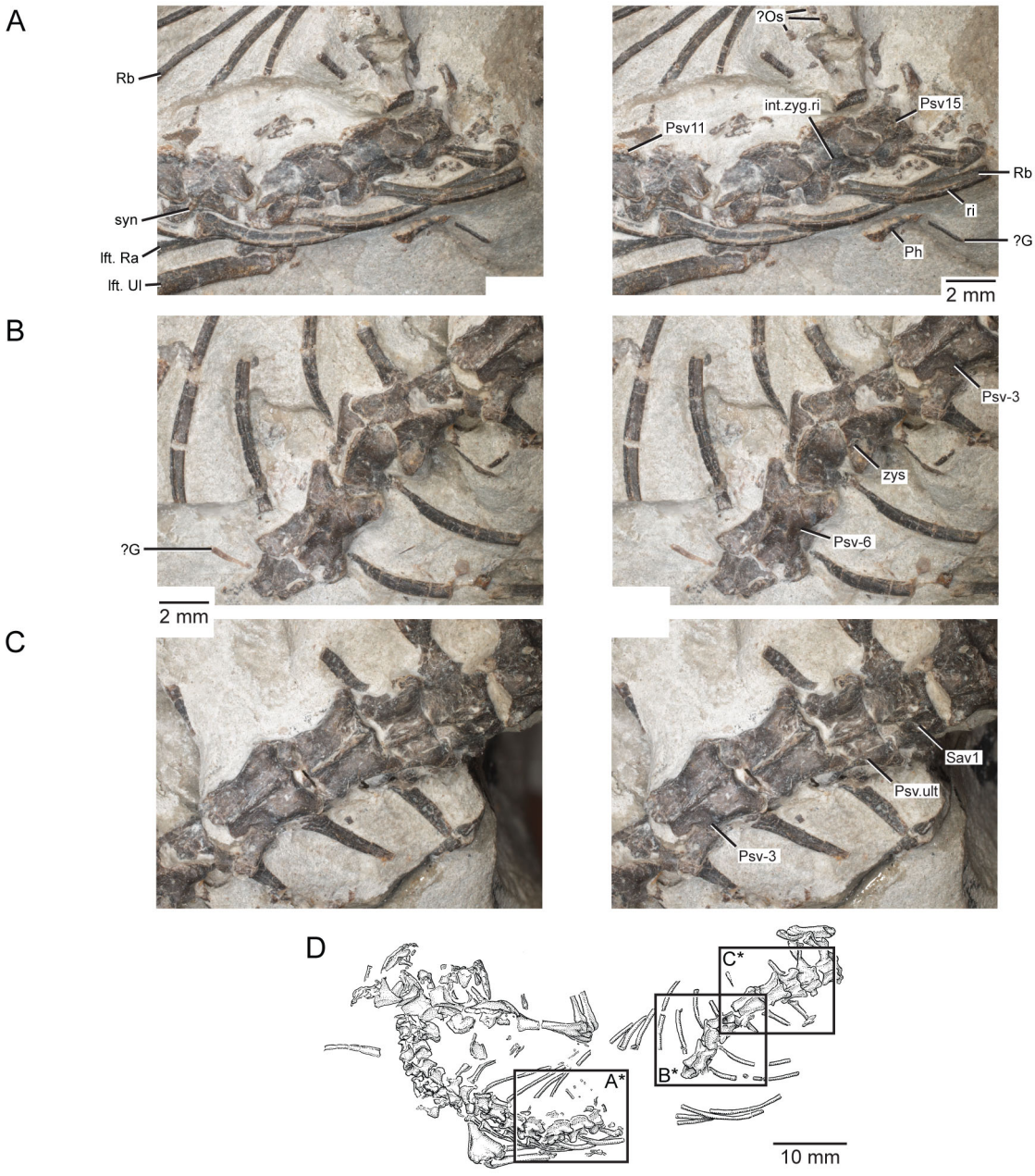

Figure 19. Presacral and sacral vertebrae of the holotype specimen (USNM PAL 722041, 'skeletal block') of *Opisthiamimus gregori* gen. et sp. nov. **A,** extended depth of field (EDF) stereophotopair of presacral vertebrae 11 to 15 in dorsal view; **B,** EDF stereophotopair of the seventh to third from last presacral vertebrae in dorsal view; **C,** EDF stereophotopair of the posterior-most four presacral vertebrae and the sacral vertebrae in dorsal view; **D,** camera lucida drawing of the skeleton in dorsal view with boxes labeled A*, B*, and C* indicating the regions shown in A–C, respectively. **Abbreviations: ?G**, possible gastralium; **int.zyg.ri**, interzygapophyseal ridge; **lft.Ra**, left radius; **lft.Ul**, left ulna; **?Os**, possible osteoderm; **Ph**, phalanx; **Psv11**, presacral vertebra no. 11; **Psv15**, presacral vertebra no. 15; **Psv-3**, third from last presacral vertebra; **Psv-6**, sixth from last presacral vertebra; **Psv.ult**, ultimate or last presacral vertebra; **Rb**, rib; **ri**, ridge; **Sav1**, sacral vertebra no. 1; **syn**, synapophysis; **zys**, zygosphene.

synapophysis joins with the interzygapophyseal ridge dorsally. The synapophyses in some of the posterior dorsals are shallowly inclined and canted more posteriorly (e.g. sixth from last presacral *vs* presacrals 10–15; Fig. 19B *vs* Fig. 19A). In some of the presacral vertebrae (e.g. presacral 12; Fig. 19A), a faint, horizontal and slightly sinuous ridge occurs at about the level where the neural arch meets the centrum. This feature possibly

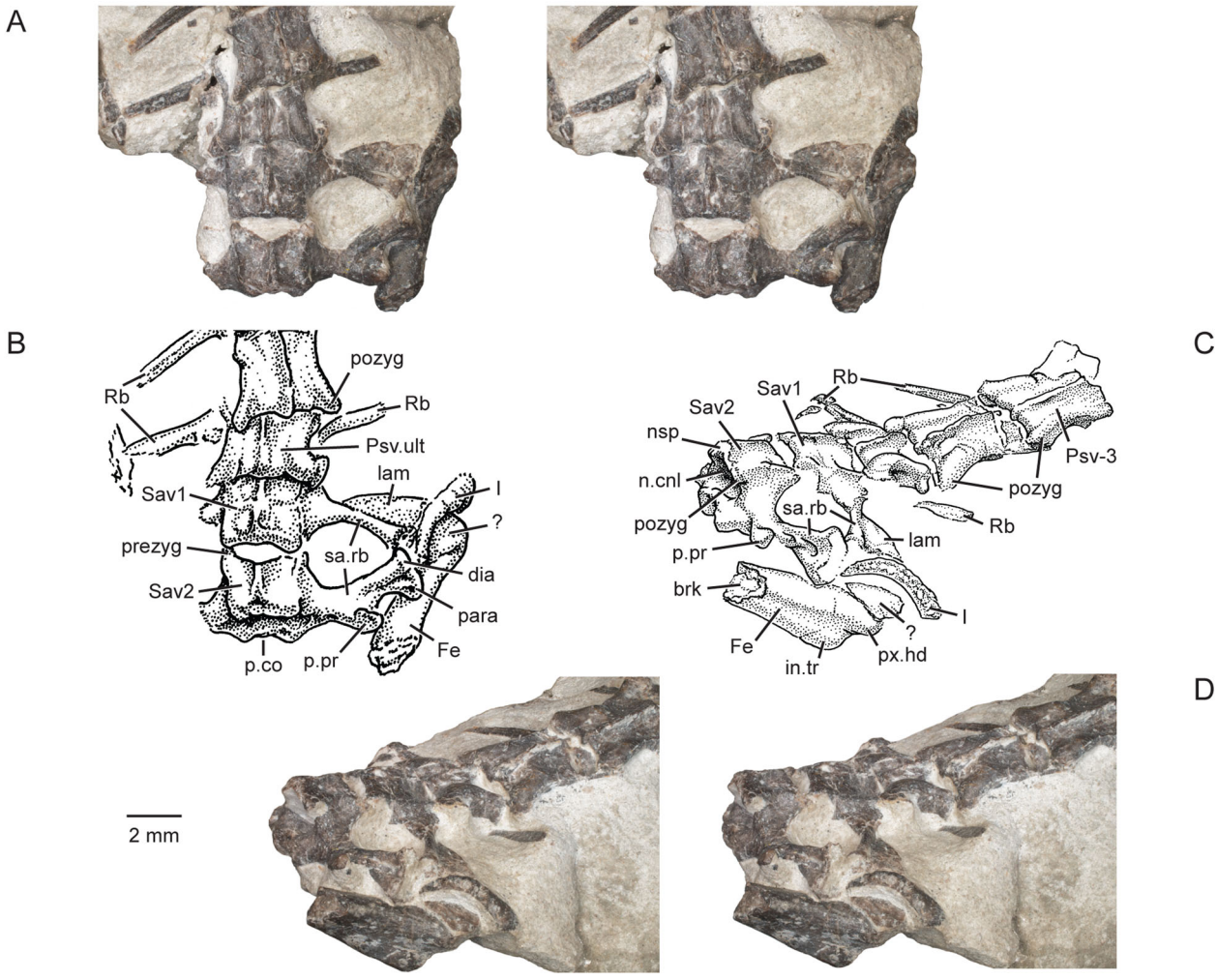

Figure 20. Sacral vertebrae of the holotype specimen (USNM PAL 722041, 'skeletal block') of *Opisthiamimus gregori* gen. et sp. nov. **A,** extended depth of field (EDF) stereophotopair of the posterior-most presacral and sacral vertebrae in dorsal view; **B,** interpretive camera lucida drawing for A; **C,** interpretive camera lucida drawing for D; **D,** EDF stereophotopair of the posterior-most presacral and sacral vertebrae in posterolateral and dorsal views. **Abbreviations: brk**, break; **dia**, diapophysis; **Fe**, femur; **I**, ilium; **in.tr**, internal trochanter; **lam**, lamina; **n.cnl**, neural canal; **nsp**, neural spine; **p.co**, posterior cotyle; **p.pr**, posterior process; **para**, parapophysis; **pozyg**, postzygapophysis; **prezyg**, prezygapophysis; **Psv-3**, third from last presacral vertebra; **Psv.ult**, ultimate or last presacral vertebra; **px.hd**, proximal head; **Rb**, rib; **sa.rb**, sacral rib; **Sav1**, sacral vertebra no. 1; **Sav2**, sacral vertebra no. 2; **?**, unidentified bone.

represents a remnant neurocentral suture. In dorsal view, the dorsolateral outline of the neural arch spanning the pre- and postzygapophyses and along the interzygapophyseal ridge of the anterior dorsal vertebrae is less laterally concave relative to the outline in the posterior dorsals (e.g. tenth presacral *vs* sixth from last presacral; Fig. 17 *vs* Fig. 19B). The anterior dorsals also have a more steeply vaulted neural arch and a slightly broader-based neural spine. Zygosphenes and zygantra are hard to discern on many of the vertebrae due to damage or articulation, but the former are clearly visible in at least the fourth from last presacral (Fig. 19B). In this vertebra, the zygosphene is small, dorsolaterally directed, and continuous with the prezygapophyseal articulation and located just up the lateral surface of the neural arch (e.g. see character 468, state 1 in Gauthier *et al*. 2012).

Sacral vertebrae. There are two slightly disarticulated and partially damaged sacral vertebrae (Figs 17, 19C, 20). The left sacral ribs are broken off laterally at slightly less than midlength; those on the right are well preserved. The centrum of the first sacral is hidden by matrix, but the second sacral centrum is partially exposed posteriorly (Fig. 20B–D). Relative to the posterior dorsals, the sacrals have anteroposteriorly shorter neural arches, postzygapophyses that lack dorsal

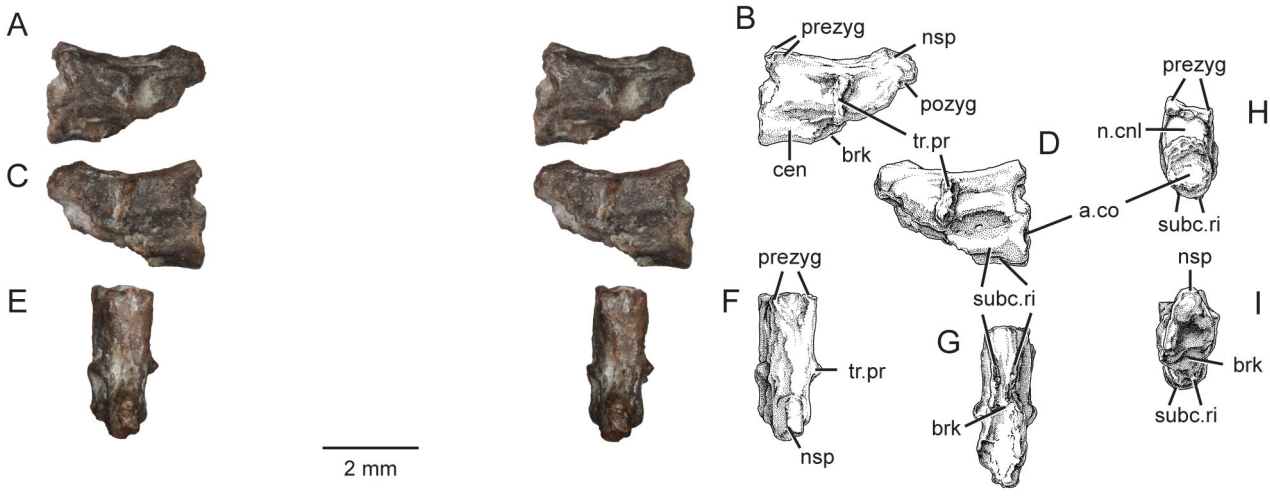

Figure 21. Caudal vertebra of the holotype specimen (USNM PAL 722041) of *Opisthiamimus gregori* gen. et sp. nov. **A,** extended depth of field (EDF) stereophotopair in left lateral view; **B,** interpretive camera lucida drawing of A; **C,** EDF stereophotopair in right lateral view; **D,** interpretive camera lucida drawing of C; **E,** EDF stereophotopair in dorsal view; **F,** interpretive camera lucida drawing of E; **G–I,** interpretive camera lucida drawings in **G,** ventral, **H,** anterior and **I,** posterior views. **Abbreviations: a.co**, anterior cotyle; **brk**, break; **cen**, centrum; **n.cnl**, neural canal; **nsp**, neural spine; **p.co**, posterior cotyle; **pozyg**, postzygapophysis; **prezyg**, prezygapophysis; **subc.ri**, subcentral ridge; **tr.pr**, transverse process.

swelling, and straight to gently concave dorsolateral margins in dorsal view. The prezygapophyses of the first sacral are similar in size to those of the posterior dorsals. Conversely, its postzygapophyses are much smaller, as are the corresponding prezygapophyses of the second sacral. The postzygapophyses of the second sacral also appear small, but some morphological details are obscured by damage to its posterior margin. The presence of a zygosphene in the first sacral could not be determined due to its tight articulation with the last dorsal. In the second sacral, the zygosphene appears absent on the left side and only weakly developed on the right. The accessory process below the neural spine posteriorly is poorly developed in the first sacral. The sacral ribs are fused to their respective vertebra with no indication of a suture. The neural spine of each sacral vertebra extends anteroposteriorly along the length of the neural arch; they are broken near the base and, therefore, their height could not be determined. Although the centrum of the second sacral vertebra is damaged along the perimeter of its posterior cotyle, it is clearly more dorsoventrally compressed relative to those of the presacral series and similar to the condition observed in *Planocephalosaurus robinsonae* (Fraser & Walkden 1984, text-fig. 8) (Fig. 20C, D).

Caudal vertebra. A single, partial caudal vertebra was found in the weathered matrix immediately surrounding the skeleton (Fig. 21). Its size is appropriate for it to have been derived from the same individual as USNM PAL 722041. The specimen is slightly plastically deformed and missing the posterior half of the centrum, the top of the neural spine, and portions of the zygapophyses. The vertebra is elongate anteroposteriorly (Fig. 21A–G), with a concave and laterally compressed, ovoid anterior cotyle (Fig. 21H). On the preserved anterior half of the centrum are a pair of parallel ridges that extend anteroposteriorly along its ventrolateral surface (Fig. 21D, G–I). The ventral margins of these ridges are situated above the ventral rim of the anterior cotyle. The neural spine is placed on the posterior half of the neural arch and has a low, short crest along its anterior half. The prezygapophyses are small, closely spaced mediolaterally, and do not extend laterally beyond the sides of the neural arch (Fig. 21E, F, H). The better preserved right prezygapophysis is chipped anteriorly but would have extended only a short distance beyond the anterior margin of the anterior cotyle. The articular facets of the prezygapophyses face mostly medially and would have clasped the postzygapophyses of the preceding caudal vertebra at the base of its neural spine ventrolaterally. The transverse process is situated at anteroposterior midlength on the lateral side of the neural arch (Fig. 21A–G). It is short dorsoventrally and mediolaterally and is either oriented nearly vertically (left side) or slanted gently anterodorsally/posteroventrally (right side). No autotomic septum (fracture plane) was observed. Combined, these features indicate that this caudal vertebra is from the distal half of the tail.

Cervical ribs. We could recognize 35 presacral ribs (20 left and 15 right; Fig. 17). Most are slightly

disarticulated from their corresponding vertebra and have rotated to expose either their posterior or anterior sides. Lying left of centra c3 and c4 is a cervical rib with its posterior side exposed (Fig. 17). Although missing its extreme distal end, it has relatively shortened proportions. The proximal half of this rib is extremely flat and thin, with a slightly chipped but equally thin head that might bear a weakly developed articular facet. The distal half of this rib is elliptical in cross-section, nearly parallel sided but slightly expanded at its distalmost end, and gently curved ventrolaterally. It likely represents the fourth cervical rib given its relatively small, gracile nature and weak or absent articular facet; it may have had a ligamentous connection with the weakly developed rib articulation of c4 (see above; Fig. 18A, B).

The proximal ends of the fifth (and possibly sixth) left cervical ribs feature a well-developed, waisted tuberculum and a rudimentary capitular protuberance (Fig. 18A, B) much like in some of the anterior cervical ribs of *Gephyrosaurus bridensis* (e.g. Evans 1981, fig. 12d, e) and *Planocephalosaurus robinsonae* (e.g. Fraser & Walkden 1984, text-fig. 11a). The flattened bone just lateral to the fifth left cervical rib possibly represents the distal end of a right cervical rib; it is parallel-sided, slightly curved, and bluntly rounded at the exposed (distal?) end. As exposed, the seventh right cervical rib is largely nondescript (Fig. 17).

Post-cervical presacral ribs. Excluding the ribs of the last four presacral vertebrae, the remaining ribs beginning at presacral eight are relatively elongate and gently curved (Figs 17, 19A, B). The exposed holocephalous rib heads (tuberculum only) of presacrals 10 and 12 are compressed anteroposteriorly and slightly waisted at mid-height. They are more gracile than the preceding rib heads (excluding cervical rib four), which match the weaker synapophyses of their corresponding vertebra. For about half their proximal length, most presacral ribs have a well-developed ridge that extends along their posterolateral margin, demarcating a costal groove that would have housed the posterior intercostal neurovasculature (Fig. 19A). Distally, these ribs become mediolaterally compressed and their tips are gently expanded anteroposteriorly. No apophyses (*sensu* Günther 1867) or uncinate processes (*sensu* Hoffstetter & Gasc 1969) were identified with certainty (but see below). The last four presacral ribs are relatively short and straight (Figs 17, 19B, C, 20A, B). In the last two presacrals, the rib slightly tapers distally, and the distal end is extremely thin dorsoventrally. None of the ribs in these last four presacrals appear fused with the vertebra but damage and/or matrix has made it difficult to confirm the presence or absence of this feature.

Sacral ribs. The first sacral rib extends away from the neural arch along a gentle ventrolateral slope; the second rib extends more laterally (Fig. 20). The base of each sacral rib is broad and becomes narrower at slightly less than mid-length. Beyond the midpoint laterally, the first sacral rib produces a thin horizontal lamina anteriorly; its posterior margin is thicker and tubular. At about mid-length on the posterior margin of the second sacral rib is a moderately developed posterior process, which extends a short distance posterolaterally; its posterior face is oriented slightly dorsally. This process is connected to the base of the synapophysis by a dorsoventrally thin horizontal lamina. Laterally, the sacral ribs are expanded to broadly contact the ilium medially (Fig. 20C, D). Much like in *Sphenodon* (e.g. Hoffstetter & Gasc 1969, fig. 30), the expanded lateral end of the first sacral rib is oriented more horizontally *vs* more vertically in the second. The articular surface of the first sacral rib is largely obscured by matrix and the ilium but appears to have a thicker posterolateral end. The end of the second rib is holocephalous with minor anteroposterior constriction between the diapophysis and parapophysis. As preserved, the first and second sacral ribs are slightly separated from each other laterally and may not have contacted each other in life (Fig. 20A).

?Gastralia. Several small, rod-like bones are scattered around the region of the mid-dorsal vertebrae and ribs (Fig. 19A, B). Most are preserved ventral to the vertebrae and ribs, indicating they are likely gastralia, although it is possible that some or all of these bones might represent disarticulated uncinate processes of the dorsal rib series or inscriptional ribs (e.g. Etheridge 1965).

Postcranial appendicular skeleton

Pectoral girdle. Most elements of the pectoral girdle are either absent or unrecognizable. We have tentatively identified only the right scapula and interclavicle.

?Scapula. A moderately thin, plate-like bone is preserved approximately where the right scapula should be anatomically: medial to the proximal end of the right humerus and lateral to presacral vertebrae seven and eight (Fig. 17). The medial-facing edge of this bone (orientation relative to the vertebrae) is abraded and chipped. Extending atop the posterior margin of the bone is a short and narrow ridge that disappears near the abraded end. Adjacent to this ridge the dorsal surface of the bone is flat. The anterior side curves anterolaterally, which might reflect *post mortem* bending of the bone if it is a scapular blade. In other rhynchocephalians (e.g. *Sphenodon punctatus*, *Clevosaurus hudsoni*) the scapular blade is mostly planar.

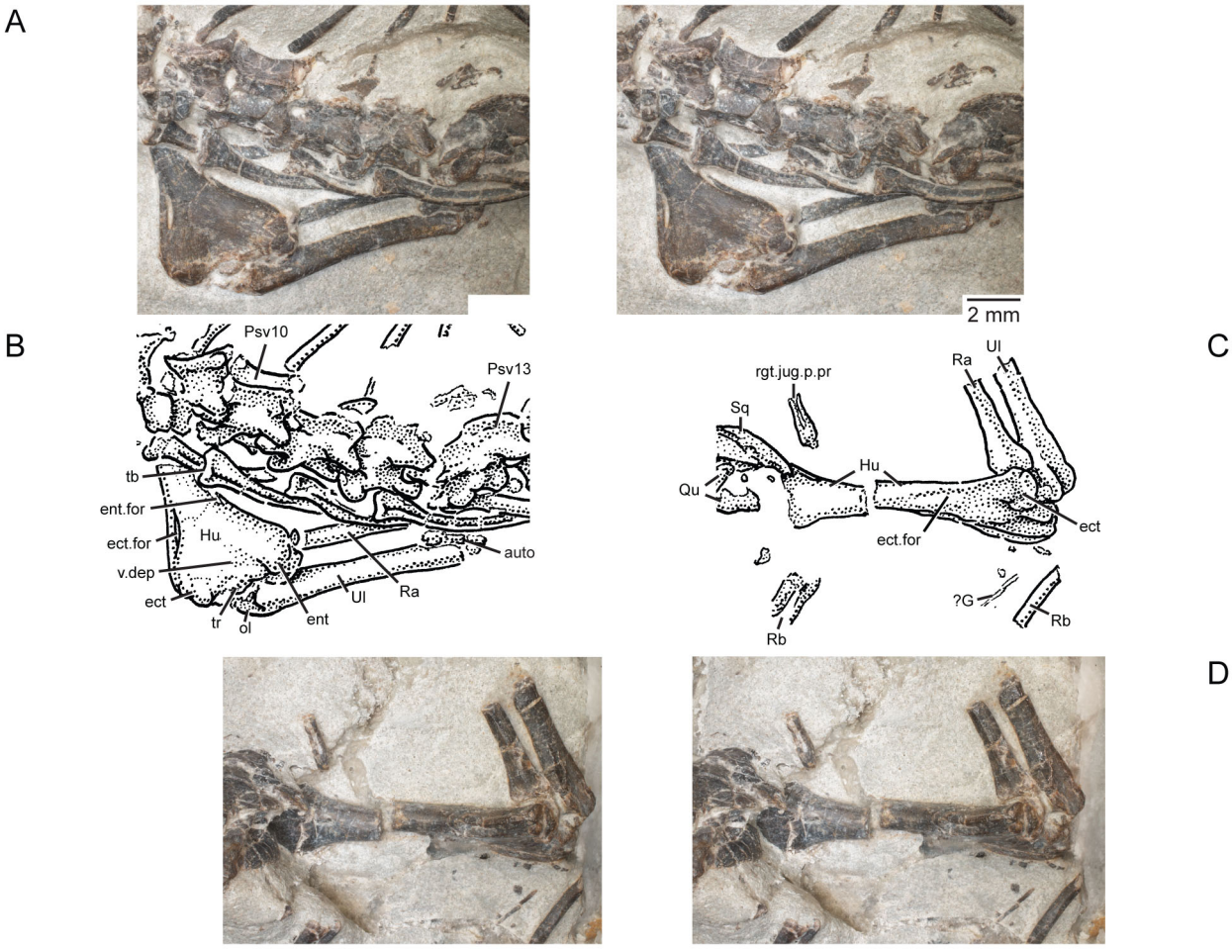

Figure 22. Forelimbs and a portion of the axial skeleton of the holotype specimen (USNM PAL 722041, 'skeletal block') of *Opisthiamimus gregori* gen. et sp. nov. **A,** extended depth of field (EDF) stereophotopair of the exposed left forelimb and several presacral vertebrae and associated ribs in dorsal view; **B,** interpretive camera lucida drawing for A; **C,** interpretive camera lucida drawing for D; **D,** EDF stereophotopair of the exposed right forelimb and adjacent bones of the skull in dorsal view. Anterior is to the left in A and B and towards the top in C and D. **Abbreviations: auto**, autopodium; **ect**, ectepicondyle; **ect.for**, ectepicondylar foramen; **ent**, entepicondyle; **ent.for**, entepicondylar foramen; **?G**, possible gastralia; **Hu**, humerus; **ol**, olecranon process; **Psv10**, presacral vertebra no. 10; **Psv13**, presacral vertebra no. 13; **Qu**, quadrate; **Ra**, radius; **Rb**, rib; **rgt.jug.p.pr**, posterior process of the right jugal; **Sq**, squamosal; **tr**, trochlea; **tu**, tuberculum; **Ul**, Ulna; **v.dep**, 'V'-shaped depression.

Interclavicle. We tentatively identify a 'T'-shaped bone located ventral to the braincase and anterior cervical series (made visible via our crude 3D reconstruction of the skeletal block) as the interclavicle. It has an elongate posterior process and anterior crossbar, each arm of which tapers laterally. The posterior process appears to be dorsoventrally flattened along its length.

Humerus. Our description of the humerus follows the figured anatomical orientations of a restored right humerus of *Clevosaurus hudsoni* (Fraser 1988, fig. 29). Both humeri are preserved in contact with their corresponding radius and ulna (Figs 17, 22). The proximal half of the left humerus is hidden under the posterior cervical and anterior dorsal vertebrae; its distal end is exposed in dorsal aspect (Fig. 22A, B). Most of the length of the right humerus is exposed except for the head, which is hidden below the right quadrate and squamosal (Fig. 22C, D). At about midshaft, the right humerus is broken and offset transversely. The distal end is slightly crushed anteroposteriorly, and a minor fracture extends through the bone, but there is no displacement; similar fracturing has occurred with the humeral head. As exposed, the anterior surface of the head faces up, and the ventral and dorsal surfaces of the distal end face posteriorly and anteriorly, respectively, relative to the orientation of the skull.

The proximal and distal ends of the humerus are expanded dorsoventrally and anteroposteriorly, respectively. The distal end is twisted relative to the proximal end. Despite the coarse resolution of our μCT scan of the skeletal block, we were able to identify the robust, anteroposteriorly flattened proximal ends of both humeri. A well-developed deltopectoral crest extends along the posteroventral margin of the humerus proximally, similar to that observed in e.g. *Clevosaurus hudsoni* (Fraser 1988, fig. 29b; O'Brien *et al*. 2018, fig. 11a, c). The humeral shaft is rounded in cross-section.

The distal end of the humerus is asymmetrical, with a well-developed and slightly larger entepicondyle relative to the ectepicondyle (Fig. 22A, B). A shallow, inverted-'V'-shaped depression sits on the dorsal surface between these condyles. The entepicondyle extends at a greater angle away from the main axis of the shaft than does the ectepicondyle. In dorsal view, the better-preserved left distal end reveals two slit-like foramina, a posteriorly placed entepicondylar foramen and an anteriorly placed ectepicondylar foramen; the former opens mostly posteriorly whereas the latter opens more dorsally (Fig. 22A, B). On the right humerus, the dorsal and ventral ectepicondylar foramina communicate obliquely through the bone via a passage that would have housed the radial nerve and associated vessels (Fig. 22C, D). The ventral entepicondylar foramen is not exposed in either humerus but is visible via μCT slices and 3D segmentation. A distally rounded trochlea between the ectepicondyle and entepicondyle articulates with the left ulna (Fig. 22A, B). The left capitellum (visible via μCT slices and 3D segmentation) is moderately expanded relative to the well-developed one in *Sphenodon punctatus* and articulated with the radius. The distal-most end of the ectepicondyle is broken off on the right humerus, and a rounded capitellum is partially exposed; the trochlea appears to be missing. The distal epiphyses appear well ossified with the rest of the humerus in both forelimbs (Fig. 22A, B).

Radius. Both radii are preserved (Fig. 17). The shaft of the left is partially exposed between the left humeral entepicondyle and the two left ribs adjacent to presacral vertebra 12 (Fig. 22A, B) The right radius is mostly exposed but broken at about mid-length to reveal a subrounded cross-section (Fig. 22C, D). Its proximal half is preserved on the skeletal block and its distal half on the hand block (Fig. 17 and Fig. 23A–C, respectively). A faint ridge extends from the proximal end distally along the lateral surface of the shaft, disappears along the midshaft, and re-occurs more prominently near the distal end. The proximal end is expanded to about twice the width of the shaft; the distal end is slightly less expanded. The proximal and distal articular ends are obscured by articulation and damage, respectively. The ratio of the proximodistal length of the right radius relative to the right humerus (as measured in 3D Slicer) is 0.65 (i.e. 8.06 mm/12.4 mm, respectively; Supplemental material, Table S1).

Ulna. Both ulnae are preserved and exposed similarly to the radii. The ulna is longer and more robust than the radius (Figs 22, 23), with an elliptical midshaft cross-section (as revealed by the broken right ulna). The lateral surface of the shaft bears a faint longitudinal ridge that may represent the attachment of the interosseous membrane. Both the proximal and distal ends are expanded relative to the shaft. The olecranon process is short proximodistally and bluntly rounded proximally (Fig. 22). Using 3D Slicer, we combined measurements of the proximal and distal portions of the right ulna to estimate a total length of 8.16 mm (Supplemental material, Table S1). The distal end of the right ulna is broadly rounded along its articular margin but somewhat crushed dorsoventrally.

Carpus and manus. Both forelimb autopodia (i.e. manus and carpi) are partially preserved, with several fractures propagating through many of the elements of the right manus (Fig. 23A–C). The left autopodium is largely hidden underneath several ribs and vertebrae at the distal end of the left forearm; a small, rounded element and a few other partially exposed bones likely represent carpal and/or manual elements (Figs 17, 19A, 22A, B). Our coarse 3D reconstruction of the skeletal block confirms the presence of several left metacarpals and phalanges in articulation. Similarly, a short distance away (∼1 cm) from these, and past the missing section of vertebrae, are two disarticulated, crisscrossing manual phalanges (presumably left); these are hidden by matrix below the four isolated and overlapping ribs to the left anterior of the sixth and seventh presacral vertebrae from the sacrum. The right autopodium – including at least two carpals, five metacarpals and 12 partial to complete phalanges – is exposed in palmar (ventral) view in the hand block (Fig. 23A, B).

Between and distal to the radius and ulna on the palmar side of the hand is an ovoid, moderately flat bone that is likely the intermedium based on its resemblance to that bone in *Sphenodon punctatus* (Fig. 23A, B *vs* Fig 23D, E). The larger carpal bone lying dorsal to the distal end of the ulna and just proximal to metacarpal IV is interpreted as distal carpal 4 based on its relative position, rounded cuboid shape, and similarity in size to distal carpal 4 of *S. punctatus* (Fig. 23C *vs* Fig. 23D, E). The smaller carpal, which is broken into dorsal and ventral halves, lies just proximal to distal carpal 4 and towards the centre of the carpus; it most likely

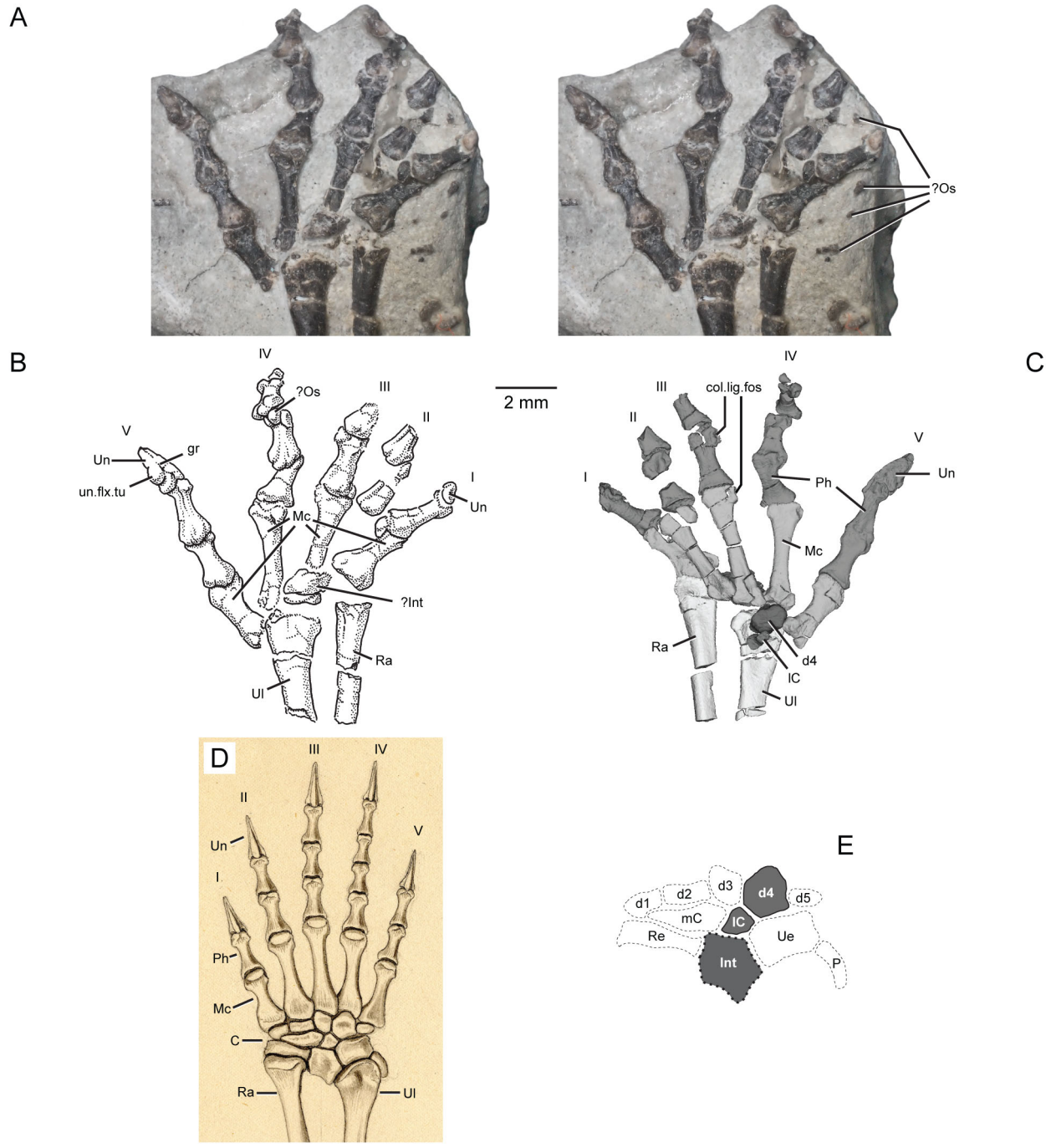

Figure 23. Distal radius and ulna, carpus and manus of the holotype specimen (USNM PAL 722041, 'hand block') of *Opisthiamimus gregori* gen. et sp. nov. (**A–C**) and *Sphenodon punctatus* (**D, E**). **A,** extended depth of field stereophotopair of the right distal forearm, carpus and manus in ventral (palmar) view; **B,** interpretive camera lucida drawing for A; **C,** virtual three-dimensional rendering of the right distal forearm, carpus and manus in dorsal view; **D,** left distal forearm, carpus and manus (reflected for ease of comparison) in dorsal view; **E,** carpus based on *S. punctatus* in D showing which elements are likely preserved in *O. gregori* (dark grey). The solid lines represent the carpals that most likely are present; the thick dashed line represents the presence only tentatively. The illustration in D is from an original, unpublished inkwash and pencil drawing made for O. C. Marsh in March, 1886 (artist unknown), and housed in the Department of Paleobiology collections at the NMNH. **Abbreviations: C**, carpus; **col.lig.fos**, collateral ligament fossa; **d1–d5**, distal carpals one to five; **gr**, groove; **I–V**, digits one to five; **?Int**, possible intermedium; **lC**, lateral centrale; **mC**, medial centrale; **Mc**, metacarpal; **?Os**, possible osteoderm; **P**, pisiform; **Ph**, phalanx; **Ra**, radius; **Re**, radiale; **Ue**, ulnare; **Ul**, ulna; **Un**, ungual; **un.flx.tu**, flexor tubercle of the ungual.

represents the lateral centrale (Fig. 23C, E). Slight dorsoventral compression has plastically deformed the metacarpals and phalanges, particularly at their proximal and distal ends. The preserved (but incomplete) phalangeal formula of the right manus is 2:2:2:3:3; evidence from the partially 3D-reconstructed left manus reveals at least one additional distal phalanx in digit III for a more complete formula of 2:2:3:3:3. Only the right digit V has an intact ungual. Assuming digit I had only two phalanges as in *S. punctatus* (phalangeal formula = 2:3:4:5:3; Günther 1867), then the broken piece of bone at the distal end of its first phalanx represents the proximal end of the ungual (Fig. 23A, B). We can also assume that unguals were present on all the digits, giving a minimum complete phalangeal formula of 2:3:4:4?:3.

The five metatarsals vary in relative size and are more elongate proximodistally when compared to their corresponding phalanges. Metatarsal III is the longest, followed by II and IV, which are sub-equal in length. Metatarsals I and V are the shortest and broadest. This pattern is similar to that observed in *Sphenodon punctatus* (Fig. 23D). The proximal and distal ends of the metatarsals are expanded transversely, and the shafts are slender with elliptical cross-sections. On each side of the distal end is an ovoid collateral ligament fossa (Fig. 23C). The ventral surface of the metatarsal bears a broadly 'U'-shaped, distally expanded depression. The articular distal end of each metatarsal is nearly single headed (with the medal and lateral edges only very weakly distinguishable) and gently convex distally, where it fits into the concave proximal end of the adjoining first phalanx.

The phalanges are broadly similar to those of other reptiles, with more distinctive medial and lateral distal condyles than the metatarsals. The nearly complete ungual phalanx of digit V is laterally compressed (Fig. 23A–C). It has a well-developed, bulbous ventral flexor tubercle positioned distal to the articular surface and separated from it by a sulcus. In lateral view, the ungual tapers to a point as it curves gently downward distally. A single vascular groove is visible on the lateral surface.

Pelvic girdle. Very little of the pelvic girdle is preserved except for part of the right iliac acetabular region and possibly a piece of the right ischium (Figs 17, 20). The ilium is broken horizontally through the top of the acetabulum, which is laterally concave to accept the head of the femur. The presumed partial ischium is a flat, otherwise nondescript piece of bone with jagged broken edges; it is preserved below the second sacral vertebra (not figured).

Femur. The proximal end of a right femur is preserved in the skeletal block, articulated with the acetabular portion of the right ilium (Figs 17, 20). As preserved, the femur is oriented parallel to the main axis of the vertebral column. A well-developed internal trochanter is observed ventral to the femoral head. Distal to the internal trochanter and where the specimen is broken, the shaft has a triangular cross-section.

Pedal? phalanx. A broken phalanx found in the weathered matrix immediately surrounding USNM PAL 722041 might belong to this individual. It is presumably from the pes but exhibits no phylogenetically informative morphology.

?Osteoderms. A small, cuboid bone with rounded edges is preserved on the palmar side of the right manus at the joint between the second and third phalanges of digit IV (Fig. 23A, B). This element was recently identified as a sesamoid bone by us in an abstract (DeMar *et al.* 2018), but here it is tentatively reidentified as a possible osteoderm. In *Sphenodon punctatus*, sesamoids of the manus are typically found at the distal end of the penultimate phalanges dorsally (i.e. penultimate phalangeal sesamoid bones or 'Sesamoidea digitorum manus'), whereas none occur on the palmar side (Regnault *et al.* 2017). Although distal metacarpal sesamoids are found in some lizards (Gauthier *et al.* 2012; Otero & Hoyos 2013), these do not occur between the phalanges but at the distal end of the metacarpals. Other similar-sized specks of bone resembling the one in digit IV are exposed at the surface near the right manus (Fig. 23A) and throughout the matrix surrounding parts of the skeleton (Figs 17, 19A). This observation, in addition to the bone's unusual position in digit IV, further suggest it is not a sesamoid. Instead, these small, scattered bones might represent osteoderms like those preserved in *Pamizinsaurus tlayuaensis* from the Early Cretaceous of Mexico (Reynoso 1997).

Other bones. Several highly incomplete postcranial and unidentifiable elements were collected from the weathered matrix associated with USNM PAL 722041. These include parts of vertebrae, ribs and possibly hind limb bones. None provide any noteworthy morphological information.

Potential non-topotypic material of *Opisthiamimus gregori*

Our review of the literature revealed only one likely and one tentative example of non-topotypic material of *Opisthiamimus gregori* gen. et sp. nov. from the Morrison Formation. The likely first example is a nearly complete left dentary (unnumbered LACM specimen;

Kirkland 2006, fig. 22J) referred to *Opisthias* sp. from Jim's Place Quarry (LACM locality 5574) in the Fruita Paleontological Area (FPA) near Fruita, Colorado (Fig. 1, locality 5; see also 'Fruita Main' localities in Foster 2003, fig. 6). This specimen is only slightly larger than the holotype dentary of *O. gregori* (tooth row length ~13.2 mm *vs* 11.4 mm, respectively), is similar in overall shape, and possesses one autapomorphy of *O. gregori*: two broadly spaced, non-hypertrophied dentary successional caniniform teeth, with the mesial caniniform positioned at the anterodorsal tip of the dentary (symphyseal). Other similarities include (1) distal additional teeth (as observed in lingual view) are non-overlapping, appear smooth without prominent grooves and ridges, and possess mesiolingual crests; (2) presence of a mesial notch above the dentary symphysis; and (3) presence of a poorly developed mentonian process. The tentative second example of *O. gregori* (also from Jim's Place Quarry) is the anterior portion of a left dentary (LACM 135516; Apesteguía 2008, fig. 65D), with a similarly spaced and positioned pair of non-hypertrophied caniniforms (for more discussion, see Supplemental material). If either of these specimens represent *O. gregori*, then the palaeobiogeographical range for this taxon would extend from north-central Wyoming to west-central Colorado. For additional comparisons with other Morrison specimens including several showing similarities with *O. gregori* but variably attributed to *Opisthias* (e.g. *Opisthias* sp., cf. *Opisthias* sp.) or to putative new taxa, see the Supplemental material.

Phylogenetic analysis results

Using maximum parsimony, our cladistic analysis recovers *Opisthiamimus gregori* gen. et sp. nov. within Eusphenodontia (Fig. 24A), as the sister taxon to a clade including all species of *Clevosaurus* and Neosphenodontia. This result effectively equates *Clevosaurus* to Clevosauridae given the definition of Hsiou *et al*. (2015, p. 4), where Clevosauridae is defined as "all taxa more closely related to *Clevosaurus* than to *Sphenodon*". Here, Neosphenodontia includes *Brachyrhinodon taylori*, *Colobops noviportensis* and a diverse clade including *Sphenodon punctatus*, Eilenodontinae, Pleurosauridae, Saphaeosauridae and other related taxa. *Polysphenodon mulleri*, from the Late Triassic of Germany (previously recognized as sharing affinity with 'clevosaurs'; e.g. Reynoso 1996), is recovered as the basal-most taxon within Eusphenodontia. *Brachyrhinodon taylori*, from the Triassic of Scotland, UK (also previously recognized as sharing affinity with 'clevosaurs'; e.g. Reynoso 1996, Chambi-Trowell *et al.* 2021), is recovered within Neosphenodontia as the sister taxon to all other neosphenodontians. The Late Triassic *C. noviportensis* from Connecticut, USA (previously described as a possible rhynchosaur [Pritchard *et al*. 2018] but more recently reestablished as a rhynchocephalian [Sues & Baird 1993; Scheyer *et al*. 2020]) is recovered immediately crownward of *B. taylori*. However, we note that Bremer, bootstrap and PP supports are poor in this region of the tree and for most more crownward nodes (Fig. 24B).

When we add *Opisthiamimus gregori* to the 35-taxon data matrix of Simões *et al*. (2020), we recover nearly identical tree topologies to some of those in Simões *et al*. (2020, fig. 2a, b) using both maximum parsimony and Bayesian analyses. The major difference (not shown here) is that *O. gregori* and all six species of *Clevosaurus* form an unresolved polytomy outside Neosphenodontia.

Our maximum parsimony consensus trees (strict and Adams; Fig. 24A, B) reveal an overall similar arrangement and recover most major clades found in several recent studies (e.g. Hsiou *et al*. 2015, 2019; Bever & Norell 2017; Herrera-Flores *et al*. 2018; Romo de Vivar *et al*. 2020; Simões *et al*. 2020; Sues & Schoch 2021), with *Gephyrosaurus bridensis* as the sister taxon to all other Rhynchocephalia, and *Diphydontosaurus avonis* as the basal-most taxon within Sphenodontia. The recently named clade Acrosphenodontia (Chambi-Trowell *et al.* 2021) also was recovered, with its basal-most taxon *Planocephalosaurus robinsonae* found in a similar position between Sphenodontia and the more crownward Eusphenodontia and with good support (Bremer = 8, PP = 1). *Polysphenodon mulleri* is recovered as the least nested member of Eusphenodontia. Clevosauridae is sister to Neosphenodontia, the latter including two major clades: Sphenodontidae and Leptorhynchia taxon nov.

Here, Sphenodontidae includes *Sphenodon punctatus* as well as taxa historically considered as members of Eilenodontinae or Opisthodontia (e.g. *Opisthias rarus*, *Eilenodon robustus*, *Toxolophosaurus cloudi*, *Sphenotitan leyesi*, *Priosphenodon avelasi*; e.g. Apesteguía & Novas 2003; Martínez *et al*. 2013; Simões *et al*. 2020, 2022; Kligman *et al*. 2021), with *Fraserosphenodon latidens* as sister to *O. rarus*. In the Adams consensus (Fig. 24B), *Pelecymala robustus* and *Kawasphenodon expectatus* + *K. peligrensis* are successively less topologically nested within the Eilenodontinae. The remaining members of Sphenodontidae, *Cynosphenodon huizachalensis* and *Sphenovipera jimmysjoyi*, do not form a monophyletic group with *S. punctatus* (which would represent Sphenodontinae) in either of our consensus trees.

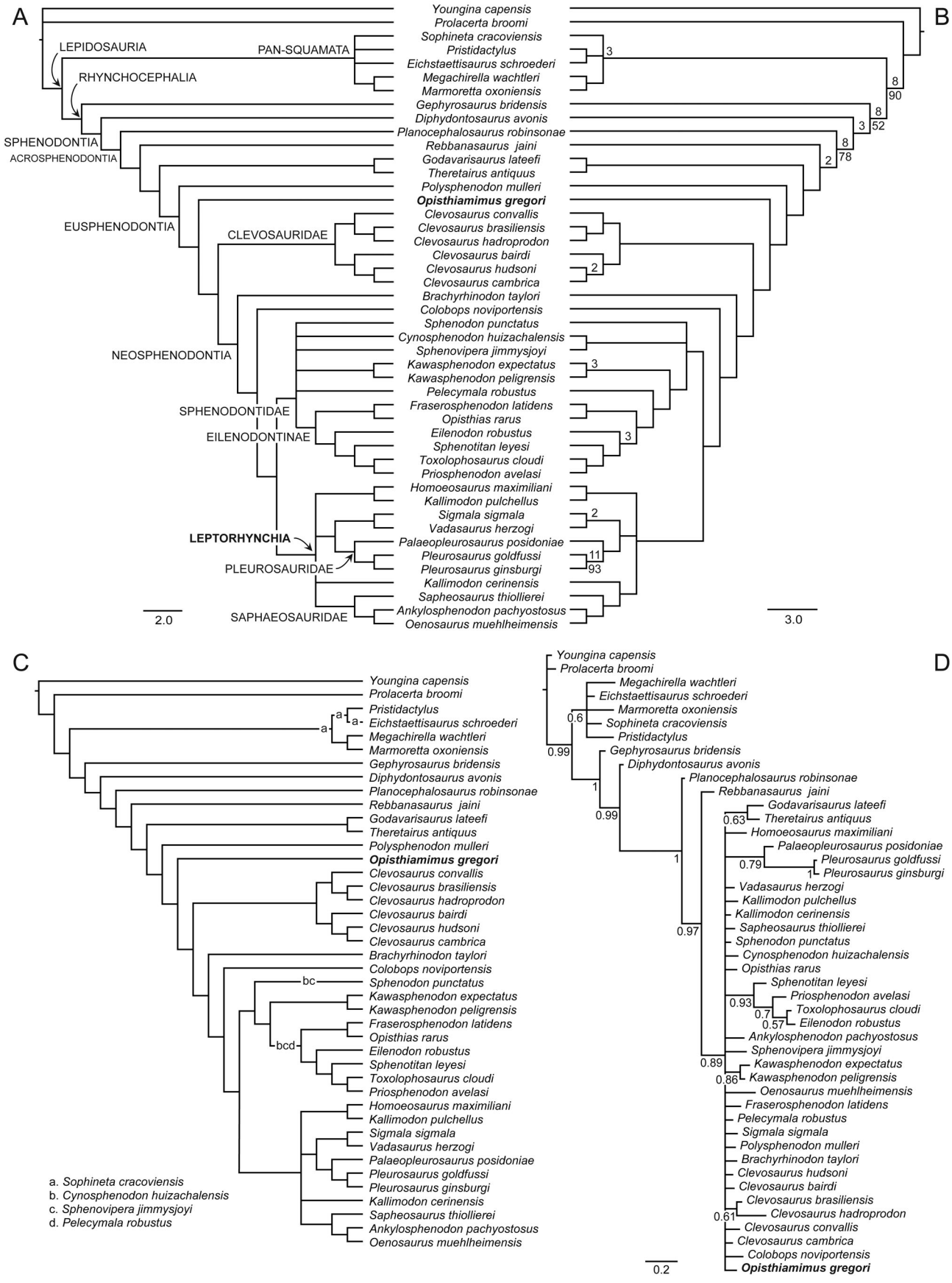
A
B
C
D
Youngina capensis
Prolacerta broomi
Sophineta cracoviensis
Pristidactylus
Eichstaettisaurus schroederi
Megachirella wachtleri
Marmoretta oxoniensis
Gephyrosaurus bridensis
Diphydontosaurus avonis
Planocephalosaurus robinsonae
Rebbanasaurus jaini
Godavarisaurus lateefi
Theretairus antiquus
Polysphenodon mulleri
Opisthiamimus gregori
Clevosaurus convallis
Clevosaurus brasiliensis
Clevosaurus hadroprodon
Clevosaurus bairdi
Clevosaurus hudsoni
Clevosaurus cambrica
Brachyrhinodon taylori
Colobops noviportensis
Sphenodon punctatus
Cynosphenodon huizachalensis
Sphenovipera jimmysjoyi
Kawasphenodon expectatus
Kawasphenodon peligrensis
Pelecymala robustus
Fraserosphenodon latidens
Opisthias rarus
Eilenodon robustus
Sphenotitan leyesi
Toxolophosaurus cloudi
Priosphenodon avelasi
Homoeosaurus maximiliani
Kallimodon pulchellus
Sigmala sigmala
Vadasaurus herzogi
Palaeopleurosaurus posidoniae
Pleurosaurus goldfussi
Pleurosaurus ginsburgi
Kallimodon cerinensis
Sapheosaurus thiollierei
Ankylosphenodon pachyostosus
Oenosaurus muehlheimensis
LEPIDOSAURIA
PAN-SQUAMATA
RHYNCHOCEPHALIA
SPHENODONTIA
ACROSPHENODONTIA
EUSPHENODONTIA
CLEVOSAURIDAE
NEOSPHENODONTIA
SPHENODONTIDAE
EILENODONTINAE
LEPTORHYNCHIA
PLEUROSAURIDAE
SAPHAEOSAURIDAE
2.0
3.0
0.2
a. Sophineta cracoviensis
b. Cynosphenodon huizachalensis
c. Sphenovipera jimmysjoyi
d. Pelecymala robustus

Results from our iterPCR analysis reveal that *C. huizachalensis*, *S. jimmysjoyi* and *P. robustus* are the unstable taxa within the Sphenodontidae, with the former two either as the sister to *S. punctatus* or with all three more closely related to the clade containing *O. rarus* and *T. cloudi* but not *Kawasphenodon* (Fig. 24C; see also Supplemental material).

Leptorhynchia taxon nov. includes primarily aquatic and semiaquatic adapted taxa (e.g. Saphaeosauridae, Pleurosauridae) and their sister taxa (e.g. *Homoeosaurus maximiliani*, *Kallimodon pulchellus*) (Figs 24–26). This clade has been recovered by previous studies but not named (e.g. Bever & Norell 2017; Sobral *et al.* 2020; Simões *et al*. 2020; Chambi-Trowell *et al.* 2021, supplemental fig. S6; Simões *et al.* 2022, fig. 8 [Clade "A"]). In analyses where this clade is not recovered the constituent taxa tend to be paraphyletic (Martínez *et al.* 2013; Apesteguía & Carballido 2014; Chambi-Trowell *et al.* 2021, fig. 16; Apesteguía *et al.* 2021; Villa *et al.* 2021) or incompletely represented in the taxon sample (e.g. Scheyer *et al.* 2020; Ford *et al.* 2021; Griffiths *et al.* 2021). The name Leptorhynchia comes from Greek 'leptós' (λεπτό ς, narrow) and 'rhúnkhos' (ρ ύγχος, beak or snout), in reference to the narrow snouts of the species it contains and as a reference to one of the first rhynchocephalians named: *Leptosaurus* Fitzinger, 1837. We define Leptorhynchia as all taxa more closely related to *Pleurosaurus goldfussi* than to *Sphenodon punctatus*. It is supported by the following four unambiguous cranial and postcranial characters: antorbital region of skull 25–33% skull length; zygosphene absent in presacral vertebrae; prominent process on posterior border of ischium; fourth metacarpal about equal in length to third metacarpal (see Supplemental material for the six ambiguous synapomorphies).

A notable departure from most other analyses is the placement of the Morrison taxon *Theretairus antiquus* away from Sphenodontinae and Neosphenodontia. Instead, our analysis recovers *T. antiquus* as a sister taxon to *Godavarisaurus lateefi* just outside Eusphenodontia. *Theretairus antiquus* and *G. lateefi* share two unambiguous synapomorphies: a moderately deep subdental ridge and mesiolingual groove on at least one dentary successional tooth. Together, these two species form the sister group to Eusphenodontia based on the absence of enamel ornamentation (e.g. striae, wide grooves) on the dentary additional teeth. On the basis of the newly referred dentary (USNM V 26088; Supplemental material, Fig. S2A–E), *T. antiquus* also is shown (for the first time) to exhibit the following dentary successional tooth features in common with *G. lateefi* and other basal rhynchocephalians: presence of non-caniniform successionals (also present in *Gephyrosaurus bridensis*, *Diphydontosaurus avonis*, *Planocephalosaurus robinsonae* and *Rebbanasaurus jaini*), lingual or labial striations (also present in *D. avonis*, *P. robinsonae* and *R. jaini*), and a mesiolingual groove. The previous association of *T. antiquus* with sphenodontines was based on the presence and number of dentary post-symphyseal caniniform teeth (posterior successionals of some authors) (e.g. Reynoso 1996, 2000, 2005; Herrera-Flores *et al*. 2018). However, *T. antiquus* lacks the pyramid-shaped additional teeth with mesiolingual and mesiolabial crests present on the dentary of *S. punctatus*, *C. huizachalensis* and *S. jimmysjoyi* (Reynoso 1996, 2005; Jones *et al*. 2012). The prominently alternate-sized additional teeth in *T. antiquus* further distinguish it from these three taxa. This feature could be attributed to immaturity, but *T. antiquus* has other features which suggest maturity – for example, the holotype and USNM PAL 720482 have a thick layer of secondary bone on the lateral side of the dentary, incised by deep maxillary tooth marks or facets (Supplemental material, Fig. S2G, J). Chambi-Trowell *et al.* (2021, fig. 16A) recovered *T. antiquus* as the sister taxon to *Zapatodon ejidoensis* (Reynoso & Clark 1998; not included in our analysis due to its presumed immature age) and within an unnamed clade found to be sister to all other neosphenodontians (but see below and the Supplemental material for this problematic result).

Another notable result is the sister-taxon relationship of *Sigmala sigmala* with *Vadasaurus herzogi*. This unexpected result is supported by two unambiguous synapomorphies: weak overlap or imbrication between the distal dentary teeth and overlap in the distal additional dentary teeth formed by the mesiolabial flange. Together, *S. sigmala* and *V. herzogi* form the sister group to the Pleurosauridae. Of the four unambiguous character states uniting these taxa, only one is scorable

Figure 24. Consensus trees based on maximum parsimony (**A–C**) and Bayesian (**D**) analyses with *Opisthiamimus gregori* gen. et sp. nov. and Leptorhynchia taxon nov. shown in bold font. **A,** strict consensus of 24 most parsimonious trees (MPTs; 436 steps each, consistency index [CI] = 0.3991, retention index [RI] = 0.6421) with clade names at their respective nodes; **B,** Adams consensus of 24 MPTs (426 steps each, CI = 0.4085, RI = 0.6557) with Bremer (>1) and bootstrap (>50) support values provided above and below each node, respectively, that is supported as such (all nodes with these values also are recovered in the strict consensus in A; **C,** strict consensus of 24 MPTs following the iterPCR protocol demonstrating the alternative positions of the most phylogenetically unstable taxa; **D,** 50% majority rule consensus tree with posterior probabilities provided.

in *S. sigmala*: dentary lateral wear facets adjacent to the additional teeth steeply oblique, discrete and nonoverlapping. Among the pleurosaurs, only *Palaeopleurosaurus posidoniae* was scorable with certainty for this same feature. Therefore, we regard this relationship with caution pending discovery of additional material of *S. sigmala*. Chambi-Trowell *et al.* (2021, fig. 16) recovered *S. sigmala* as the sister taxon to *Clevosaurus convalis* within Clevosauridae.

Our Bayesian analysis (Fig. 24D) recovered a similar and strongly supported outer branching topology (PP = 0.97–1) to our maximum parsimony analysis, but crownward of *Rebbanosaurus jaini* the tree becomes poorly resolved with fewer clades recovered. Eusphenodontia (PP = 0.89) is recovered but with *Godavarisaurus lateefi* + *Theretairus antiquus* as members of that clade rather than its sister group. *Opisthiamimus gregori* is again recovered as a eusphenodontian. Only Pleurosauridae (PP = 0.79) and a less inclusive Eilenodontinae (PP = 0.93) are recovered as monophyletic clades. *Kawasphenodon expectatus* + *K. peligrensis* and *Clevosaurus brasiliensis* + *C. hadroprodon* are the remaining resolved clades but they are poorly supported sister pairs (PP = 0.86 and 0.61, respectively).

Discussion

Opisthiamimus gregori gen. et sp. nov. is the first rhynchocephalian from the Morrison Formation to be named on the basis of articulated cranial and postcranial material including an almost complete skeleton. Previous Morrison records mainly comprise isolated and incomplete lower jaws, as was the case for the type specimens of all three previously named taxa: *Opisthias rarus* (Gilmore 1909), *Theretairus antiquus* (Simpson 1926) and *Eilenodon robustus* (Rasmussen & Callison 1981). Thus, the type and referred specimens of *O. gregori* offer an exceptional opportunity to study the cranial and postcranial anatomy of a Late Jurassic rhynchocephalian from North America. Furthermore, the new material allows us to re-evaluate the higher-level taxonomy, evolutionary history and ecomorphological diversity of Rhynchocephalia within the Morrison Formation.

Phylogenetic implications

On the basis of previous phylogenetic hypotheses, rhynchocephalians yielded from the Morrison Formation were all deeply nested members of the group (all within Eusphenodontia) (e.g. Herrera-Flores *et al.* 2018; Romo de Vivar *et al.* 2020; Simões *et al.* 2020; Chambi-Trowell *et al.* 2021; Kligman *et al.* 2021). Our phylogenetic results corroborate the deeply nested phylogenetic positions of *Opisthias rarus* and *Eilenodon robustus* but call into question the crownward position of *Theretairus antiquus* (also implied in the results of Bever & Norell 2017, fig. 5a). Nevertheless, *Opisthiamimus gregori* represents the first unambiguous basal eusphenodontian known from the Morrison Formation. These results indicate the spatiotemporal overlap between at least one basal rhynchocephalian (*O. gregori*) and multiple more deeply nested and morphologically derived taxa (*O. rarus*, *E. robustus*) during the Late Jurassic in North America (Figs 25, 26). Thus, not only was there greater alpha-level taxon diversity in the Morrison Formation (at least four species in as many genera), but this diversity also reflects higher-level taxon diversity because it derives from disparate regions of the phylogeny.

The sister-taxon relationship of *Theretairus antiquus* and *Godavarisaurus lateefi* (Figs 24–26) poses an interesting palaeobiogeographical scenario, as the former taxon is from the Late Jurassic of North America (Simpson 1926) and the latter is from the Early–Middle Jurassic of India (Evans *et al.* 2001; but see Vijaya & Prasad [2001] for a potential late Middle Jurassic to Early Cretaceous age for the Kota Formation). *Godavarisaurus lateefi* has previously been recovered as the sister taxon to *Sphenocondor gracilis* from the Middle Jurassic of Argentina (Apesteguía *et al.* 2012, 2014; Herrera-Flores *et al.* 2018; Romo de Vivar *et al.* 2020). Although we removed *S. gracilis* from our final dataset due to the presumed immature status of its holotype and only known specimen, it possesses one of the synapomorphies uniting *T. antiquus* and *G. lateefi* (presence of a mesiolingual groove on at least one dentary successional tooth) and at least two other seemingly important dentary successional tooth features (the presence of non-caniniform successionals, and lingual or labial striations). A close relationship between *T. antiquus* and *G. lateefi* is surprising given their ages and geographic origins. However, Rhynchocephalia are known to have been both diverse (e.g. Fraser 1986; Heckert 2004; Meloro & Jones 2012; Martínez *et al.* 2013; Kligman *et al.* 2021) and biogeographically widespread by the Middle–Late Triassic (e.g. Shubin & Sues 1991; Ezcurra 2010). Given the persistently patchy Mesozoic fossil record of small vertebrates, seemingly complex biogeographic signals should not be unexpected.

The less deeply nested position of *Theretairus antiquus* might also be reflected in the shape of its additional teeth, which bear similarities to several *Planocephalosaurus*-like dentaries (*per* Fraser 1993) from the Late Triassic (Norian) of Arizona, USA, including teeth acrodont, triangular, labiolingually

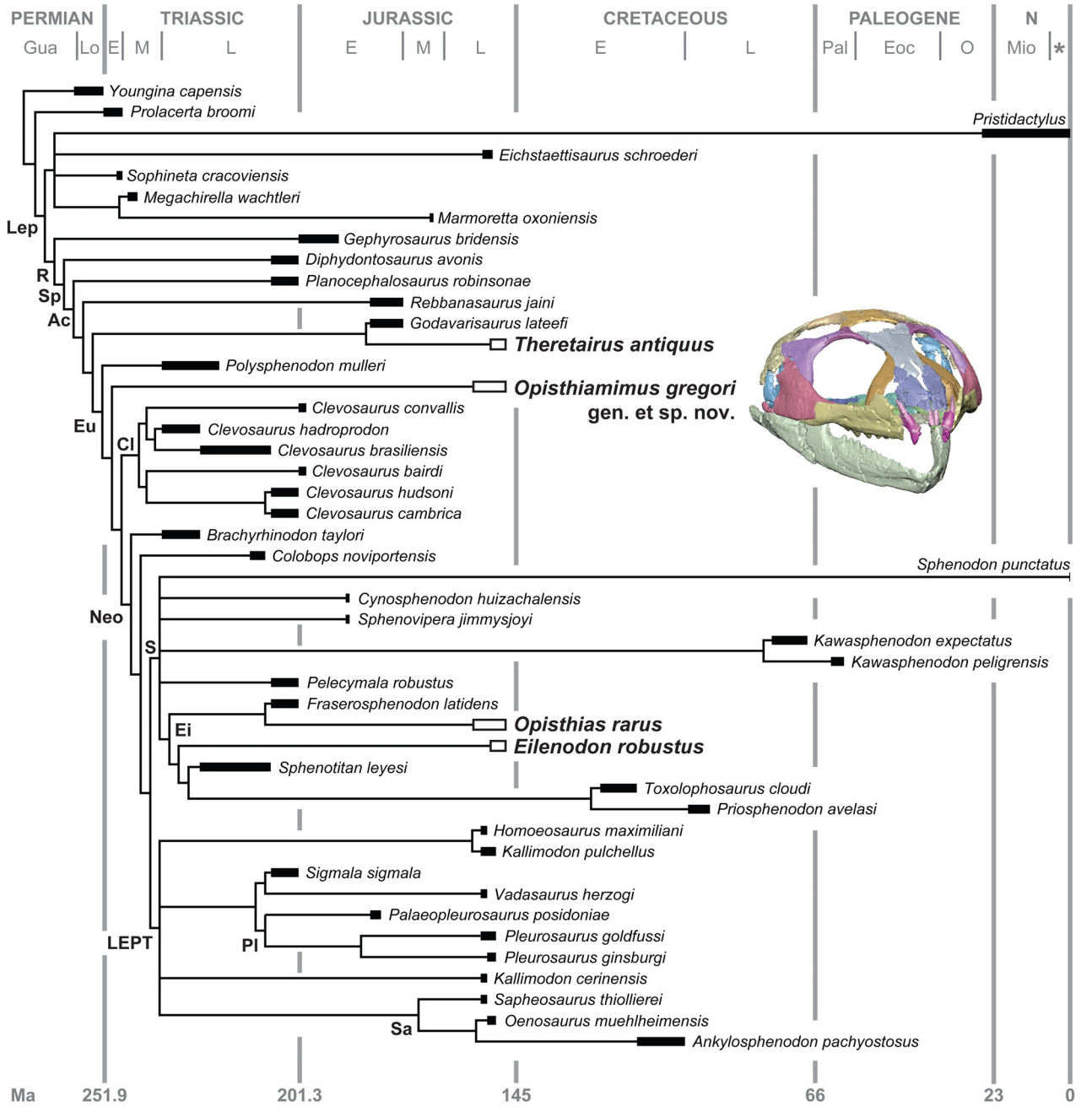

Figure 25. A time-calibrated phylogeny of Rhynchocephalia (and outgroups) based on the strict consensus presented in Figure 24A. The thick bars and boxes at the branch tips represent the temporal ranges for each species. The Morrison Formation taxa are emphasized by the enlarged bold font and black-bordered white boxes. Boundary dates are based on Walker *et al*. (2018). The three-dimensional reconstructed skull of *Opisthiamimus gregori* gen. et sp. nov. is shown in oblique anterodorsolateral view. **Abbreviations: Ac**, Acrosphenodontia; **Cl**, Clevosauridae; **E**, Early; **Ei**, Eilenodontinae; **Eoc**, Eocene; **Eu**, Eusphenodontia; **Gua**, Guadalupian; **L**, Late; **Lep**, Lepidosauria; **LEPT**, Leptorhynchia taxon nov.; **Lo**, Lopingian; **M**, Middle; **Ma**, million years ago: **Mio**, Miocene; **N,** Neogene; **Neo**, Neosphenodontia; **O**, Oligocene; **Pal**, Paleocene; **Pl**, Pleurosauridae; **R**, Rhynchocephalia; **S**, Sphenodontidae; **Sa**, Saphaeosauridae; **Sp**, Sphenodontia; *, Pliocene, Pleistocene and Holocene.

compressed and alternate in size (Kaye & Padian 1994, figs 9.55–9.57 *vs* Simpson 1926, fig. 1 and Supplemental material, Fig. S2F–J). Therefore, we cautiously accept our phylogenetic results pending an in-progress formal revision of *T. antiquus* based on re-description of the holotype and new descriptions of

recently identified topotypic material including two partial dentaries (USNM PAL 720482, USNM V 26088; see Supplemental material) and a nearly complete maxilla (USNM PAL 720478; DGD, pers. obs.). Similarly, if the recent referral of an undescribed crushed skull (DINO 16454) from the Morrison Formation of Utah, USA, to *T. antiquus* is correct (Chambi-Trowell *et al.* 2021), then DINO 16454 would significantly improve our understanding of this taxon's cranial anatomy and perhaps its phylogenetic position. However, we find this referral problematic (for our assessment, see Supplemental material) and thus consider the phylogenetic position of *T. antiquus* as presented in Chambi-Trowell *et al.* (2021) suspect.

Anatomical comparisons

Opisthiamimus gregori gen. et sp. nov. has many craniodental features in common with several of the less phylogenetically nested Rhynchocephalia included in our dataset. For example, it has large orbits and small upper and lower temporal fenestrae relative to the size of its skull (see characters 2–5 in the Supplemental material). These proportions are very similar to those of several of the least nested rhynchocephalians (i.e. *Gephyrosaurus bridensis*, *Diphydontosaurus avonis*, *Planocephalosaurus robinsonae* and *Polysphenodon mulleri*). Similarly, among the rhynchocephalians in our data set, *O. gregori* possesses several characters found principally in most or all members of Clevosauridae and *Brachyrhinodon taylori* and *Polysphenodon mulleri*: premaxilla excludes maxilla from the external naris; maxilla premaxillary process short anteroposteriorly; prefrontal-jugal contact present; poorly developed parietal parasagittal crest (also present in *G. bridensis*, *D. avonis* and *P. robinsonae* but better developed in the former two); parietal foramen positioned posterior to the anterior border of the upper temporal fenestra (also present in *G. bridensis*, *D. avonis* and *P. robinsonae*); palatine with a single lateral tooth row plus one isolated tooth; pterygoid with two tooth rows (also present in *P. robinsonae*); and subdental ridge dorsoventrally deep at mid tooth row length relative to total height of dentary at that point ($\geq$ 60%; also present in *P. robinsonae* and *Rebbanasaurus jaini*).

The postcranial skeleton of *Opisthiamimus gregori* is similar in form and proportions to those of several extinct rhynchocephalians as well as *Sphenodon punctatus* (e.g. Fraser 1988, fig. 36; Fraser & Benton 1989, fig. 5), exhibiting a typical terrestrial sphenodontian bauplan. Many postcranial characters that occur commonly (but not necessarily ubiquitously) in Rhynchocephalia also are present in *O. gregori*: 24 or 25 presacral vertebrae; centra amphicoelous and notochordal; presence of the zygosphene/zygantrum articulation and accessory process at the base of the neural arch posteriorly in the presacral vertebrae; most presacral ribs holocephalous; transverse process of second sacral rib laterally bifurcated with a posterior process; and interclavicle 'T'-shaped. The distal end of the humerus in *O. gregori* features an expanded radial condyle (= capitellum), an uncommon but widely distributed (i.e. homoplastic) rhynchocephalian character that also occurs in *Clevosaurus cambrica*, *Kallimodon pulchellus*, *Leptosaurus neptunius*, *S. punctatus* and the recently described *Navajosphenodon sani* (e.g. Keeble *et al.* 2018; Simões *et al.* 2020, 2022).

The manus in *Opisthiamimus gregori* is quite similar to that of *S. punctatus* (Fig. 23), which, together, are the only taxa in our data set (albeit few are scorable) to share the following unique combination of character states: breadth of metacarpal I sub-equal to metacarpals II–IV; length of metacarpal I between 60% and 80% that of metacarpal II; and metacarpal IV shorter than metacarpal III. This last feature perhaps is the single most important postcranial character present in *O. gregori* as it unambiguously unites it with all more crownward taxa (i.e. Clevosauridae + Neosphenodontia; Figs 24–26).

The evolution of the postcranial skeleton in Rhynchocephalia is not well understood, particularly in comparison to that of the cranium, lower jaw, and dentition. However, well-preserved postcranial remains do exist for several taxa, including the Triassic–Jurassic fissure-fill taxa of the UK (e.g. Evans 1981; Fraser 1982, 1988; Fraser & Walkden 1984; Keeble *et al.* 2018; O'Brien *et al.* 2018; Chambi-Trowell *et al.* 2019); *Brachyrhinodon taylori* from the Triassic of Scotland (Fraser & Benton 1989); *Polysphenodon mulleri* from a Late Triassic borehole of Germany (Fraser & Benton 1989); *Clevosaurus brasiliensis* from the Late Triassic of Brazil (Arantes *et al.* 2009); *Palaeopleurosaurus posidoniae* from the Early Jurassic of Germany (Carroll 1985); several taxa from the Jurassic of Europe (e.g. Cocude-Michel 1963; Carroll & Wild 1994; Dupret 2004; Rauhut & López-Arbarello 2016; Bever & Norell 2017; Villa *et al.* 2021), and Cretaceous taxa from Italy (Cau *et al.* 2014) and Mexico (e.g. Reynoso 1997, 2000). There also are several postcranial records that remain incompletely described (e.g. Apesteguía 2008). Of the several postcranial records from North America (e.g. Sues *et al.* 1994a, Fraser & Wu 1998; Kirkland 2006; Simões *et al.* 2022), that of *Opisthiamimus gregori* is the most thoroughly described.

Among Rhynchocephalia, broad comparisons of the postcrania generally have been limited to limb dimensions (e.g. Cocude-Michel 1963; Reynoso 2000, table 2;

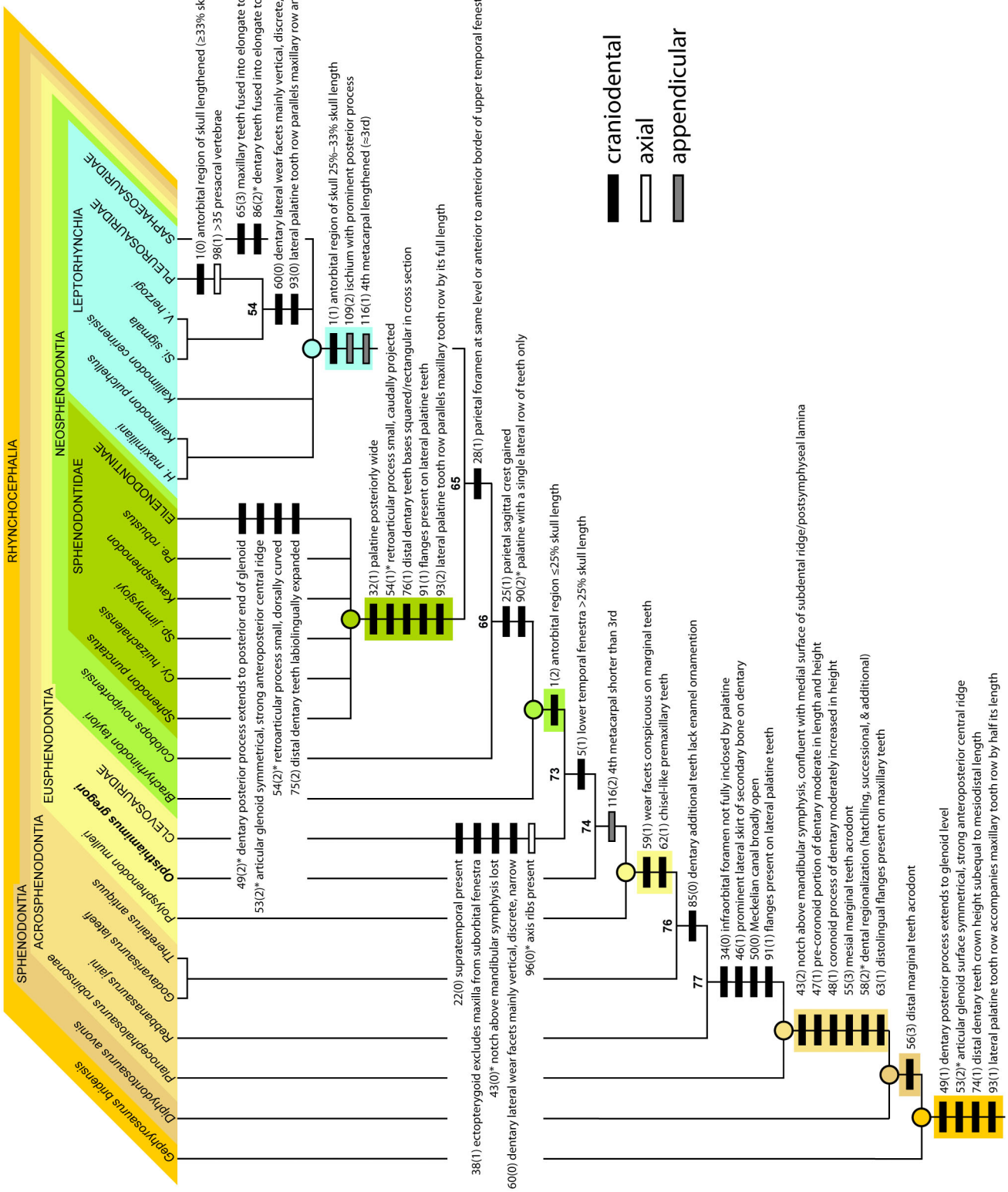
RHYNCHOCEPHALIA
SPHENODONTIA
ACROSPHENODONTIA
EUSPHENODONTIA
NEOSPHENODONTIA
LEPTORHYNCHIA
SPHENODONTIDAE
EILENODONTINAE
SAPHAEOSAURIDAE
PLEURosAURIDAE
Gephyrosaurus bridensis
Diphydontosaurus avonis
Planocephalosaurus robinsonae
Rebbanasaurus jaini
Godavarisaurus latefi
Theretairus antiquus
Polysphenodon muelleri
Opisthiamimus gregori
CLEVOSAURIDAE
Brachyrhinodon taylori
Coloborhynchus clackamasensis
Sphenodon punctatus
Cy. huizachalensis
Sp. jimmysioyi
Kawasphenodon peligrensis
Pe. robustus
H. maximiliani
Kallimodon pulchelus
Si. sigmala
V. herzogi
1(0) antorbital region of skull lengthened (≥33% skull length)
98(1) >35 presacral vertebrae
65(3) maxillary teeth fused into elongate tooth plate
86(2)* dentary teeth fused into elongate tooth plate
60(0) dentary lateral wear facets mainly vertical, discrete, narrow
93(0) lateral palatine tooth row parallels maxillary row anteriorly only
1(1) antorbital region of skull 25%–33% skull length
109(2) ischium with prominent posterior process
116(1) 4th metacarpal lengthened (≈3rd)
49(2)* dentary posterior process extends to posterior end of glenoid
53(2)* articular glenoid symmetrical, strong anteroposterior central ridge
54(2)* retroarticular process small, dorsally curved
75(2) distal dentary teeth labiolingually expanded
32(1) palatine posteriorly wide
54(1)* retroarticular process small, caudally projected
76(1) distal dentary teeth bases squared/rectangular in cross section
91(1) flanges present on lateral palatine teeth
93(2) lateral palatine tooth row parallels maxillary tooth row by its full length
28(1) parietal foramen at same level or anterior to anterior border of upper temporal fenestra
25(1) parietal sagittal crest gained
90(2)* palatine with a single lateral row of teeth only
1(2) antorbital region ≤25% skull length
5(1) lower temporal fenestra >25% skull length
116(2) 4th metacarpal shorter than 3rd
59(1) wear facets conspicuous on marginal teeth
62(1) chisel-like premaxillary teeth
85(0) dentary additional teeth lack enamel ornamention
34(0) infraorbital foramen not fully inclosed by palatine
46(1) prominent lateral skirt of secondary bone on dentary
50(0) Meckelian canal broadly open
91(1) flanges present on lateral palatine teeth
43(2) notch above mandibular symphysis, confluent with medial surface of subdental ridge/postsymphyseal lamina
47(1) pre-coronoid portion of dentary moderate in length and height
48(1) coronoid process of dentary moderately increased in height
55(3) mesial marginal teeth acrodont
58(2)* dental regionalization (hatchling, successional, & additional)
63(1) distolingual flanges present on maxillary teeth
56(3) distal marginal teeth acrodont
49(1) dentary posterior process extends to glenoid level
53(2)* articular glenoid surface symmetrical, strong anteroposterior central ridge
74(1) distal dentary teeth crown height subequal to mesiodistal length
93(1) lateral palatine tooth row accompanies maxillary tooth row by half its length
22(0) supratemporal present
38(1) ectopterygoid excludes maxilla from suborbital fenestra
43(0)* notch above mandibular symphysis lost
60(0) dentary lateral wear facets mainly vertical, discrete, narrow
96(0)* axis ribs present
54
65
66
73
74
76
77
craniodental
axial
appendicular

Figure 26. Distributions of some of the major synapomorphies in Rhynchocephalia as mapped onto the maximum parsimony strict consensus tree, including many that are hypothesized to be associated with proal and orthal jaw movements (e.g. characters 46, 53, 59, 60, 63, 90, 91, 93). Major clade nodes are indicated with coloured circles. Bold numbers above nodes represent those listed in the full apomorphy list for the strict consensus (see Supplemental material). The coloured circles and boxes at and below the nodes correspond to those bracketing the major clades at the top of the figure. The horizontal rectangles on the stem below each major node indicate some or all of the unambiguous or ambiguous character states supporting that node; ambiguous character states are denoted with an asterisk (*). Black rectangles = cranial, lower jaw or dental characters. White-filled rectangles = axial skeleton characters. Grey-filled rectangles = appendicular skeleton characters. Numbers and numbers in parentheses in the form of X(Y) and next to the rectangles represent the character and character state numbers presented in the character and apomorphy lists (see Supplemental material). **Abbreviations:** ***Cy***., *Cynosphenodon*; ***H***., *Homoeosaurus*; ***Pe***., *Pelecymala*; ***Si***., *Sigmala*; ***Sp***., *Sphenovipera*; ***V***., *Vadasaurus*.

Bever & Norell 2017), and postcranial characters have played a somewhat secondary role in phylogenetic analyses compared to lower jaws and teeth. In our character/taxon data matrix only 19 (~49%) of the 39 rhynchocephalian operational taxonomic units (OTUs) included have postcrania that could be scored for the 22 postcranial characters. Furthermore, for these 19 species only 253 (~30%) out of 858 possible character states were codable. As a consequence, our maximum parsimony strict consensus (Fig. 24A) revealed few unambiguous postcranial synapomorphies outside Leptorhynchia taxon nov. (e.g. Fig. 26; see summarized apomorphy list in the Supplemental material). Future studies would benefit from more detailed descriptions and figures of postcranial elements, including provision of digital scan models (e.g. X-ray μCT; O'Brien *et al.* 2018). This additional information would facilitate cross-taxon comparisons and allow identification of new phylogenetic characters and evolutionary patterns related to ecomorphology and locomotion.

Palaeobiological interpretations

Ontogenetic stage. With estimated skull and snout-vent lengths of approximately 20.5 mm and 85 mm, respectively (Supplemental material, Table S1), *Opisthiamimus gregori* is among the smallest rhynchocephalians known. It is similar in size to several taxa, mostly from the Late Triassic and Early Jurassic, that are based on reasonably complete material of inferred mature individuals: *Planocephalosaurus robinsonae*, *Polysphenodon mulleri*, *Brachyrhinodon taylori*, several species of *Clevosaurus* (e.g. *C. bairdi*, *C. brasiliensis*, *C. cambrica*) and *Homoeosaurus maximiliani* (Late Jurassic) all possess skulls with estimated lengths of between 16 and 24 mm (Fraser & Benton 1989; Wu 1991; Sues *et al*. 1994a; Bonaparte & Sues 2006; Chambi-Trowell *et al*. 2019; see also Molero & Jones 2012, table 1, Apesteguía *et al*. 2014, suppl-table 2, and Apesteguía & Carballido 2014, appendix 1 for size estimates of some of these and other rhynchocephalians). Based on lower jaws alone, *Theretairus antiquus* and *Sphenovipera jimmysjoyi* also are estimated to have had similar-sized skulls (lengths ~20 mm and 21 mm, respectively; Apesteguía *et al*. 2014, suppl-table 2).

Despite their small size, all specimens of *Opisthiamimus gregori* are considered mature individuals based on ontogenetic variables observed in *Sphenodon punctatus* (e.g. Howes & Swinnerton 1901; Hoffstetter & Gasc 1969; Robinson 1976; Jones 2008; Jones & Lappin 2009; Jones *et al*. 2009a) and size-related variables observed in fossil taxa known from larger sample sizes (e.g. Fraser 1986; Whiteside 1986; Apesteguía & Carballido 2014): all are from similar-sized individuals; tooth wear is moderate to severe on the marginal and palatal dentitions; the bases of non-hatchling teeth are obscured by a thickened layer of secondary bone; maxillary tooth marks are moderately to deeply incised into the thickened layer or 'lip' of secondary bone on the dorsolateral surface of the dentary; a 'lip' of secondary bone also present on maxilla; the atlas and axis centra and axis intercentrum fused into a single element; vertebral neurocentral sutures are obscured or obliterated; and the capitellum and trochlea are well ossified with the humerus. Another possible but unconfirmed piece of evidence supporting a mature age in *O. gregori* is the lack of apparent braincase sutures in the holotype. In adult specimens of *S. punctatus* the bones of the braincase fuse together, nearly obliterating the sutures. In less mature individuals the bones are not fused, retaining visible sutures (e.g. Howes & Swinnerton 1901; Evans 2008). However, if our identifications of the possible disarticulated right prootic/opisthotic and left exoccipital are correct then the mature status for *O. gregori* might be rejected on these grounds.

Jaw function. Interpreting jaw movement in a fossil tetrapod is difficult, but some tentative inferences can be made according to the shape of the jaw joint and form of wear on the teeth and jaws. The extant *Sphenodon punctatus* also provides an important baseline for comparisons given that its jaw movements and tooth wear are relatively well known (e.g. Robinson 1976; Gorniak *et al*. 1982; Curtis *et al*. 2010; Jones *et al*. 2012). In *S. punctatus* and some fossil taxa (e.g. *Gephyrosaurus bridensis*, *Diphydontosaurus avonis*, *Eilenodon robustus*) the anteroposterior length of the articular surface of the lower jaw is greater than it is for the quadrate condyle (Evans 1980; Whiteside 1986; Jones *et al*. 2012). This difference in length allows for proal movement of the lower jaw (Jones *et al.* 2012): a forward power stroke following jaw closure. In *Clevosaurus* these jaw joint surfaces are more similar in anteroposterior dimension (e.g. Fraser 1988) indicating a more orthal, scissor-like movement of the lower jaw. The length of the quadrate condyle in *Opisthiamimus gregori* is short relative to the elongate articular surface of the lower jaw (Fig. 27B *vs* Fig. 11L, M) and is more similar to that in *Sphenodon* than to *Clevosaurus*.

Wear facets might also be informative for inferring jaw motion, but because the additional teeth are not replaced in rhynchocephalians, they could document wear that occurred earlier in ontogeny (e.g. Robinson 1976; also see remarks for character 60 in the character list in the Supplemental material). Nevertheless, dramatic oblique wear facets that do not or largely do not overlap likely indicate orthal wear (e.g. *Clevosaurus*

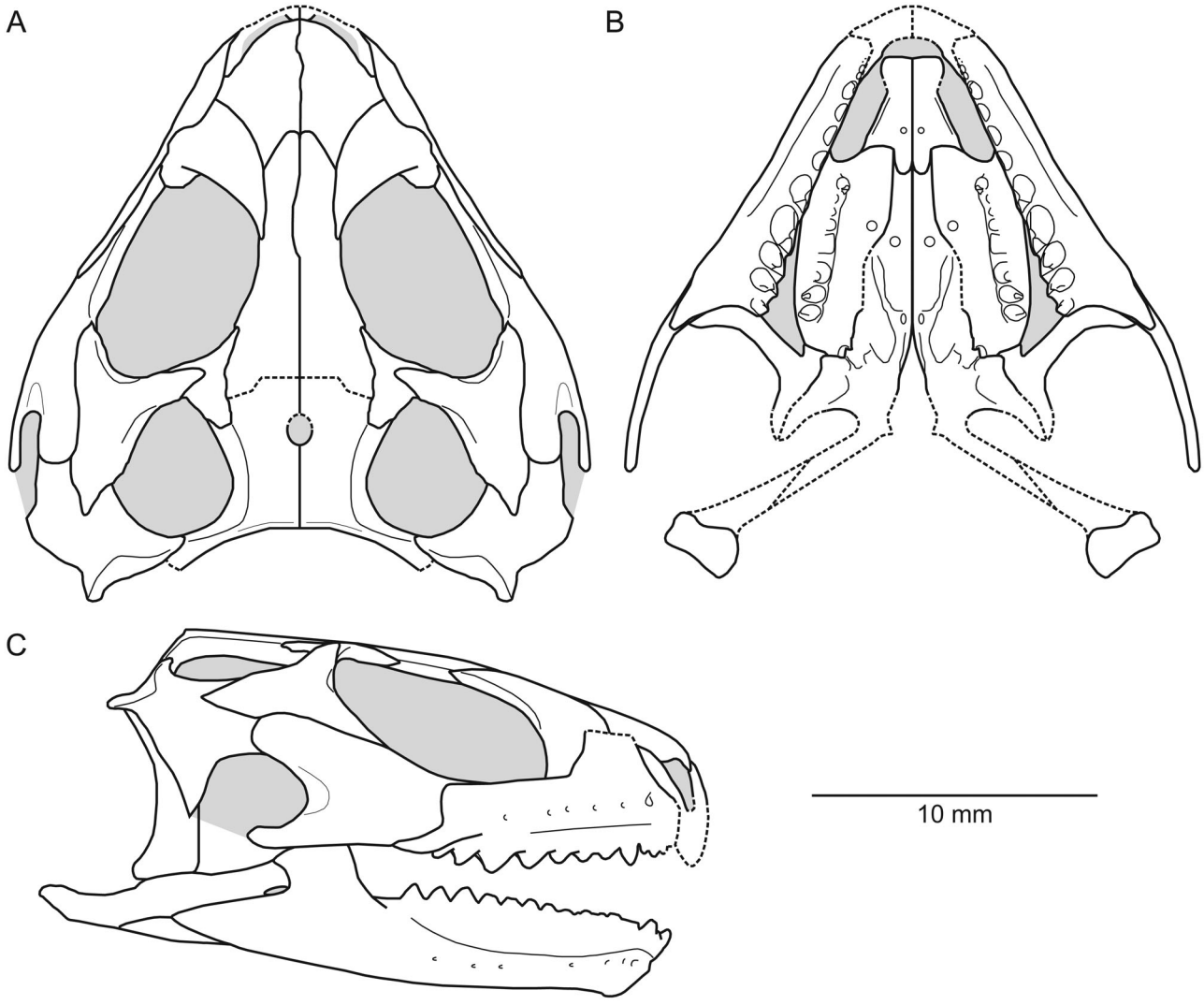

Figure 27. Line drawing reconstruction of the skull (minus the braincase) and lower jaws of *Opisthiamimus gregori* gen. et sp. nov. based on observations of the holotype and referred specimens (USNM PAL 720475, 720476, 722041) and our three-dimensional reconstructions (e.g. Fig. 4; Supplemental material, Fig. S4). **A,** dorsal view; **B,** ventral view; **C,** right lateral view. Light grey represents cranial openings (i.e. orbit, choana, upper and lower temporal, infraorbital and suborbital fenestrae, external nares) and foramina (i.e. parietal, mandibular); dashed lines represent hypothesized contours.

hudsoni: Fraser 1988, fig. 19c, pl. 3, fig. 20; Chambi-Trowell *et al*. 2019, fig. 3D, F), whereas elongate and overlapping wear facets likely indicate proal movement (e.g. *Sphenodon punctatus*: Robinson 1976, fig. 4, pl. 1B, C). Slightly elongate and non-overlapping, crescent-shaped wear facets have been observed in e.g. *Rebbanasaurus jaini* (Evans *et al*. 2001, figs 2D, 7G) and *Kawasphenodon expectatus* (Apesteguía 2005, fig. 2B), and these might indicate some proal movement, less tightly opposed upper and lower jaws, or both. In *Opisthiamimus gregori*, the dentary wear facets made by the maxillary dentition, in particular the elongate anterior wear facet, suggest some proal jaw movement (Fig. 12A). These traits suggest oral food processing in a manner similar to that in *S. punctatus* (Jones *et al*. 2012). The orientation of the flanges on the dentary and maxillary teeth, and relative parasagittal orientation of the entire lateral palatine tooth row, are consistent with this ability. *Gephyrosaurus bridensis* and *Diphydontosaurus avonis* also show evidence of an elongate articular surface (Evans 1980; Whiteside 1986), but at least some species of *Clevosaurus* have a short articular surface (e.g. Fraser 1988). Therefore, the pattern of character distribution suggests that some form of proal jaw movement is plesiomorphic among rhynchocephalians (Fig. 26). The shearing associated with this

type of jaw movement was enhanced in some taxa by the presence of flanges and tooth-on-tooth wear, and the number of cutting edges involved in each power stroke (Throckmorton *et al*. 1981; Jones 2008, 2009; Jones *et al*. 2012, 2018). However, proal movement was replaced by orthal movement in at least some clevosaurs that retain tooth-on-tooth wear but typically have a smaller number of long cutting edges (Fraser 1988; Jones 2008, 2009; Jones *et al*. 2012; Fig. 25). A similar type of orthal shearing bite was probably also acquired in pleurosaurs. Larger postorbital regions in Eusphenodontia are associated with greater capacity for jaw muscles (Jones 2008). A secondary layer of bone (skirt or lip) increases the cross-sectional area of the jaws making them stronger and better able to withstand greater stress from bite forces (Jones & Lappin 2009).

Palaeoecological diversity. Rhynchocephalians are among the most specimen- and site-abundant vertebrates from the Morrison Formation throughout its stratigraphic thickness (e.g. Foster 2007, figs 7.1, 7.3 and appendix). As such, they likely played an important ecological role among small-bodied terrestrial vertebrates, perhaps more so than the relatively less abundant squamates. The presence of at least four rhynchocephalians (and likely others; see Supplemental material) in the Morrison Formation implies a substantial concomitant palaeoecological diversity among these small-bodied lepidosaurs. This pattern was likely the case even though site-level alpha diversity was lower than whole-formation diversity – and it is possible that some of these species were chronologically and palaeobiogeographically separated. Nevertheless, there is evidence for direct overlap of multiple species at several localities.

Several options were available for these Morrison species to avoid extended direct competition in these palaeoenvironments. Such avoidance might have occurred, in part, due to differences in body size and dietary preferences. For example, the small-bodied *Opisthiamimus gregori* (snout-vent length ~85 mm) most likely was an invertivore feeding primarily on insects and possibly small terrestrial gastropods. Using body size data of 86 extant legged lizard species with snout-vent length between 80 and 90 mm (Meiri 2010), we estimate the body mass of *O. gregori* at about 16 g (see Supplemental material). Minimum and maximum mass likely would have been between about 3.9 g (greatest mass of the lightest taxon *Nactus pelagicus*) and 43.6 g (mean mass of the heaviest taxon *Sceloporus magister*), respectively. This body mass range falls on the lower end of the range (<50–100 g) occupied by strictly 'carnivorous' lizards (Pough 1973). Given the moderate to extreme marginal and palatal tooth wear, *O. gregori* probably incorporated a high percentage of resistant food types in its diet, such as insects with hard keratinous exoskeletons (e.g. beetles). Moreover, the proal jaw motion, *Sphenodon*-like maxillary, dentary and lateral palatine dentitions, and moderately robust and rigidly built skull and lower jaws in *O. gregori* (Figs 4, 27) would have permitted oral processing for tearing apart resistant food items, as demonstrated in *Sphenodon punctatus* (e.g. Jones *et al*. 2011, 2012). *Theretairus antiquus* was likely insectivorous as well given its similarly small body size, but the lack of well-developed wear facets on at least its dentary teeth suggest it fed primarily on softer-bodied prey, e.g. annelids. The enlarged successional caniniforms and triangular additional teeth appear well suited for piercing and holding on to such prey.

Opisthias rarus, with an estimated skull length of about 42 mm (Apesteguía *et al*. 2014, Supplemental material, Table S2), was substantially larger than *Opisthiamimus gregori* (e.g. Fig. 15G *vs* Fig. 15M) and *Theretairus antiquus*. Although only about two-thirds the size of the largest individuals of *Sphenodon punctatus* (e.g. skull length of LDUCZ x036 = 67.5 mm; Supplemental material, Table S2), *O. rarus* likely had a similar diet consisting of insects, arachnids and gastropods (e.g. Walls 1981; Ussher 1999; Foster 2003, 2007; Jones & Cree 2012) and was large enough to have preyed on relatively smaller-bodied vertebrates of the Morrison Formation such as anurans, squamates, other rhynchocephalians (including juveniles of its own species), and mammals. *Opisthias rarus* might also have eaten plants given it has dentary teeth that are more tightly packed, wider than long and with moderately well-developed mesial flanges for shredding. Biplots of linear tooth measurements from *O. rarus* plot at the base and in a similar area to those from the herbivorous eilenodontines with shredding and grinding dentitions (Jones 2006c, fig. 1). Therefore, *O. rarus* likely was an animal-dominated omnivore. *Eilenodon robustus* was the largest Morrison rhynchocephalian with an estimated skull length of *c*. 109 mm (Apesteguía *et al*. 2014, suppl-table 2), more than double that of *O. rarus*. *Eilenodon robustus* was likely herbivorous on the basis of its deep dentary and transversely widened marginal dentition with thickened enamel and extensive wear facets (Rasmussen & Callison 1981; Jones 2006c; Jones *et al*. 2018). Its relatively large body size might have aided it metabolically in digesting plant material (e.g. Pough 1973; Espinoza *et al*. 2004).

Conclusions

Here we document a new, small-bodied rhynchocephalian taxon, *Opisthiamimus gregori* gen. et sp. nov., from

the Upper Jurassic Morrison Formation of Wyoming, USA. Much of the skull and skeleton of the holotype is preserved, and our detailed anatomical study reveals its distinctiveness from all previously described rhynchocephalian taxa. The skull of *O. gregori* has many features in common with several non-neosphenodontian rhynchocephalians (e.g. *Planocephalosaurus*, *Clevosaurus*) yet exhibits craniodental features related to the proal shearing mechanism that becomes increasingly elaborated in more phylogenetically nested taxa (e.g. *Sphenodon*, *Eilenodon*). The postcranial skeleton of *O. gregori* is broadly similar to that of other terrestrial rhynchocephalians and possesses at least one phylogenetically informative postcranial character (fourth metacarpal shorter than third). Additionally, and if confirmed, the presence of osteoderms in *O. gregori* would be only the second case of these structures identified in a rhynchocephalian (*Pamizinsaurus* being the other) and potentially could be phylogenetically and/or ecomorphologically informative if additional discoveries of taxa with preserved osteoderms are made.

Our phylogenetic analyses support placement of *Opisthiamimus gregori* as a eusphenodontian, but not particularly closely related to the other Morrison taxa (i.e. *Opisthias rarus*, *Theretairus antiquus* or *Eilenodon robustus*). Differences in jaw and tooth morphology, dental wear patterns and body size also indicate dietary differences among the Morrison taxa that likely resulted in ecologically meaningful distinctions. Thus, the discovery of *O. gregori* increases both the alpha and beta taxonomic diversities and the ecomorphological diversity of Morrison Rhynchocephalia.

As highlighted by this study, much is yet to be gleaned from the rhynchocephalian fossil record of the Morrison Formation, from the Fox Mesa locality, and from existing specimens of *Opisthiamimus gregori*. For example, new scans (e.g. X-ray synchrotron tomography) of the holotype skeletal block of *O. gregori* might allow us to confirm its hypothesized mature age (e.g. fusion of the braincase) and provide higher-resolution data for identifying and reconstructing other parts of its skeleton (e.g. quadratojugal, scapula). Furthermore, a redescription of *Theretairus antiquus* on the basis of its holotype dentary and the new topotypic material cited herein will aid in better understanding its morphology and phylogenetic relationships. Lastly, future endeavours to re-evaluate the taxonomic identity(ies) and phylogenetic position(s) of the many published (and unpublished) Morrison specimens (mostly attributed to *Opisthias* as outlined in our Supplemental material) are warranted and will allow for the execution of more accurate studies on the diversity, palaeobiogeography and stratigraphic distributions of taxa. As such, and in conjunction with a similar investigation of the Morrison squamates, a more thorough understanding of the underlying mechanism(s) that allowed squamates to become the predominant lepidosaurs around the close of the Jurassic may come to light.

Acknowledgements

We are grateful to the many NMNH colleagues whose work contributed to the discovery, preparation and curation of these materials: in particular, we thank A. Millhouse for collections access and curatorial assistance; M. Brett-Surman, P. Kroehler, S. Jabo, J. Guibord, M. Oreska and C. Peredo for fieldwork; and J. Gregor and P. Kroehler for their careful preparation work. J. Hill, H. Little and S. Whittaker (NMNH), D. White (GWU, previously NMNH), A. Pritchard (VMNH, previously NMNH), J. Gladman and M. Walters (DU), and S. Taft and M. Fagan (UOHUK) helped facilitate and assist with μCT scans and/or processing of the digital data using 3D hardware and software. S. Whittaker provided access to and assistance with digital microscopy in the Scientific Imaging Lab at the NMNH. We especially thank J. Morrison (NMNH) for his skillfully rendered interpretive drawings in Figures 2, 3, 6, 13-15 and 17-23. K. de Queiroz (NMNH) provided access to the Amphibians and Reptiles collections in the Department of Vertebrate Zoology at the NMNH. G. Bever (JHMI), R. Martínez (UNSJ), A. Pritchard and V. Reynoso (UNAM) kindly provided digital images of *Theretairus*, *Sphenotitan*, *Planocephalosaurus* and *Zapatodon*, respectively, for character reassessment and scoring. J. Foster (UFHNH SPM), J. Kirkland (UGS), H.-D. Sues (NMNH) and K. Trujillo (LCCC) provided additional information on other North American rhynchocephalian specimens known to them. We thank M. Bies and the Bureau of Land Management for land access, assistance and special use permits (PA99-WY-054, PA03-WY-102) for collection of the fossils described herein. We are further grateful to H.-D. Sues and A. Pritchard for conversations on rhynchocephalian morphology and evolution. We are indebted to Editor-in-Chief P. Barrett for allowing us to submit our lengthy manuscript to the *Journal of Systematic Palaeontology* and to J. Olori (Associate Editor) and two anonymous reviewers for their constructive reviews and/or editorial assistance that improved our manuscript. Funding was provided by Smithsonian Small Grants to MTC. MEHJ was supported by the Australian Research Council (DE130101567) and was hosted by Elizabeth Freeland and David Land during visits to Washington.

Supplemental material

Supplemental material for this article can be accessed here: https://doi.org/10.1080/14772019.2022.2093139.

ORCID

David G. DeMar http://orcid.org/0000-0001-5426-0471
Marc E. H. Jones http://orcid.org/0000-0002-0146-9623
Matthew T. Carrano http://orcid.org/0000-0003-2129-1612

References

Apesteguía, S. 2005. A late Campanian sphenodontid (Reptilia, Diapsida) from northern Patagonia. *Comptes Rendus Palevol*, **4**, 663–669. doi:10.1016/j.crpv.2005.06.003

Apesteguía, S. 2008. *Esfenodontes (Reptilia, Lepidosauria) del Cretácico Superior de Patagonia: anatomía y filogenia*. Unpublished PhD dissertation, Universidad Nacional de La Plata, 535 pp.

Apesteguía, S. & Novas, F. E. 2003. Large Cretaceous sphenodontian from Patagonia provides insight into lepidosaur evolution in Gondwana. *Nature*, **425**, 609–612.

Apesteguía, S., Gómez, R. O. & Rougier, G. W. 2012. A basal sphenodontian (Lepidosauria) from the Jurassic of Patagonia: new insights on the phylogeny and biogeography of Gondwanan rhynchocephalians. *Zoological Journal of the Linnean Society*, **166**, 342–360. doi:10.1111/j.1096-3642.2012.00837.x

Apesteguía, S. & Carballido, J. L. 2014. A new eilenodontine (Lepidosauria, Sphenodontidae) from the Lower Cretaceous of central Patagonia. *Journal of Vertebrate Paleontology*, **34**, 303–317. doi:10.1080/02724634.2013.803974

Apesteguía, S., Gómez, R. O. & Rougier, G. W. 2014. The youngest South American rhynchocephalian, a survivor of the K/Pg extinction. *Proceedings of the Royal Society B*, **281**, 1–6. doi:10.1098/rspb.2014.0811

Apesteguía, S., Garberoglio, F. F. & Gómez, R. O. 2021. Earliest tuatara relative (Lepidosauria: Sphenodontinae) from southern continents. *Ameghiniana*, **58**, 416–441.

Arantes, B. de A., Soares, M. B. & Schultz, C. L. 2009. *Clevosaurus brasiliensis* (Lepidosauria, Sphenodontia) from the Upper Triassic of Rio Grande do Sul: post-cranial anatomy and phylogenetic relationships. *Revista Brasileira de Paleontologia*, **12**, 43–54. doi:10.4072/rbp.2009.1.04

Baur, G. 1895. Bemerkungen über die Osteologie der Schläfengegend der höheren Wirbeltiere. *Anatomischer Anzeiger*, **10**, 315–330.

Bever, G. S. & Norell, M. A. 2017. A new rhynchocephalian (Reptilia: Lepidosauria) from the Late Jurassic of Solnhofen (Germany) and the origin of the marine Pleurosauridae. *Royal Society Open Science*, **4**, 170570. doi:10.1098/rsos.170570

Bonaparte, J. F. & Sues, H.-D. 2006. A new species of *Clevosaurus* (Lepidosauria: Rhynchocephalia) from the Upper Triassic of Rio Grande do Sul, Brazil. *Palaeontology*, **49**, 917–923.

Brett-Surman, M., Jabo, S., Kroehler, P. A., Carrano, M. T. & Kvale, E. P. 2005. A new microvertebrate assemblage from the Upper Jurassic Morrison Formation, including mammals, theropods, and sphenodontians. *Journal of Vertebrate Paleontology*, **25**(3, suppl.), 39A.

Broom, R. 1914. A new thecodont reptile. *Proceedings of the Zoological Society of London*, **1914**, 1072–1077.

Burbrink, F. T., Grazziotin, F. G., Pyron, R. A., Cundall, D., Donnellan, S., Irish, F., Keogh, J. S., Kraus, F., Murphy, R. W., Noonan, B., Raxworthy, C. J., Ruane, S., Lemmon, A. R., Lemmon, E. M. & Zaher, H. 2020. Interrogating genomic-scale data for Squamata (lizards, snakes, and amphisbaenians) shows no support for key traditional morphological relationships. *Systematic Biology*, **69**, 502–520. doi:10.1093/sysbio/syz062

Carrano, M. T. & Velez-Juarbe, J. 2006. Paleoecology of the Quarry 9 vertebrate assemblage from Como Bluff, Wyoming (Morrison Formation, Late Jurassic). *Palaeogeography, Palaeoclimatology, and Palaeoecology*, **237**, 147–159. doi:10.1016/j.palaeo.2005.11.018

Carrano, M. T., Mateus, O. & Mitchell, J. 2013. First definitive association between embryonic *Allosaurus* bones and *Prismatoolithus* eggs in the Morrison Formation (Upper Jurassic, Wyoming, USA). *Journal of Vertebrate Paleontology, Program & Abstracts*, **2013**, 101.

Carroll, R. L. 1985. A pleurosaur from the Lower Jurassic and the taxonomic position of the Sphenodontida. *Palaeontographica Abteilung A*, **189**, 1–28.

Carroll, R. L. & Wild, R. 1994. Marine members of the Sphenodontia. Pp. 70–83 in N. C. Fraser & H.-D. Sues (eds) *In the shadow of the dinosaurs*. Cambridge University Press, Cambridge.

Cau, A., Baiano, M. A. & Raia, P. 2014. A new sphenodontian (Reptilia, Lepidosauria) from the Lower Cretaceous of Southern Italy and the phylogenetic affinities of the Pietraroia Plattenkalk rhynchocephalians. *Cretaceous Research*, **49**, 172–180. doi:10.1016/j.cretres.2014.02.001

Chambi-Trowell, S. A. V., Whiteside, D. I. & Benton, M. J. 2019. Diversity in rhynchocephalian *Clevosaurus* skulls based on CT reconstruction of two Late Triassic species from Great Britain. *Acta Palaeontologica Polonica*, **64**, 41–64. doi:10.4202/app.00569.2018

Chambi-Trowell, S. A. V., Martinelli, A. G., Whiteside, D. I., Romo de Vivar, P. R., Soares, M. B., Schultz, C. L., Gill, P. G., Benton, M. J., & Rayfield, E. J. 2021. The diversity of Triassic South American sphenodontians: a new basal form, clevosaurs, and a revision of rhynchocephalian phylogeny. *Journal of Systematic Palaeontology*, **19**, 787–820. doi:10.1080/14772019.2021.1976292

Cleary, T. J., Benson, R. B. J., Evans, S. E. & Barrett, P. M. 2018. Lepidosaurian diversity in the Mesozoic–Palaeogene: the potential roles of sampling biases and environmental drivers. *Royal Society Open Science*, **5**, 171830. doi:10.1098/rsos.171830

Cocude-Michel, M. 1963. Les rhynchocéphales et les sauriens des calcaires lithographiques (Jurassique supérieur)

d'Europe occidentale. *Nouvelles archives du Muséum d'histoire naturelle de Lyon*, **7**, 3–224.

Cope, E. D. 1871. On the homologies of some of the cranial bones of the Reptilia, and on the systematic arrangement of the class. *Proceedings of the American Association for the Advancment of Science*, **19**, 194–247.

Cree, A. 2014. *Tuatara: biology and conservation of a venerable survivor*. Canterbury University Press, Christchurch, New Zealand, 583 pp.

Curtis, N., **Jones, M. E. H.**, **Evans, S. E.**, **Shi, J.**, **O'Higgins, P.** & **Fagan, M. J.** 2010. Predicting muscle activation patterns from motion and anatomy: modelling the skull of *Sphenodon* (Diapsida: Rhynchocephalia). *Journal of The Royal Society Interface*, **7**, 153–160. doi:10.1098/rsif.2009.0139

DeMar, D. G. Jr., **Jones, M. E. H.** & **Carrano, M. T.** 2018. New rhynchocephalian (Reptilia, Lepidosauria) material from the Upper Jurassic Morrison Formation, north-central Wyoming, USA consolidates a clade of American Sphenodontinae. *Journal of Vertebrate Paleontology, Program & Abstracts*, **2018**, 114.

de Queiroz, K. & **Gauthier, J. A.** 2020. Lepidosauria. Pp. 1079–1085 in K. de Queiroz, P. D. Cantino & J. A. Gauthier (eds) *Phylonyms: a companion to the PhyloCode*. CRC Press, Boca Raton.

Dupret, V. 2004. The pleurosaurs: anatomy and phylogeny. *Revue de Paléobiologie*, **9**, 61–80.

Espinoza, R. E., **Wiens, J. J.** & **Tracy, C. R.** 2004. Recurrent evolution of herbivory in small, cold-climate lizards: breaking the ecophysiological rules of reptilian herbivory. *Proceedings of the National Academy of Sciences of the United States*, **101**, 16819–16824. doi:10.1073/pnas.0401226101

Etheridge, R. 1965. The abdominal skeleton of lizards in the Family Iguanidae. *Herpetologica*, **21**, 161–168.

Evans, S. E. 1980. The skull of a new eosuchian reptile from the Lower Jurassic of South Wales. *Zoological Journal of the Linnean Society*, **70**, 203–264. doi:10.1111/j.1096-3642.1980.tb00852.x

Evans, S. E. 1981. The postcranial skeleton of the Lower Jurassic eosuchian *Gephyrosaurus bridensis*. *Zoological Journal of the Linnean Society*, **73**, 81–116. doi:10.1111/j.1096-3642.1981.tb01580.x

Evans, S. E. 1984. The classification of the Lepidosauria. *Zoological Journal of the Linnean Society*, **82**, 87–100. doi:10.1111/j.1096-3642.1984.tb00537.x

Evans, S. E. 1995. Lizards: evolution, early radiation and biogeography. Pp. 271–283 in A. Sun & Y. Wang (eds) *Sixth symposium on Mesozoic terrestrial ecosystems and biota, short papers*. China Ocean Press, Beijing.

Evans, S. E. 2003. At the feet of the dinosaurs: the early history and radiation of lizards. *Biological Reviews*, **78**, 513–551. doi:10.1017/S1464793103006134

Evans, S. E. 2008. The skull of lizards and tuatara. Pp. 1–347 in C. Gans, A. S. Gaunt & K. Adler (eds) *Biology of the Reptilia*, *Volume 20*, *Morphology H: the skull of Lepidosauria*. Society for the Study of Amphibians and Reptiles, Ithaca, New York.

Evans, S. E. & **Fraser, N. C.** 1992. A sphenodontid jaw (Reptilia: Lepidosauria) from the Upper Jurassic of Dorset. *Proceedings of the Dorset Natural History Society*, **1992**, 199–200.

Evans, S. E., **Prasad, G. V. R.** & **Manhas, B. K.** 2001. Rhynchocephalians (Diapsida: Lepidosauria) from the Jurassic Kota Formation of India. *Zoological Journal of the Linnean Society*, **133**, 309–334. doi:10.1111/j.1096-3642.2001.tb00629.x

Evans, S. E. & **Jones, M. E. H.** 2010. The origin, early history and diversification of lepidosauromorph reptiles. Pp. 27–44 in S. Bandyopadhyay (ed.) *New aspects of Mesozoic biodiversity*. Springer Berlin Heidelberg, Berlin, Heidelberg.

Ezcurra, M. D. 2010. Biogeography of Triassic tetrapods: evidence for provincialism and driven sympatric cladogenesis in the early evolution of modern tetrapod lineages. *Proceedings of the Royal Society B*, **277**, 2547–2552. doi:10.1098/rspb.2010.0508

Fitzinger, L. J. 1837. Ueber *Palaeosaurus sternbergii*, eine neue Gattung vorweltlicher Reptilien und die Stellung dieser Tiere im Systeme überhaupt. *Annalen des Wiener Museums der Naturgeschichte*, **2**, 171.

Ford, D. P., **Evans, S. E.**, **Choiniere, J. N.**, **Fernandez, V.** & **Benson, R. B.** 2021. A reassessment of the enigmatic diapsid *Paliguana whitei* and the early history of Lepidosauromorpha. *Proceedings of the Royal Society B*, **288**, 20211084.

Foster, J. R. 2003. Paleoecological analysis of the vertebrate fauna of the Morrison Formation (Upper Jurassic), Rocky Mountain region, USA. *New Mexico Museum of Natural History and Science Bulletin*, **23**, 1–95.

Foster, J. R. 2007. *Jurassic West: the dinosaurs of the Morrison Formation and their world*. Indiana University Press, Bloomington, 389 pp.

Fraser, N. C. 1982. A new rhynchocephalian from the British Upper Trias. *Palaeontology*, **25**, 709–725.

Fraser, N. C. 1986. New Triassic sphenodontids from south-west England and a review of their classification. *Palaeontology*, **29**, 165–186.

Fraser, N. C. 1988. The osteology and relationships of *Clevosaurus* (Reptilia: Sphenodontida). *Philosophical Transactions of the Royal Society of London, Series B, Biological Sciences*, **321**, 125–178. doi:10.1098/rstb.1988.0092

Fraser, N. C. 1993. A new sphenodontian from the early Mesozoic of England and North America: implications for correlating early Mesozoic continental deposits. *New Mexico Museum of Natural History and Science Bulletin*, **3**, 135–139.

Fraser, N. C. & **Walkden, G. M.** 1984. The postcranial skeleton of the Upper Triassic sphenodontid *Planocephalosaurus robinsonae*. *Palaeontology*, **27**, 575–595.

Fraser, N. C. & **Benton, M. J.** 1989. The Triassic reptiles *Brachyrhinodon* and *Polysphenodon* and the relationships of the sphenodontids. *Zoological Journal of the Linnean Society*, **96**, 413–445. doi:10.1111/j.1096-3642.1989.tb02521.x

Fraser, N. C. & **Wu, X.-C.** 1998. Sphenodontians from the Brushy Basin Member of the Morrison Formation in Dinosaur National Monument. *Modern Geology*, **23**, 17–34.

Gauthier, Jacques A., **Estes, R.** & **de Queiroz, K.** 1988. A phylogenetic analysis of Lepidosauromorpha. Pp. 15–98 in R. Estes & G. Pregill (eds) *Phylogenetic relationships of the lizard families*. Stanford University Press, Stanford.

Gauthier, J. A., **Kearney, M.**, **Maisano, J. A.**, **Rieppel, O.** & **Behlke, A. D. B.** 2012. Assembling the squamate tree of life: perspectives from the phenotype and the fossil

record. *Bulletin of the Peabody Museum of Natural History*, **53**, 3–308. doi:10.3374/014.053.0101

Gemmell, N. J., Rutherford, K., Prost, S., Tollis, M., Winter, D., Macey, J. R., Adelson, D. L., Suh, A., Bertozzi, T., Grau, J. H., Organ, C., Gardner, P. P., Muffato, M., Patricio, M., Billis, K., Martin, F. J., Flicek, P., Petersen, B., Kang, L., Michalak, P., Buckley, T. R., Wilson, M., Cheng, Y., Miller, H., Schott, R. K., Jordan, M. D., Newcomb, R. D., Arroyo, J. I., Valenzuela, N., Hore, T. A., Renart, J., Peona, V., Peart, C. R., Warmuth, V. M., Zeng, L., Kortschak, R. D., Raison, J. M., Zapata, V. V., Wu, Z., Santesmasses, D., Mariotti, M., Guigó, R., Rupp, S. M., Twort, V. G., Dussex, N., Taylor, H., Abe, H., Bond, D. M., Paterson, J. M., Mulcahy, D. G., Gonzalez, V. L., Barbieri, C. G., DeMeo, D. P., Pabinger, S., Van Stijn, T., Clarke, S., Ryder, O., Edwards, S. V., Salzberg, S. L., Anderson, L., Nelson, N., Stone, C., Ngatiwai Trust Board, Stone, C., Smillie, J. & Edmonds, H. 2020. The tuatara genome reveals ancient features of amniote evolution. *Nature*, **584**, 403–409. doi:10.1038/s41586-020-2561-9

Gilmore, C. W. 1909. A new rhynchocephalian reptile from the Jurassic of Wyoming, with notes on the fauna of 'Quarry 9'. *Proceedings of the United States National Museum*, **37**, 35–42.

Goloboff, P. A., Farris, J. S. & Nixon, K. C. 2008. TNT, a free program for phylogenetic analysis. *Cladistics*, **24**, 774–786. doi:10.1111/j.1096-0031.2008.00217.x

Gorniak, G. C., Rosenberg, H. I. & Gans, C. 1982. Mastication in the tuatara, *Sphenodon punctatus* (Reptilia: Rhynchocephalia): structure and activity of the motor system. *Journal of Morphology*, **171**, 321–353. doi:10.1002/jmor.1051710307

Griffiths, E. F., Ford, D. P., Benson, R. B. & Evans, S. E. 2021. New information on the Jurassic lepidosauromorph *Marmoretta oxoniensis*. *Papers in Palaeontology*, **7**, 2255–2278.

Günther, A. 1867. Contribution to the anatomy of *Hatteria* (Rhynchocephalus, Owen). *Philosophical Transactions of the Royal Society of London*, **157**, 595–629.

Haeckel, E. 1866. *Generelle Morphologie der Organismen. II: Allgemeine Entwicklungsgeschichte der Organismen*. Verlag Georg Reimer, Berlin, 574 pp.

Hay, J. M., Sarre, S. D., Lambert, D. M., Allendorf, F. W. & Daugherty, C. H. 2010. Genetic diversity and taxonomy: a reassessment of species designation in tuatara (*Sphenodon*: Reptilia). *Conservation Genetics*, **11**, 1063–1081. doi:10.1007/s10592-009-9952-7

Heckert, A. B. 2004. Late Triassic microvertebrates from the lower Chinle Group (Otischalkian–Adamanian: Carnian), southwestern USA. *New Mexico Museum of Natural History and Science Bulletin*, **27**, 1–170.

Heckert, A. B., Lucas, S. G., Rinehart, L. F. & Hunt, A. P. 2008. A new genus and species of sphenodontian from the Ghost Ranch *Coelophysis* quarry (Upper Triassic: Apachean), Rock Point Formation, New Mexico, USA. *Palaeontology*, **51**, 827–845. doi:10.1111/j.1475-4983.2008.00786.x

Herrera-Flores, J. A., Stubbs, T. L., Elsler, A. & Benton, M. J. 2018. Taxonomic reassessment of *Clevosaurus latidens* Fraser, 1993 (Lepidosauria, Rhynchocephalia) and rhynchocephalian phylogeny based on parsimony and Bayesian inference. *Journal of Paleontology*, **92**, 734–742. doi:10.1017/jpa.2017.136

Herrera-Flores, J. A., Stubbs, T. L. & Benton, M. J. 2021. Ecomorphological diversification of squamates in the Cretaceous. *Royal Society Open Science*, **8**, 201961. doi:10.1098/rsos.201961

Hoffstetter, R. & Gasc, J.-P. 1969. Vertebrae and ribs of modern reptiles. Pp. 201–310 in C. Gans, A. d'A. Bellairs & T. S. Parsons (eds) *Biology of the Reptilia*. Academic Press, London and New York.

Howes, G. B. & Swinnerton, H. H. 1901. On the development of the skeleton of the tuatara, *Sphenodon punctatus*; with remarks on the egg, on the hatching, and on the hatched young. *Transactions of the Zoological Society of London*, **16**, 1–84.

Hsiou, A. S., De França, M. A. G. & Ferigolo, J. 2015. New data on the *Clevosaurus* (Sphenodontia: Clevosauridae) from the Upper Triassic of southern Brazil. *PLoS ONE*, **10**, e0137523. doi:10.1371/journal.pone.0137523

Hsiou, A. S., Nydam, R. L., Simões, T. R., Pretto, F. A., Onary, S., Martinelli, A. G., Liparini, A., Martínez, P. R. R. de V., Soares, M. B., Schultz, C. L. & Caldwell, M. W. 2019. A new clevosaurid from the Triassic (Carnian) of Brazil and the rise of sphenodontians in Gondwana. *Scientific Reports*, **9**, 11821. doi:10.1038/s41598-019-48297-9

Huelsenbeck, J. P. & Ronquist, F. 2001. MRBAYES: Bayesian inference of phylogeny. *Bioinformatics*, **17**, 754–755.

Jenkins, F. A. Jr., Shubin, N. H., Amaral, W. W., Gatesy, S. M., Schaff, C. R., Clemmensen, L. B., Downs, W. R., Davidson, A. R., Bonde, N. & Osbaeck, F. 1994. Late Triassic continental vertebrates and depositional environments of the Fleming Fjord Formation, Jameson Land, East Greenland. *Meddelelser om Grønland, Geoscience*, **32**, 1–25.

Jenkins, K. M., Jones, M. E. H., Zikmund, T., Boyde, A., Daza, J. D. 2017. A review of tooth implantation among rhynchocephalians (Lepidosauria). *Journal of Herpetology*, **51**(3), 300–306.

Jones, M. E. H. 2006a. *Skull evolution and functional morphology in* Sphenodon *and other Rhynchocephalia (Diapsida: Lepidosauria*). Unpublished PhD dissertation, University of London, 567 pp.

Jones, M. E. H. 2006b. The Early Jurassic *Clevosaurus* from China (Diapsida: Lepidosauria). *New Mexico Museum of Natural History and Science Bulletin*, **37**, 548–562.

Jones, M. E. H. 2006c. Tooth diversity and function in the Rhynchocephalia (Diapsida: Lepidosauria). Pp. 55–58 in P. M. Barrett & S. E. Evans (eds) *Ninth international symposium on Mesozoic terrestrial ecosystems and biota*. Natural History Museum, London.

Jones, M. E. H. 2008. Skull shape and feeding strategy in *Sphenodon* and other Rhynchocephalia (Diapsida: Lepidosauria). *Journal of Morphology*, **269**, 945–966. doi:10.1002/jmor.10634

Jones, M. E. H. 2009. Dentary tooth shape in *Sphenodon* and its fossil relatives (Diapsida: Lepidosauria: Rhynchocephalia). Pp. 9–15 in T. Koppe, G. Meyer & K. W. Alt (eds) *Interdisciplinary dental morphology, frontiers of oral biology*, *Volume 13*. Karger, Greifswald.

Jones, M. E. H., Curtis, N., O'Higgins, P., Fagan, M. & Evans, S. E. 2009a. The head and neck muscles associated with feeding in *Sphenodon* (Reptilia:

Lepidosauria: Rhynchocephalia). *Palaeontologia Electronica*, **12**(2), 7A. https://palaeo-electronica.org/2009_2/179/index.html

Jones, M. E. H. & **Lappin, A. K.** 2009. Bite-force performance of the last rhynchocephalian (Lepidosauria: *Sphenodon*). *Journal of the Royal Society of New Zealand*, **39**, 71–83. doi:10.1080/03014220909510565

Jones, M. E. H, **Tennyson, A. J. D.**, **Worthy, J. P.**, **Evans, S. E.** & **Worthy, T. H.** 2009b. A sphenodontine (Rhynchocephalia) from the Miocene of New Zealand and palaeobiogeography of the tuatara (*Sphenodon*). *Proceedings of the Royal Society B*, **276**, 1385–1390. doi:10.1098/rspb.2008.1785

Jones, M. E. H., Curtis, N., O'Higgins, P., Fagan, M. J. & **Evans, S. E.** 2011. Hard tissue anatomy of the cranial joints in *Sphenodon* (Rhynchocephalia): sutures, kinesis, and skull mechanics. *Palaeontologia Electronica*, **14**(2), 17A. https://palaeo-electronica.org/2011_2/251/index.html

Jones, M. E. H. & **Cree, A.** 2012. Tuatara. *Current Biology*, **22**, R986–R987. doi:10.1016/j.cub.2012.10.049

Jones, M. E. H., O'Higgins, P., Fagan, M. J., Evans, S. E. & **Curtis, N.** 2012. Shearing mechanics and the influence of a flexible symphysis during oral food processing in *Sphenodon* (Lepidosauria: Rhynchocephalia). *The Anatomical Record*, **295**, 1075–1091. doi:10.1002/ar.22487

Jones, M. E. H., Anderson, C., Hipsley, C. A., Müller, J., Evans, S. E. & **Schoch, R. R.** 2013. Integration of molecules and new fossils supports a Triassic origin for Lepidosauria (lizards, snakes, and tuatara). *BMC Evolutionary Biology*, **13**, 208. doi:10.1186/1471-2148-13-208

Jones, M. E. H., Lucas, P. W., Tucker, A. S., Watson, A. P., Sertich, J. J. W., Foster, J. R., Williams, R., Garbe, U., Bevitt, J. J. & **Salvemini, F.** 2018. Neutron scanning reveals unexpected complexity in the enamel thickness of an herbivorous Jurassic reptile. *Journal of The Royal Society Interface*, **15**, 20180039. doi:10.1098/rsif.2018.0039

Kaye, F. & **Padian, K.** 1994. Microvertebrates from the Placerias Quarry: a window on Late Triassic vertebrate diversity in the American Southwest. Pp. 171–196 in N. C. Fraser & H.-D. Sues (eds) In *the shadow of the dinosaurs: Early Mesozoic tetrapods*. Cambridge University Press, Cambridge.

Keeble, E., Whiteside, D. I. & **Benton, M. J.** 2018. The terrestrial fauna of the Late Triassic Pant-y-ffynnon Quarry fissures, South Wales, UK and a new species of *Clevosaurus* (Lepidosauria: Rhynchocephalia). *Proceedings of the Geologists' Association*, **129**, 99–119. doi:10.1016/j.pgeola.2017.11.001

Kirkland, J. I. 2006. Fruita Paleontological Area (Upper Jurassic, Morrison Formation), western Colorado: an example of terrestrial taphofacies analysis. *New Mexico Museum of Natural History and Science Bulletin*, **36**, 67–95.

Kligman, B. T., McClure, W. C., Korbitz, M. & **Schumacher, B. A.** 2021. New sphenodontian (Reptilia: Lepidosauria) from a novel Late Triassic paleobiota in western North America sheds light on the earliest radiation of herbivorous lepidosaurs. *Journal of Paleontology*, **95**, 827–844. doi:10.1017/jpa.2021.22

Lamar, S. K., Nelson, N. J., Moore, J. A., Taylor, H. R., Keall, S. N. & **Ormsby, D. K.** 2021. Initial collection, characterization, and storage of tuatara (*Sphenodon punctatus*) sperm offers insight into their unique reproductive system. *PLoS ONE*, **16**, e0253628. doi:10.1371/journal.pone.0253628

LeBlanc, A. R. H., Apesteguía, S., Larsson, H. C. E. & **Caldwell, M. W.** 2020. Unique tooth morphology and prismatic enamel in Late Cretaceous sphenodontians from Argentina. *Current Biology*, **30**, 1755–1761. doi:10.1016/j.cub.2020.02.071

Lydekker, R. 1888. *Catalogue of the fossil Reptilia and Amphibia in the British Museum (Natural History). Part I. Containing the orders Ornithosauria, Crocodilia, Dinosauria, Squamata, Rhynchocephalia, and Proterosauria*. British Museum (Natural History), London, 309 pp. doi:10.5962/bhl.title.61848

Maddison, W. P. & **Maddison, D. R.** 2018. *Mesquite: a modular system for evolutionary analysis*. Version 3.40. Updated at http://www.mesquiteproject.org, accessed 23 March 2018.

Maidment, S. C. R. & **Muxworthy, A.** 2019. A chronostratigraphic framework for the Upper Jurassic Morrison Formation, western USA. *Journal of Sedimentary Research*, **89**, 1017–1038. doi:10.2110/jsr.2019.54

Martínez, R. N., Apaldetti, C., Colombi, C. E., Praderio, A., Fernandez, E., Malnis, P. S., Correa, G. A., Abelin, D. & **Alcober, O.** 2013. A new sphenodontian (Lepidosauria: Rhynchocephalia) from the Late Triassic of Argentina and the early origin of the herbivore opisthodontians. *Proceedings of the Royal Society B*, **280**, 20132057. doi:10.1098/rspb.2013.2057

Meiri, S. 2010. Length–weight allometries in lizards. *Journal of Zoology*, **281**, 218–226. doi:10.1111/j.1469-7998.2010.00696.x

Meloro, C. & **Jones, M. E. H.** 2012. Tooth and cranial disparity in the fossil relatives of *Sphenodon* (Rhynchocephalia) dispute the persistent 'living fossil' label. *Journal of Evolutionary Biology*, **25**, 2194–2209. doi:10.1111/j.1420-9101.2012.02595.x

Müller, J., Scheyer, T. M., Head, J. J., Barrett, P. M., Werneburg, I., Ericson, P. G. P., Pol, D. & **Sánchez-Villagra, M. R.** 2010. Homeotic effects, somitogenesis and the evolution of vertebral numbers in recent and fossil amniotes. *Proceedings of the National Academy of Sciences of the United States*, **107**, 2118–2123. doi:10.1073/pnas.0912622107

Nopcsa, F. 1923. *Die Familien der Reptilien*. *Fortschritte der Geologie und Palaeontologie 2*. Verlag von Gebrüder Borntraeger, Berlin, 210 pp.

Nopcsa, F. 1928. The genera of reptiles. *Palaeobiologica*, **1**, 163–188.

O'Brien, A., Whiteside, D. I. & **Marshall, J. E. A.** 2018. Anatomical study of two previously undescribed specimens of *Clevosaurus hudsoni* (Lepidosauria: Rhynchocephalia) from Cromhall Quarry, UK, aided by computed tomography, yields additional information on the skeleton and hitherto undescribed bones. *Zoological Journal of the Linnean Society*, **183**, 163–195. doi:10.1093/zoolinnean/zlx087

Otero, T. & **Hoyos, J. M.** 2013. Sesamoid elements in lizards. *Herpetological Journal*, **23**, 105–114.

Pol, D. & **Escapa, I. H.** 2009. Unstable taxa in cladistic analysis: identification and the assessment of relevant characters. *Cladistics*, **25**, 515–527. doi:10.1111/j.1096-0031.2009.00258.x

Pough, F. H. 1973. Lizard energetics and diet. *Ecology*, **54**, 837–844. doi:10.2307/1935678

Pritchard, A. C., **Gauthier, J. A.**, **Hanson, M.**, **Bever, G. S.** & **Bhullar, B.-A. S.** 2018. A tiny Triassic saurian from Connecticut and the early evolution of the diapsid feeding apparatus. *Nature Communications*, **9**, 1213. doi:10.1038/s41467-018-03508-1

Rasmussen, T. E. & **Callison, G.** 1981. A new herbivorous sphenodontid (Rhynchocephalia: Reptilia) from the Jurassic of Colorado. *Journal of Paleontology*, **55**, 1109–1116.

Rauhut, O. W. M., **Heyng, A. M.**, **López-Arbarello, A.** & **Hecker, A.** 2012. A new rhynchocephalian from the Late Jurassic of Germany with a dentition that is unique amongst tetrapods. *PloS ONE*, **7**, e46839. doi:10.1371/journal.pone.0046839

Rauhut, O. W. M. & **López-Arbarello, A.** 2016. Zur taxonomie der Brückenechse aus dem oberen Jura von Schamhaupten. *Archaeopteryx*, **33**, 1–11.

Regnault, S., **Hutchinson, J. R.** & **Jones, M. E. H.** 2017. Sesamoid bones in tuatara (*Sphenodon punctatus*) investigated with X-ray microtomography, and implications for sesamoid evolution in Lepidosauria. *Journal of Morphology*, **278**, 62–72. doi:10.1002/jmor.20619

Reynoso, V.-H. 1996. A Middle Jurassic *Sphenodon*-like sphenodontian (Diapsida: Lepidosauria) from Huizachal Canyon, Tamaulipas, Mexico. *Journal of Vertebrate Paleontology*, **16**, 210–221.

Reynoso, V.-H. 1997. A 'beaded' sphenodontian (Diapsida: Lepidosauria) from the Early Cretaceous of Central Mexico. *Journal of Vertebrate Paleontology*, **17**, 52–59.

Reynoso, V.-H. 2000. An unusual aquatic sphenodontian (Reptilia: Diapsida) from the Tlayua Formation (Albian), Central Mexico. *Journal of Paleontology*, **74**, 133–148.

Reynoso, V.-H. 2005. Possible evidence of a venom apparatus in a Middle Jurassic sphenodontian from the Huizachal Red Beds of Tamaulipas, México. *Journal of Vertebrate Paleontology*, **25**, 646–654.

Reynoso, V.-H. & **Clark, J. M.** 1998. A dwarf sphenodontian from the Jurassic La Boca Formation of Tamaulipas, México. *Journal of Vertebrate Paleontology*, **18**, 333–339.

Robinson, P. L. 1976. How *Sphenodon* and *Uromastyx* grow their teeth and use them. Pp. 43–64 in A. d'A. Bellairs & C. B. Cox (eds) *Morphology and biology of reptiles*. Academic Press, London.

Romo de Vivar, P. R., **Martinelli, A. G.**, **Schmaltz Hsiou, A.** & **Soares, M. B.** 2020. A new rhynchocephalian from the Late Triassic of southern Brazil enhances eusphenodontian diversity. *Journal of Systematic Palaeontology*, **18**, 1103–1126. doi:10.1080/14772019.2020.1732488

Säilä, L. K. 2005. A new species of the sphenodontian reptile *Clevosaurus* from the Lower Jurassic of South Wales. *Palaeontology*, **48**, 817–831. doi:10.1111/j.1475-4983.2005.00486.x

Scheyer, T. M., **Spiekman, S. N. F.**, **Sues, H.-D.**, **Ezcurra, M. D.**, **Butler, R. J.** & **Jones, M. E. H.** 2020. *Colobops*: a juvenile rhynchocephalian reptile (Lepidosauromorpha), not a diminutive archosauromorph with an unusually strong bite. *Royal Society Open Science*, **7**, 192179. doi:10.1098/rsos.192179

Shubin, N. H. & **Sues, H.-D.** 1991. Biogeography of early Mesozoic continental tetrapods: patterns and implications. *Paleobiology*, **17**, 214–230. doi:10.1017/S0094837300010575

Simões, T. R., **Caldwell, M. W.**, **Tałanda, M.**, **Bernardi, M.**, **Palci, A.**, **Vernygora, O.**, **Bernardini, F.**, **Mancini, L.** & **Nydam, R. L.** 2018. The origin of squamates revealed by a Middle Triassic lizard from the Italian Alps. *Nature*, **557**, 706–709. doi:10.1038/s41586-018-0093-3

Simões, T. R., **Caldwell, M. W.** & **Pierce, S. E.** 2020. Sphenodontian phylogeny and the impact of model choice in Bayesian morphological clock estimates of divergence times and evolutionary rates. *BMC Biology*, **18**, 191. doi:10.1186/s12915-020-00901-5

Simões, T. R., **Kinney-Broderick, G.** & **Pierce, S. E.** 2022. An exceptionally preserved *Sphenodon*-like sphenodontian reveals deep time conservation of the tuatara skeleton and ontogeny. *Communications Biology*, **5**, 195. doi:10.1038/s42003-022-03144-y

Simpson, G. G. 1926. American terrestrial Rhynchocephalia. *American Journal of Science*, **12**, 12–16.

Smith, J. B. & **Dodson, P.** 2003. A proposal for a standard terminology of anatomical notation and orientation in fossil vertebrate dentitions. *Journal of Vertebrate Paleontology*, **23**, 1–12. doi:10.1671/0272-4634(2003)23[1:APFAST]2.0.CO;2

Sobral, G., **Simões, T. R.** & **Schoch, R. R.** 2020. A tiny new Middle Triassic stem-lepidosauromorph from Germany: implications for the early evolution of lepidosauromorphs and the Vellberg fauna. *Scientific Reports*, **10**, 2273. doi:10.1038/s41598-020-58883-x

Sues, H.-D. & **Baird, D.** 1993. A skull of a sphenodontian lepidosaur from the New Haven Arkose (Upper Triassic: Norian) of Connecticut. *Journal of Vertebrate Paleontology*, **13**, 370–372. doi:10.1080/02724634.1993.10011517

Sues, H.-D., **Shubin, N. H.** & **Olsen, P. E.** 1994a. A new sphenodontian (Lepidosauria: Rhynchocephalia) from the McCoy Brook Formation (Lower Jurassic) of Nova Scotia, Canada. *Journal of Vertebrate Paleontology*, **14**, 327–340. doi:10.1080/02724634.1994.10011563

Sues, H.-D., **Olsen, P. E.** & **Kroehler, P. A.** 1994b. Small tetrapods from the Upper Triassic of the Richmond basin of Virginia. Pp. 161–170 in N. C. Fraser & H.-D. Sues (eds) *In the shadow of the dinosaurs: Early Mesozoic tetrapods*. Cambridge University Press, New York.

Sues, H.-D. & **Schoch, R. R.** 2021. A new early-diverging sphenodontian (Lepidosauria, Rhynchocephalia) from the Upper Triassic of Virginia, USA. *Journal of Paleontology*, **95**, 344–350. doi:10.1017/jpa.2020.87

Swofford, D. L. 2003. *PAUP*. Phylogenetic analysis using parsimony (*and other methods)*. Version 4a. Sinauer Associates, Sunderland, Massachusetts.

Throckmorton, G. S., **Hopson, J. A.** & **Parks, P.** 1981. A redescription of *Toxolophosaurus cloudi* Olson, a Lower Cretaceous herbivorous sphenodontian reptile. *Journal of Paleontology*, **55**, 586–597.

Trujillo, K. C. & **Kowallis, B. J.** 2015. Recalibrated legacy $^{40}Ar/^{39}Ar$ ages for the Upper Jurassic Morrison Formation, Western Interior, USA. *Geology of the Intermountain West*, **2**, 1–8.

Uetz, P., Freed, P., Aguilar, R. & **Hošek, J. (eds).** 2022. *The reptile database*. Updated at: http://www.reptile-database.org, accessed 21 March 2022.

Ussher, G. T. 1999. Tuatara (*Sphenodon punctatus*) feeding ecology in the presence of kiore (*Rattus exulans*). *New*

Zealand Journal of Zoology, **26**, 117–125. doi:10.1080/03014223.1999.9518183

Vijaya & **Prasad, G. V. R.** 2001. Age of the Kota Formation, Pranhita-Godavari Valley, India. A palynological approach. *Journal of the Palaeontological Society of India*, **46**, 77–93.

Villa, A., **Montie, R.**, **Röper, M.**, **Rothgaenger, M.** & **Rauhut, O. W. M.** 2021. *Sphenofontis velserae* gen. et sp. nov., a new rhynchocephalian from the Late Jurassic of Brunn (Solnhofen Archipelago, southern Germany). *PeerJ*, **9**, e11363. doi:10.7717/peerj.11363

Walker, J. D., Geissman, J. W., Bowring, S. A. & **Babcock, L. E.** 2018. *GSA geologic time scale v.* 5.0. Geological Society of America. doi:10.1130/2018.CTS005R3C

Walls, G. Y. 1981. Feeding ecology of the Tuatara (*Sphenodon punctatus*) on Stephens Island, Cook Strait. *New Zealand Journal of Ecology*, **4**, 89–97.

Whiteside, D. I. 1986. The head skeleton of the Rhaetian sphenodontid *Diphydontosaurus avonis* gen. et sp. nov. and the modernizing of a living fossil. *Philosophical Transactions of the Royal Society of London, Series B*, **312**, 379–430. doi:10.1098/rstb.1986.0014

Williston, S. W. 1925. *The osteology of the reptiles*. Harvard University Press, Cambridge, 300 pp.

Wu, X.-C. 1991. *The comparative anatomy and systematics of Mesozoic sphenodontians*. Unpublished PhD dissertation, McGill University, 229 pp.

Wu, X.-C. 1994. Late Triassic–Early Jurassic sphenodontians from China and the phylogeny of the Sphenodontia. Pp. 38–69 in N. C. Fraser & H.-D. Sues (eds) In *the shadow of the dinosaurs: Early Mesozoic tetrapods*. Cambridge University Press, Cambridge.

Zardoya, R. & **Meyer, A.** 1998. Complete mitochondrial genome suggests diapsid affinities of turtles. *Proceedings of the National Academy of Sciences of the United States*, **95**, 14226. doi:10.1073/pnas.95.24.14226

Associate Editor: Jennifer Olori